

University of Hertfordshire
School of Engineering and Technology
Aeronautics and Space Division

Satellite Drag Analysis using Direct Simulation Monte Carlo (DSMC)

By Jacob Bullard

A Thesis Submitted to the University of Hertfordshire
in partial fulfilment of the requirements of the degree of
Master of Science by Research

March 2018

Abstract

High altitude research into free molecular flow properties has become more prominent in the aerospace field in recent years due to the rise of private aerospace firms. This led to an increase in satellite launches and greater interest in the behaviour of rarefied gasses and their effect on satellites, spacecraft and space stations. The advancement in research in this field can influence the design of these space vehicles. Direct Simulation Monte Carlo (DSMC) is a reliable simulation tool for high altitude flow which has proven its worth over the past 40-50 years.

This report lays the foundation for research into the effect of varying geometric shapes of satellites in Low Earth Orbit (LEO) and whether factors such as atmospheric density and temperature have an effect on the coefficient of drag. It shows that the coefficient of drag of the satellite can increase dramatically with a rise in atmospheric temperature with most structures.

A variety of DSMC simulations were also carried out on a satellite with a drag plate, which was shown to produce a significant decrease in the orbital life of satellites in LEO. These simulations were carried out on generic shaped satellites as a base, then the GRACE satellite was tested. It was shown through numerical simulation that the addition of a drag plate to a satellite in LEO can alter the orbital life and rate of decay of that satellite; these rates varied depending on different orbital conditions.

Future work for this project was also discussed with the emphasis on further research into the drag plate design and mechanics; this project has demonstrated the proof of concept for the drag plate well.

TABLE OF CONTENTS

	Page
Abstract.....	ii
List of Tables.....	vi
List of Figures	vii
Nomenclature.....	10
1. Introduction	12
1.1 Background	12
1.2 Aim and Objectives	14
1.3 Approach.....	15
1.4 Report Structure	17
1.5 Summary.....	17
2. Literature Review	18
2.1 Characterisation of LEO Atmosphere.....	18
2.1.1 F10.7 Solar Index.....	22
2.2 Previous Work Undertaken	23
2.3 Analytical Methods	30
2.3.1 Orbital Decay	34
2.4 Summary.....	35
3. DSMC Modelling	36
3.1 Direct Simulation Monte Carlo Method (Numerical Method) 2.4.....	36
3.1.1 DSMC Program Structure.....	37
3.1.2 Momentum and Molecule Collisions	38
3.1.3 Molecular Model for DSMC	42

3.1.4 Direct Simulation 3D Visualisation (DS3V) Program	44
3.2 DSMC Validation	47
3.2.1 Validation against Experimental Data	47
3.2.1.1 Flow past a 70° Blunt Cone	47
3.2.2 DSMC Validation against Analytical Data	50
3.3 Validation Results.....	51
3.4 Summary.....	61
4. Modelling Satellite Coefficient of Drag Values	62
4.1 Impact of Freestream Temperature on Coefficient of Drag	63
4.1.1 Simulation conditions.....	63
4.1.2 Results and Discussions.....	65
4.2 Impact of LEO Atmospheric Density on Coefficient of Drag.....	66
4.2.1 Simulation Conditions.....	67
4.2.2 Results and Discussions.....	68
4.3 Effect of Drag Increase Devices on Satellites in LEO.....	69
4.3.1 Initial Model Development	70
4.3.2 Drag plate development.....	71
4.3.3 Physics modelling	72
4.3.4 Computational Results	73
4.4 Modelling Orbital Decay	80
4.5 Drag Plate Simulations on GRACE Satellite	83
4.5.1 GRACE Model	84
4.5.2 Physics Modelling for GRACE Satellite	87
4.5.3 Results and Discussions.....	88
4.6 Summary.....	94
5. Conclusions	95
5.1 Future Work.....	97
REFERENCES	99

APPENDIX A	103
APPENDIX B	105

List of Tables

Table	Page
Table 1: Vacuum types against no. density and mean free path.....	20
Table 2: Freestream parameters for 70° blunt nose simulations	48
Table 3: Important free stream values for DSMC simulations for Analytical vs DSMC Validation	51
Table 4: Coefficient of drag, experimental vs DSMC data	52
Table 5: Coefficient of Lift, experimental vs DSMC data	53
Table 6: Values used for Drag plate simulations.....	73
Table 7: Values used in the GRACE DSMC Simulations.....	88
Table 8: Drag and C_D of GRACE satellite with and without drag plate.....	93
Table 9: 1976 US Standard Atmosphere (Important values)	105
Table 10: Important values of gasses for VHS molecular model	106

List of Figures

Figure	Page
Figure 1: Height of the ISS above mean sea level over time. Height decreases due to skin friction drag, sudden increases are boosts initiated to increase orbit [47]	13
Figure 2 Chart of the gas composition of LEO atmosphere from 100km to 500km.....	19
Figure 3 shows the rough estimation for validation of flows in terms of Knudsen Number	22
Figure 4: Solar flux index of the sun taken from 1945 to 2013 [9]	23
Figure 5: Comparison of Diffuse reflection (shown on the left) compared to Quasi-Specular reflection	31
Figure 6: Flow Chart for DSMC Program; most DSMC codes follow this process [7]	37
Figure 7: Planer Representation of a collision in the laboratory frame of reference [6]	41
Figure 8: Binary collision in the centre of mass frame reference [6].....	41
Figure 9: Interaction of the reduced mass particle with a fixed scattering centre [6]	42
Figure 10: 3D mesh of geometry used in the DS3V program	49
Figure 11: Geometry of model used for experimental wind tunnel experiments.....	49
Figure 12: Typical Cell adaptation for the DS3V program	49
Figure 13: Analytical data from closed-form equations	52
Figure 14: Plot showing Cd plotted against the angle of attack of the Blunt Cone	53
Figure 15: Plot showing Cl plotted against the angle of attack for the Blunt Cone.....	54
Figure 16: Density contours of blunt cone 0 - 15 degrees.....	55
Figure 17: Density contours of blunt cone 20 - 30 degrees.....	56
Figure 18: Temperature contours of blunt cone 0 - 15 degrees.....	57
Figure 19: Temperature contours of blunt cone 20 - 30 degrees.....	58

Figure 20: Pressure distributions on blunt cone 0 - 15 degrees	59
Figure 21: Pressure distributions of blunt cone 20 - 30 degrees.....	60
Figure 22: Dimensionless density and Temperature contours from simulations carried out by Moss et al [39].....	60
Figure 24: Typical Temperature flow patterns of geometry in LEO.....	64
Figure 23: Molecular density formation on the surface of a satellite in LEO	64
Figure 25: Coefficient of Drag calculated on different geometries at a wide range of freestream temperatures.....	66
Figure 26: Coefficient of drag on Geometries in LEO against Atmospheric number density; Computational and Analytical	68
Figure 27: Dimensions (in mm) for the 'generic' satellite for initial testing	70
Figure 28: Isometric view of the initial generic satellite.....	70
Figure 29: Example of 3D CAD Models for the satellite Drag Plate Experiments	72
Figure 30: Simulation result for Drag plate size against coefficient of drag.....	74
Figure 31: Density flow of the satellites of drag plates from 0 - 2.5m ²	75
Figure 32: Density flow of the satellites of drag plates from 3 - 5m ²	76
Figure 33: Pressure distribution of satellite drag plates 0 - 2.5m ²	77
Figure 34: Pressure distribution of satellite drag plates 3 - 5m ²	78
Figure 35: Orbital Decay paths of satellites with drag plates	80
Figure 36: Orbital decay paths of no drag plate and the large drag plate from 50 – 300 sfu	81
Figure 37: Inside view of the GRACE Satellite.....	84
Figure 38: Front on view of Grace Satellite with Dimensions.....	85
Figure 39: Side on view of GRACE Satellite with Dimensions	86
Figure 40: 3D CAD model of GRACE Satellite without drag plate.....	86
Figure 41: 3D CAD model of GRACE Satellite with large Drag Plate	87

Figure 42: Comparison of the GRACE Satellite with and without an attached drag plate	89
Figure 43: Density of flow around GRACE Satellite looking in Y and Z direction.....	90
Figure 44: Temperature contours for GRACE satellite without drag plate in Y and Z direction	90
Figure 45: Pressure distribution for GRACE satellite without drag plate	91
Figure 46: Density contours of GRACE satellite with drag plate.....	91
Figure 47: Temperature contours of GRACE satellite with drag plate.....	92
Figure 48: Pressure distribution on GRACE satellite with drag plate attached	92

Nomenclature

a	Semi major Axis
a_{drag}	Acceleration
A	Cross Sectional Area
A_e	Effective Area
C_D	Coefficient of Drag
d	Molecular Diameter
$DS2V$	Direct Simulation 2D Visualisation
$DS3V$	Direct Simulation 3D Visualisation
$DSMC$	Direct Simulation Monte Carlo
E_i	Kinetic Energy (Incident)
E_r	Kinetic Energy (Reemitted)
E_w	Kinetic Energy (Carry Away)
erf	Gauss Error Function
G	Gravitational Constant
GHS	General Hard Sphere
HS	Hard Sphere
ISS	International Space Station
k_B	Boltzmann Constant
Kn	Knudsen Number
L	Characteristic Length
LEO	Low Earth Orbit
m	Mass
m_g	Molecular Mass
M	Mach Number
M_e	Mass of the Earth

<i>MEO</i>	Medium Earth Orbit
<i>P</i>	Orbital Period
<i>r</i>	Effective Radius
<i>R_e</i>	Reynold's Number
<i>s</i>	Speed Ratio
<i>T</i>	Temperature
<i>T_{ki}</i>	Temperature (Incident)
<i>T_{kr}</i>	Temperature (reemitted)
<i>T_w</i>	Temperature (Carry away)
<i>T_∞</i>	Temperature (Freestream)
<i>v</i>	Velocity
<i>V_{rel}</i>	Relative Velocity
<i>V_{mp}</i>	Particle Incident Velocity
<i>VHS</i>	Variable Hard Sphere
<i>VSS</i>	Variable Soft Sphere
<i>α</i>	Accommodation Coefficient
<i>γ</i>	Specific Heat Ratio
<i>λ</i>	Mean Free Path
<i>ρ</i>	Density
<i>σ</i>	Collision Cross Section

1. Introduction

1.1 Background

It is often thought that in Low Earth Orbit (LEO) the air density is so low that it does not have an impact on any satellite or spacecraft moving through it. However, Particles in the upper atmosphere interact with the surface of the object, and these collisions cause a change in momentum of the object. When the number of collisions is magnified over $7E+15$ times (average number of particles at a given height in LEO [1]) the overall effect could potentially cause an object to slow down, this event is called 'Orbital Decay'. Understanding the mechanics behind orbital decay, and when a satellite will eventually decay from LEO is vitally important for the aerospace industry. It allows us to know when a satellite or space station needs to be boosted back up into a higher orbit, or to arrange a new satellite to replace the decaying one. One example of a space vehicle needing re-boosting into a higher orbit is the International Space Station (ISS), which needs a boost on average every month to maintain its orbit [2]. This is a prime example of how particles in the earth's upper atmosphere can influence the drag and orbital decay of space vehicle. Figure 1 shows a chart of the altitude of the ISS against time. Satellites are hugely important to civilisation, we wouldn't be the society we are without them, so understanding all aspects of the science and engineering behind them is vital, including a full appreciation and understanding of Drag in LEO.

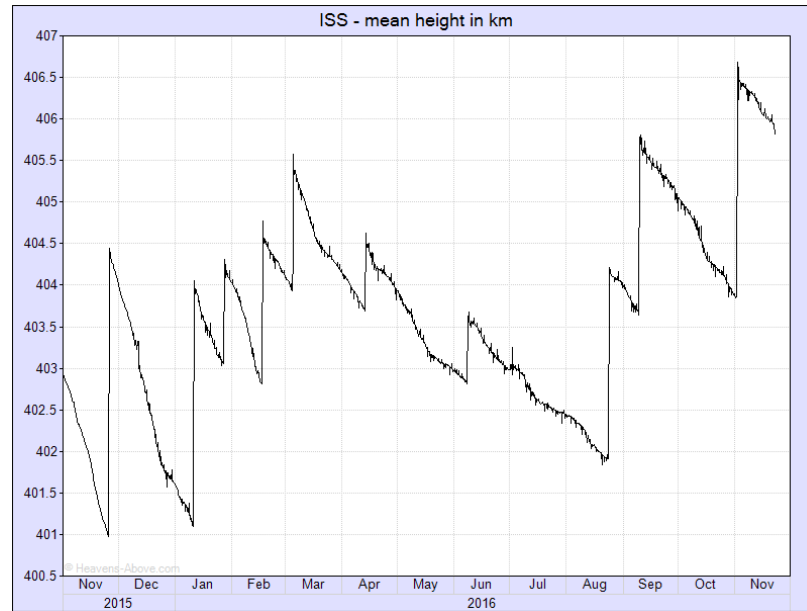


Figure 1: Height of the ISS above mean sea level over time. Height decreases due to skin friction drag, sudden increases are boosts initiated to increase orbit [49]

Much work has been put in over the last 50 years to understand the aerodynamics of a space capsule re-entering the earth's atmosphere, but not much work has been put into extending or decreasing the orbital life of these satellites. Extending the life could save companies the cost of replacing satellites for several years, while extendable high drag devices could bring a satellite down from its orbit at a faster rate and reduce satellites in graveyard orbits. Looking at the geometries of satellites and the aerodynamics at high altitudes could help us understand more about the coefficient of drag at these altitudes.

Aerodynamic packages are not used now on satellites in LEO, due to the limited space that rockets have on them, and how much it costs to send a satellite into orbit; roughly between \$50 million and \$400 million (depending on size and weight) [3]. Due to this limited space and the cost, satellites are designed without aerodynamic components as they take up a great amount of room inside the rocket. Aerodynamic fairings are designed to reduce the drag of the object without

adding too much mass to the rocket. With the current advancements in rocket technology, conventional rocket systems may be a thing of the past. Conventional Take-off and Landing (CTOL) orbital vehicles are at the height of research, and could potentially vastly reduce the cost of putting satellites into orbit, whilst allowing room for slightly larger volume satellites with the potential for modified geometries. The benefit of these CTOL spaceplanes is their ability to take off from any conventional runway. These vehicles (i.e. Reaction Engine Ltd. Skylon) could potentially accommodate these satellites in their cargo bays [4].

Satellites with limited life spans are starting to cause a problem for other satellites in low earth orbit, with hundreds of thousands of pieces of junk that could potentially destroy other satellites. It was reported at the end of 2011 that there were roughly 16000 catalogued objects in LEO, MEO, and Geostationary orbit. These objects include satellites, spacecraft (current and old), as well as fragmentation debris [5]. Getting rid of these satellites after they have finished their purpose has become more relevant in recent times. While long life satellites include thrusters which can easily deorbit satellites, this can be very expensive for the shorter life span satellites; the inclusion of drag increase devices that can be deployed at a satellite's end-of-life could prove advantageous for the future of low orbiting satellites.

Identifying the key aims and objectives of this thesis is highly important. Before beginning the project, an extensive literature study was carried out to see if there were similar papers in this field. This helped to scope the project and it provides a platform to verify any results that are obtained.

1.2 Aim and Objectives

The aim of this project is to gain a further understanding of the aerodynamic forces on bodies in Low Earth Orbit. Although the atmosphere is extremely rarefied at these altitudes, there are potentially enough particles to make a significant impact

on the drag figures, If this is the case, then further design considerations may have to be applied to satellites in the future by satellite manufacturers.

In order to achieve this aim the project will carry out simulations using the DSMC method, and in particular will use this method to simulate the flow in LEO rarefied conditions. The physics and molecular conditions will be input into the simulation program to make sure that all simulations are as close to realistic as possible. During the course of the project, data will be compared to existing data trends to see how they compare and can be validated. As well as numerical data collected from DSMC, analytical data will also be calculated and compared using well established equations which have already been verified. The simulations will also give the opportunity to look at how the particles flow over the satellite, so that the model can be refined and retested. The simulations will allow us to look at the velocity, temperature, pressure and density of the flow around the satellite.

The objective of this project also includes an analysis of drag plates attached to satellites to see whether they can de-orbit satellites at a faster rate from LEO. This will be done using DSMC; Drag values will be calculated and used to calculate the orbital decay of the satellite. All the collected data will be analysed to determine whether the drag plate proof of concept is worth further research.

1.3 Approach

Here is the outline of the main steps that will be taken:

- Research into previous papers that may be relevant to this field, which may be helpful to the research carried out in this project. This will include studying areas such as DSMC, satellites, Molecular dynamics and experimental data.
- Verify and validate DS3V and the DSMC method. Replicate the results from a simulation that has already been carried out. Examples of this are simulations carried out by G. A. Bird [6] [7] where there is detailed analysis

of 2D and 3D Simulations. This section will also give an opportunity to learn and understand the DS3V software

- Verify and validate the DSMC method compared to analytical data and experiment data collect. This will include simulating a simple object (such as a basic sphere), and comparing it to analytical data collected from equations. These results will then be compared to experimental data from satellites which contain specialist equipment like accelerometers. If the results compare well, then this will validate later results from the work carried out.
- Build a satellite model using CAD Software, from this, simulations can be refined more accurately to the real world; this will include implementing realistic physics progressively. This will include accurate molecular setup, as well as more representative build-up of earth's upper atmosphere.
- From data collected from the previous simulations, aerodynamic modifications will be made to the satellite model and retested by simulation. Different additions will be added to the satellite to see if they have an effect of the C_D calculations.
- Lastly a conclusion will be drawn from the simulation data. All the data will be presented and discussed along with future work. This conclusion will include whether the geometry of satellites has an effect on the C_D of the satellite.

A Project Gantt Chart has been included in the appendix of this report, which outlines the steps that will be taken, along with the time span of the project.

1.4 Report Structure

The organisation of the final thesis content will go as follows:

- Literature review – This section will consider the background research of molecular gas dynamics, including previous work undertaken in this or similar fields. The theory behind theoretical data and analytical data will be studied.
- Validation of DSMC Simulations – This section will compare computational data from DSMC to experimental data. An in-depth explanation to the numerical model will also be studied. Experimental data will be collect from technical reports.
- Simulations/ Data results from simulations – Main satellite simulations will be carried out and results will be compared against each other.
- Conclusions & Future work – Final results will be discussed and conclusions drawn against the original aims and objectives. Potential future work will be discussed.

1.5 Summary

In this section we have looked at a general outline of the project as well as a break down of all the components that will be studied throughout. This includes a basic background and reasoning behind the study, as well as various sections that will be covered.

2. Literature Review

2.1 Characterisation of LEO Atmosphere

Many of the satellites that orbit the earth, orbit in LEO, which is between 160km and 2000km above mean sea level, this is a very wide range where the regime changes vastly. The composition of the atmosphere from sea level to around 85km is fairly constant, with the composition being roughly 78% nitrogen, 21% oxygen and 1% other gases. Above this height different particles are detected; due to the ionising nature of solar radiation, unstable, ionised and lighter particles, such as hydrogen, helium and atomic (free radical) oxygen which tend not to be found naturally occurring near sea level. It can be seen from Figure 2 how the composition of different gasses changes as the altitude increases. It is noticed how the lighter particles like helium and hydrogen stay near constant. Hydrogen and Helium become the most prominent gasses at 1000km [1].

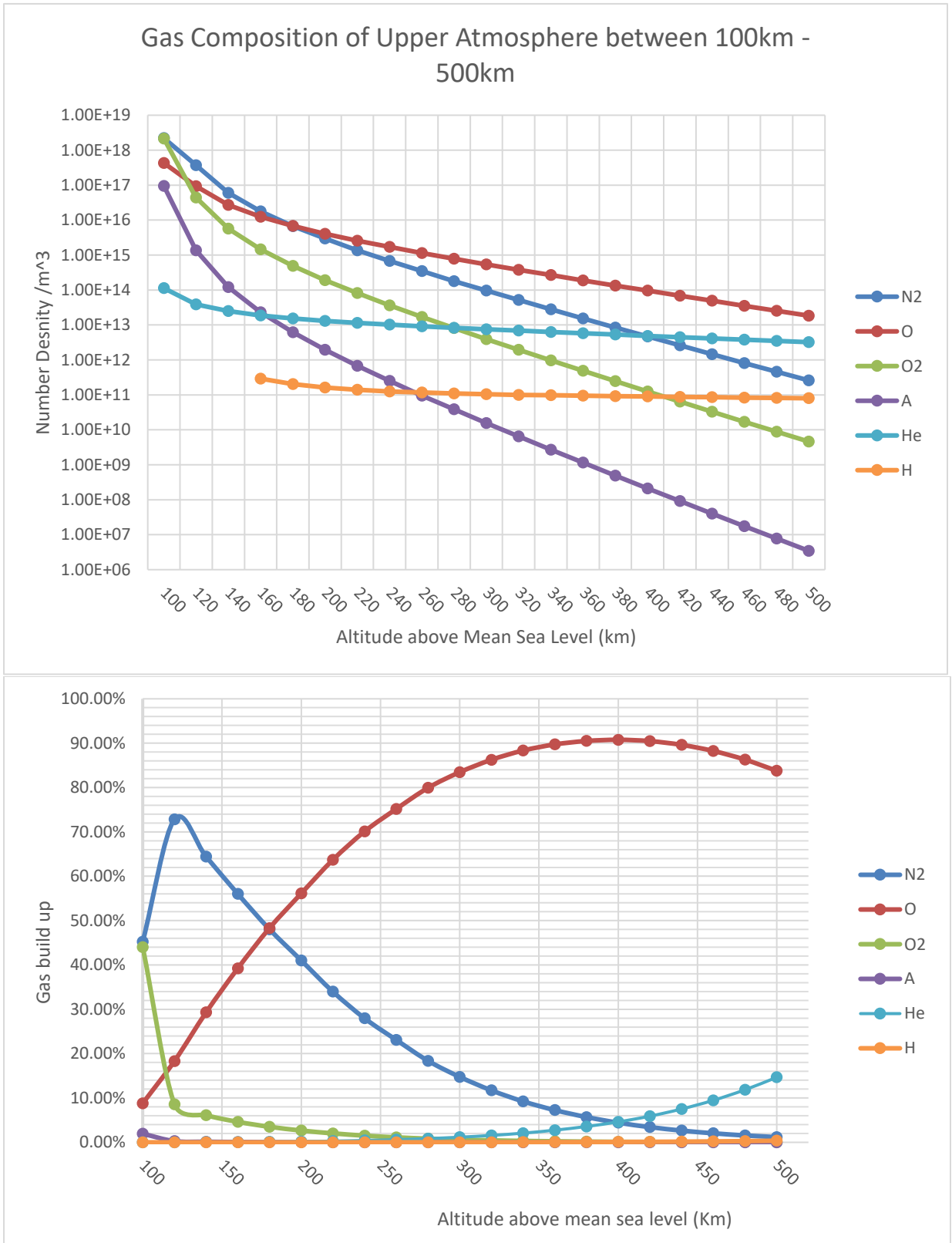


Figure 2 Chart of the gas composition of LEO atmosphere from 100km to 500km.

These values are not fixed values and can vary due to solar activity, as the sun's radiation can agitate the molecules in the upper atmosphere. Particle temperatures can vary between 200K and 2000K at a fixed altitude, and the density can vary by as much as 20% [8].

The density and pressure are key properties affected as the altitude increases. The mean free path between the particles increases as the density decreases. It is this mean free path between the particles that can help characterise the flow, and characterise what level of vacuum the regime is at. At ambient pressures, the mean free path between particles can be as low as 60nm, while in LEO the mean free path can be between 1cm and 1km. Below is a table of the vacuum range against the molecules and mean free path of the particles. The bottom end of LEO falls between medium and high vacuum. It is very difficult to achieve a true vacuum naturally, the only place that could achieve this level of vacuum would be the space between galaxies (Inter-galactic space), and any molecules in this space would have a near infinite mean free path.

Table 1: Vacuum types against no. density and mean free path

<i>Vacuum Range</i>	<i>Molecules (No. m⁻³)</i>	<i>Mean Free Path</i>	<i>Altitude</i>
<i>Ambient Pressure</i>	2.7×10^{25}	68nm	0m
<i>Low Vacuum</i>	$10^{25} - 10^{22}$	0.1 - 100µm	0m – 75km
<i>Medium Vacuum</i>	$10^{22} - 10^{19}$	0.1 – 100mm	75km – 98km
<i>High Vacuum</i>	$10^{19} - 10^{15}$	10cm – 1km	98km – 110km
<i>Ultra-High Vacuum</i>	$10^{15} - 10^{10}$	1 – 10^5 km	110km – 520km
<i>Extremely High Vacuum</i>	$<10^{10}$	$>10^5$ km	>520 km

As stated before, the mean free path between the particles can characterise the flow in a given case, this can help determine which mechanics can be used. At low m.f.p distances, continuum mechanics can be used to help solve flow problems, an example of continuum mechanics is Navier-Stokes Equations. In Continuum mechanics, the m.f.p between particles is assumed to be zero, this can help the computational time in CFD calculations, but limits the use to near earth altitudes. The Navier Stokes equations arise from Newton's second law of motion, where momentum is conserved, therefore the overall change in the system is zero.

The Knudsen number can be calculated in flow cases to see which mechanics would be valid for that particular case. The Knudsen (Kn) number is defined as:

$$Kn = \frac{\lambda}{L} \quad (2.1.1)$$

Where λ is the mean free path of the gas and L is the characteristic length of the object that is being tested. As the characteristic length cannot define a single Knudsen number for the entire flow, a local Knudsen number can be defined with L as scale length of macroscopic elements [6]:

$$L = \frac{\rho}{d\rho/dx} \quad (2.1.2)$$

From these equations, we can calculate which flow mechanics can be employed. If the $Kn < 0.001$, then continuum mechanics (such as Navier-Stokes/CFD) can be used. If $0.001 < Kn < 0.01$, then modified continuum methods can be used, (such as the Burnett Equations, shown in figure 3). For any Knudsen number above 0.01, then discrete particle methods will need to be used. These discrete particle methods do not neglect the mean free path. This can become more computationally intensive. It should be noted that the Knudsen number can also be related to the Reynolds Number (Re), the Mach Number (M) and the Specific Heat Ratio by the Equation:

$$(Re) = \frac{16}{5} \left(\frac{\gamma}{2\pi} \right)^{0.5} \frac{M}{(Kn)} \quad (2.1.3)$$

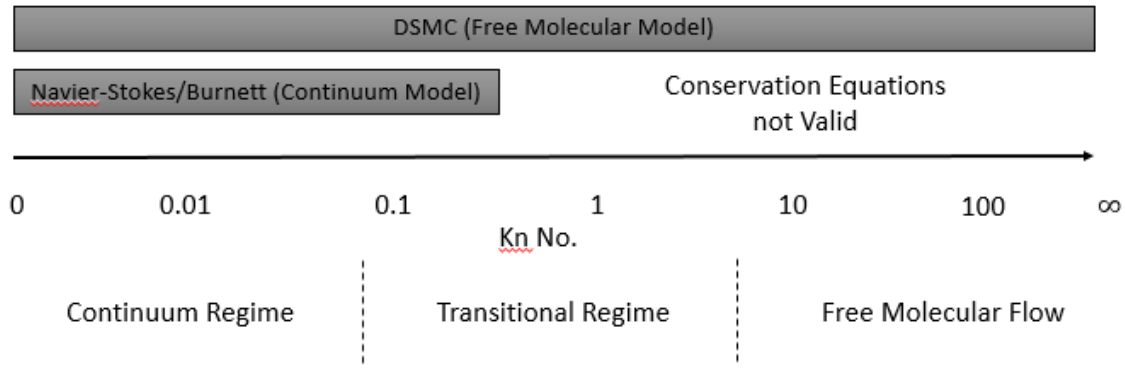


Figure 3 shows the rough estimation for validation of flows in terms of Knudsen Number

Here you can see in figure 3 that methods like CFD, which can solve for the Euler Equations, Navier-Stokes and Burnett equations would not be valid for high altitude or LEO altitudes. For this we would need to use the molecular model, which solves the Boltzmann Equation for finite Knudsen numbers.

2.1.1 F10.7 Solar Index

The 10.7cm solar radio flux (or F10.7 index for short) is a widely used measure for solar activity from our sun and is used to determine the position along a solar cycle and to measure sun spot activity. This measures the radio emissions from the sun at a wavelength of 10.7cm (2800Mhz ±50MHz) averaged over an hour, and is measured in *sfu* which stands for 'Solar Flux Unit' where 1 sfu = 10E-22 W m⁻²Hz⁻¹ [9]. The F10.7 index of the sun varies between 50sfu and 300sfu (which is the theoretical maximum and minimum) over roughly 10-year cycles. This measurement was first taken in 1947 in Canada and has been taken regularly since then. This has been made possible due to the ease of taking this measurement from the surface of the earth.

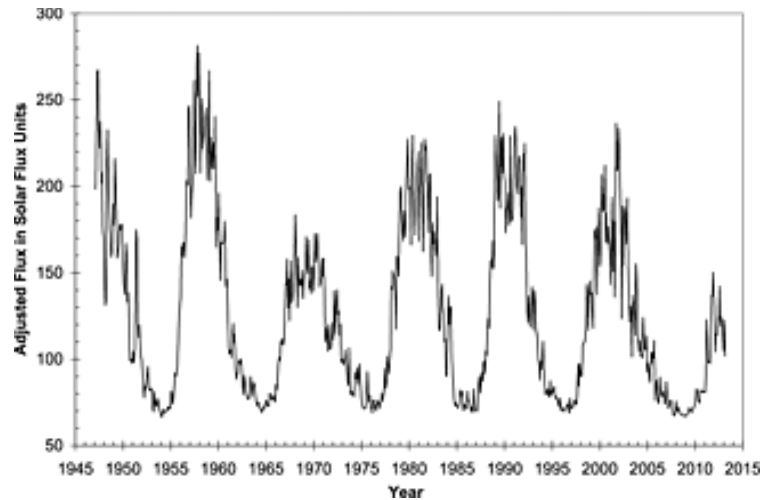


Figure 4: Solar flux index of the sun taken from 1945 to 2013 [9]

The F10.7 index is a helpful tool as it has an impact on a number of other factors, including radio communication, the climate and chemistry of the atmosphere as well as the orbital paths of satellites. It has been seen that F10.7 index readings have an effect upon local densities in the atmosphere at altitudes ranging roughly from 250km to 1000km [10]. It can also be seen that the Extreme Ultra Violet (EUV) emission from the sun that hit the earth's upper atmosphere have an effect on the molecular activity of the particles; making the particles more agitated increases the local temperature which could have an effect on the satellites drag.

2.2 Previous Work Undertaken

One of the pioneers of molecular gas dynamics was Martin Knudsen (who derived the equation for the 'Knudsen Number' in 2.1), Knudsen's work included in-depth research into kinetic theory of gases, which he outlines and concludes results in his 1934 book [11]. The findings from his work have led to the development of several concepts, including:

- Knudsen Flow – This is molecular flow that is characterised when the characteristic length of an object in a flow scenario is the same length as the mean free path
- Knudsen Gas – This is when the mean free path of the gas is equal to or larger than the container it is in. An example of this is a container at extremely high vacuum level
- Knudsen Layer – Layer of gas that sits above a solid or liquid, this layer only tends to be a few mean free path lengths thick
- Knudsen Diffusion – Diffusion that occurs when particles bounce around the sides of small tubes or ‘pores’. This theory is similar to Knudsen Flow.

Knudsen’s work on basic kinetic theory laid more foundations for the work that led onto molecular gas dynamics, and the basis of DSMC Methods.

The aim of gaining a deeper knowledge of drag coefficients on satellites has been around since the first satellites themselves, and there has always been huge doubt regarding their calculation. The earliest work has always used a value of 2.2 for the drag coefficient, but doubts about this came around in the 1960’s, example of this work was by Cook [12], where it was concluded that height could be considered independent from the drag coefficient calculation. One of the uncertainties that needs to be considered is the orientation of the satellite with reference to its velocity. As the satellite continues around its orbit it keeps a fixed axis, meaning that the reference area of the satellite is constantly changing throughout its orbit. Although this variable is easily predicted, other variables can come into effect, including the solar activity, which can cause huge variations in local densities. Information on these densities are documented in many journals, including the ‘Journal of Atmospheric Sciences’, more specifically, Albert D Anderson’s section on density fluctuation between 200km and 800km [8]. In this journal, experimental data is collected from 4 different satellites over their orbits, and a density model is built from the data, assuming that there is a direct proportion between the density and the 10.7cm solar radio flux measurements (a standard

measurement which is associated with solar activity). Data shows that there are huge variations between day and night, as well as solar activity itself, this has the potential to cause different levels of drag on an orbiting body. The data collected and modelled from this report can help in the process of producing accurate simulations for satellites in LEO.

This conclusion from Cook comes partly from the detailed computational and experimental analysis of the upper atmosphere in the US Standard Atmosphere [1] (1962 versions used by Cook, but the 1976 updated version will be used instead). This document gives a detailed study of the rarefied conditions at altitudes up to 1000km above sea level. This document contains important information for this project, including the temperature, molecular weight, density, gas composition and many other variables. The US Standard Atmosphere has been considered a reliable source for a very long time and it will be treated as such for this project.

Other notable works include the report from Lee Sentman, 1961 [13], which includes detailed introduction to free molecular flow problems; this paper was written from the point of view of someone who has little knowledge or experience in this field of study. Equations are derived and theories presented for calculating the forces and moments on a body that is subject to free molecular flow. These equations prove useful in predicting the C_D of a satellite in orbit without already having the drag force data, and have been used in many papers, including works involving the calculation of C_D on satellites such as GRACE [14] and looking at the gas-surface interactions of molecules to form values for the C_D . Sentman also derives free molecular flow equations for other forces that are experienced by bodies in LEO.

The Direct Simulation Monte Carlo Method was created by Prof. Graeme A. Bird [6] [7] of the University of Sydney, and it has become one of the most important techniques for solving rarefied gas flow simulations. Bird has written many books and journals in this field, and used this knowledge to develop DSMC Simulations. The books included detailed theory of molecular gas dynamics as well

as specific books which look at DSMC simulations themselves. There are many other applications of DSMC which Bird has shown, these include:

- Re-entry of space Vehicles, such as capsules – DSMC has been used extensively to look at the aerothermodynamics of re—entry vehicles. Important drag and pressure readings can be taken from the simulations and used in structural and material analysis. Re-entry is a very violent aerodynamic process, so accurate DSMC simulations can prove to be a valuable tool.
- Rocket Nozzle Expansion into a vacuum – can be used to simulate the exhaust plume of a rocket engine while in rarefied conditions. This data can be used to refine rocket nozzle designs and to test efficiency.
- Flow through slits/ orifice – an example of which is allowing a reservoir of gas to leak through a hole, leading into a vacuum or area with lower pressure. As the DSMC method simulates individual particles, it is possible to simulate microflows.

These are just a few examples of applications of the DSMC method. DSMC simulations can be used in the majority of high mean free path situations. A noticeable example of re-entry simulation using DSMC method was for the Apollo 14 capsule [15]. DSMC was used to simulate the hypersonic flow around the capsule in the transitional mean free path range (~100-200km above the earth's atmosphere). A full range of simulations were carried out which calculated the various aerodynamic coefficients such as C_D , C_L , C_N and C_A . A number of re-entry and geometric orientation variables were changed and simulated; this included:

- Re-entry from lunar and Mars return velocities (~ 7.7 – 15 kms⁻¹)
- Angle of incidence of the stream against the capsule, this varied from 0° to 180°
- Several different gas compositions. This is due to the composition changing over altitude, solar index, and other factors. This demonstrated how sensitive the aerodynamics forces are to changes in the rarefied gas.

Initial values for the simulations on the capsule are taken from theoretical and computation data from the various Apollo missions.

Many advancements have been made since the DSMC method was created by Bird, including our understanding of how the particles are re-emitted after they interact with the surface of a satellite. Work by M. Moe and K. Moe has looked into this [16] [17] [18]. Specially designed satellites have looked at the energy accommodation and angular dispersal of particles from the surface. It has been found that at certain altitudes in LEO, molecules are stuck, or 'absorbed' onto the surface of the satellite; this can cause the reflection type to change which effects the C_D . Data was collected for this from a variety of sensors attached to satellites, including accelerometers and mass spectrometers. From this data, more accurate calculations were produced from the use of Sentman's model for the C_D calculation [13] [17].

Sentman's C_D model has been widely used in rarefied gas dynamics, one notable example of this is the use of it is to calculate the drag coefficient on the GRACE Satellite [14]. Computed data from accelerometers inside the satellite are compared next to DSMC simulations. The computation data from the DSMC simulations come within 1% of the experimental data computed from the satellite. This is a great example of work similar to which will be done during this project. Work from Mehta *et al* also extended to running DSMC simulations on basic shapes, to calculate the C_D on them [19]. These shapes include a sphere, a flat plate and a number of different cylinders. Work by Mehta *et al* has shown the closest similarities to this project, most notably the work with DSMC simulations, the original 3D DSMC program (DS3V), and the work on using DSMC simulations to calculate drag coefficients on orbiting bodies and satellites. These papers provide useful insight into computational and closed-form calculations for drag coefficients.

Also of interest was the work done by Horsley [20] which investigated the potential use of drag plates attached to CubeSats to induce differential drag and allow the CubeSat's to move relative to each other. This idea extended from need

to have CubeSat's in formation with other CubeSat's while in LEO. Due to solar flux variations and general density fluctuations in earth's upper atmosphere, this can cause CubeSat's to move out of formation with each other. Further reading found that this was not a new concept, and there were many investigations before this into the use of differential drag, including the work from Leonard *et al* [21]. In both of these reports, equations are derived for the motion and forces. In the report by Horsley, it is shown that drag plates can give a small amount of control to the CubeSat's while in orbit. Experimental data was collected and equations were derived directly from free molecular data collected from the CHAMP satellite in the report by Sutton *et al* [22]; these equations were used by Horsley and included closed form expressions for the Drag and Lift Coefficients. This research from Sutton *et al* and Horsley has shown that the use of geometry, such as an angled flat plat, can alter the path of a satellite; this theory can also be applied to expanding the orbital lifespan of a satellite.

Significant research has been carried out in the transitional regime (seen in figure 3) on space re-entry vehicles. In part of this regime CFD and DSMC are both valid methods of simulation and have been compared next to each other to show whether both these methods are viable approaches for the same problem, this has been shown in detail by Votta *et al* [23]. This transitional regime roughly translates to altitudes of 75km to 125km; this is significantly lower than any satellite will ever orbit the earth, but this method could be considered for any satellite de-orbit or return to earth simulation. Experimental data used from a Plasma Wind Tunnel (PWT) was compared next to CFD with slip and DSMC and shown to have good correlation. This work is similar in context to the work carried out by Mungiguerra *et al* in which DSMC simulations were carried out on a deployable re-entry vehicle at a wide range of angle of attacks to determine the various aerodynamic coefficients during the re-entry process [24]. In this study, Bird's 3D DS3V DSMC software [25] has been used to carry out simulations and is seen as a widely used software in the rarefied dynamics community.

There are many examples of this area of study into the molecular transitional regime, including in recent years where DSMC simulations have been carried out on satellites to work out possible decay times for the orbit, but none have been focusing on using this tool for the design of the satellite to increase its orbital life.

There are three main ways used in engineering to calculate the solution to a given problem. They are Experimentally, Analytically and Numerically. For the purpose of this thesis, analytical and numerical data will be compared to previous experimental data. Traditional calculations from equations will form the basis of the analytical work, while the numerical data will be collected from DSMC simulations.

2.3 Analytical Methods

Calculating the drag coefficient on a body in orbit around the earth has always had a great amount of uncertainty. The theoretical drag on an orbital body is:

$$\vec{a}_{drag} = -\frac{1}{2} \rho \frac{C_D A}{m} v_r^2 \frac{\vec{v}_r}{|v_r|} \quad (2.3.1)$$

where A is the cross-sectional area of the body perpendicular to the velocity component, C_D is the coefficient of drag for that particular body, ρ is the local density (this value may fluctuate intensively, as discussed early), m is the mass of the body, and v is the velocity of the satellite relative to the atmosphere. The two biggest forms of uncertainty for this calculation are the density and the coefficient of drag. For the purpose of this project, the US Standard Atmosphere [1] will be used as the reliable source of data for all atmospheric conditions to allow for accurate result comparisons. C_D can be defined in a number of ways for use in calculations. One of those is a fixed C_D where a constant drag coefficient is used. In the case of satellites in LEO this value is usually given as 2.2 [12]. The other way C_D is defined is the physical drag coefficient [14], this is calculated from the momentum and energy transferred from free stream particles to the satellite surface in the upper atmosphere [26]. This value is considered to be a lot more accurate than a fixed value.



Figure 5: Comparison of Diffuse reflection (shown on the left) compared to Quasi-Specular reflection

Physical drag coefficient considers the way particles interact with the surface of the satellite, this is called the gas-surface interaction [17], and it looks at how the particle transfers its momentum and energy to the surface, and how the particle is reflected and re-emitted into the flow. At high altitudes, it is expected that the particles would be re-emitted in a specular fashion, due to low density and high mean free path between the atoms. However, this is not the case. Atomic Oxygen in LEO contaminates the surface of the satellite and effectively sticks to the surface and any other particles that come into contact with the surface, either absorb or get reflected in a chaotic manner [18]. This atomic Oxygen layer can be measured with testing equipment attached to satellites. Particles at higher altitudes (above 500km) will stand to behave more in a specular fashion again, this is due to there being less atomic oxygen, and more hydrogen and helium; these particles are not absorbed by the surface of the satellite. Figure 5 shows representations of diffuse reflection and partial specular reflection.

The Kinetic energy lost in the reflection by the particle can be calculated with the use of specialised equipment attached to satellites, and can measure the kinetic energy lost with diffuse or more specular particle reflection. This is called the Accommodation Coefficient, and is given by the equation:

$$\alpha = \frac{E_i + E_r}{E_i + E_w} \quad (2.3.2)$$

where E_i is the kinetic energy of the incident molecule, E_r is the kinetic energy of the reemitted molecule, and E_w is the average energy the molecules would carry away if they came into thermal equilibrium with the surface [Watt & Moreton 1964] [27].

The accommodation coefficient (or energy accommodation) can be written in the form of temperature and was originally derived by Knudsen in 1934 [11]. This can be written as:

$$\alpha = \frac{T_{k,i} - T_{k,r}}{T_{k,i} - T_w} \quad (2.3.3)$$

Where $T_{k,i}$ is the kinetic temperature of the incident molecule and is defined by:

$$T_{k,i} = \frac{m_g v_{rel}^2}{3k_B} \quad (2.3.4)$$

$T_{k,r}$ is the temperature of the reemitted molecule and is defined by:

$$T_{k,r} = T_{k,i}(1 - \alpha) + \alpha T_w \quad (2.3.5)$$

and T_w is the temperature of the surface (in this case the wall of the satellite). All of these equations are only valid if the gas is modelled to have Maxwell velocity distributions, and that the particles diffuse from the surface rather than reflect in a specular fashion. Expressions can be derived for the coefficient of drag on various shapes to form closed form expressions, this was done by Sentman in 1961 [13]. They have been put in the form as seen on the paper from Mehta et al [14]. All the equations for C_D are only valid if the Knudsen number is above 1 (this includes LEO altitudes and above); given below are the C_D equations for a sphere and a flat plate:

$$C_{D,sp} = \frac{4s^4 + 4s^2 - 1}{2s^4} \text{erf}(s) + \frac{2s^2 + 1}{\sqrt{\pi}s^3} e^{-s^2} + \frac{2\sqrt{\pi}}{3s} \sqrt{\frac{T_{k,r}}{T_\infty}} \quad (2.3.6)$$

$$C_{D,fl} = \left(1 + \frac{1}{s^2}\right) \text{erf}(s) + \frac{2}{\sqrt{\pi}s} e^{-s^2} + \frac{\sqrt{\pi}}{s} \sqrt{\frac{T_{k,r}}{T_\infty}} \quad (2.3.7)$$

Where s is the speed ratio and is defined by:

$$s = \frac{v_{rel}}{v_{mp}} \quad (2.3.8)$$

and is the ratio of the satellite speed relative to the atmosphere (v_{rel}) to the speed of the incident molecule that contacts the surface of the satellite (v_{mp}), and this value for the incident molecule speed is given by:

$$v_{mp} = \sqrt{\frac{2k_B T_\infty}{m_g}} \quad (2.3.9)$$

The error function ($\text{erf}(x)$) is given as the standard Gauss Error function for diffusion used in probability and statistics problems, this is given as:

$$\text{erf}(x) = \frac{2}{\sqrt{\pi}} \int_0^x e^{-t^2} dt \quad (2.3.10)$$

2.3.1 Orbital Decay

The orbital decay of the satellite is the amount of orbit (distance or period) a satellite will lose on each orbit it completes around a body due to the drag experienced by the satellite. Correct calculation of orbital decay can help manufacturers and space agencies predict times to re-enter into earth's atmosphere.

A derivative of equation 2.3.1 for theoretical drag force, along with Newton's second law and equation relating to circular motion, can be used to derive an equation that relates the orbital period of a satellite with its semi major axis. This is given by:

$$P^2 GM_e = 4\pi^2 a^3 \quad (2.3.11)$$

Where P is the orbital period of the satellite, G is the gravitational constant ($6.67408 \times 10^{-11} \text{ m}^3 \text{ kg}^{-1} \text{ s}^{-2}$), M_e is the mass of the earth ($5.972 \times 10^{24} \text{ kg}$), and a is the semi major axis of the orbit. The reduction in the time period of the orbit due to the atmospheric drag in LEO is then given by:

$$\frac{dP}{dt} = -3\pi a \rho \left(\frac{A_e}{m} \right) \quad (2.3.12)$$

Where A_e is the effective area of the satellite and is given by the C_D and the area of the satellite ($A_e = A C_D$) and m is the atmospheric molar mass. These two equations can be used in conjunction to form iterative solutions to the orbital decay problem [28] [29].

2.4 Summary

This chapter has looked at an extensive literature review in which the various methods used in this projects (and theory behind them) were researched and discussed, as it is important to fully understand the material before carrying out any research. Analytical methods and equations for calculating drag and orbital decay were discussed as well as molecular and interaction theory.

3. DSMC Modelling

Ensuring accurate representation between the real world and computational data is vital to engineering. It is important to be able to rely on computational data from simulations as experimental data can be expensive to obtain due to the nature and difficulty of obtaining low density flow, so computational data can reduce the costs of a project. Validation simulations will be carried out, which will compare the physical models to real world data.

This process differs from the verification of a code, which involves seeing if the code accurately represents the original developer's model. As this project uses the original developer's code, no verification will be carried out.

One more experiment that will be carried out during this project will compare the analytical/ closed form equations to computational data, and will show how close the two methods correlate to each other.

3.1 Direct Simulation Monte Carlo Method (Numerical Method) 2.4

The direct simulation Monte Carlo method is the numerical method that will be used during this project to simulate the rarefied gas flow in the LEO regime. This method uses Monte Carlo mathematical model of random probabilistic sampling to achieve a solution. Several real, individual molecules are given a location and movements, collisions and molecular interactions are recorded over a change of time, then the process repeats [6]. Billions of interactions can be simulated over the course of a simulation, although only a fraction of the real molecules are simulated. Basic DSMC simulations with grid sizes tending to infinity have been shown to have a solution to the Boltzmann equation, this can only be said for the original DSMC codes [30]. Modern codes have changed their procedures to become more complicated and haven't been verified and validated to the extent of the original Bird Code.

Many variables can be changed to make DSMC simulations as accurate as possible, including changes to the exact composition and fraction of gasses in a flow, the rotational spin of the molecules, chemical reactions between molecules (dissociation and recombination), as well as other settings that will be discussed later in this chapter.

3.1.1 DSMC Program Structure

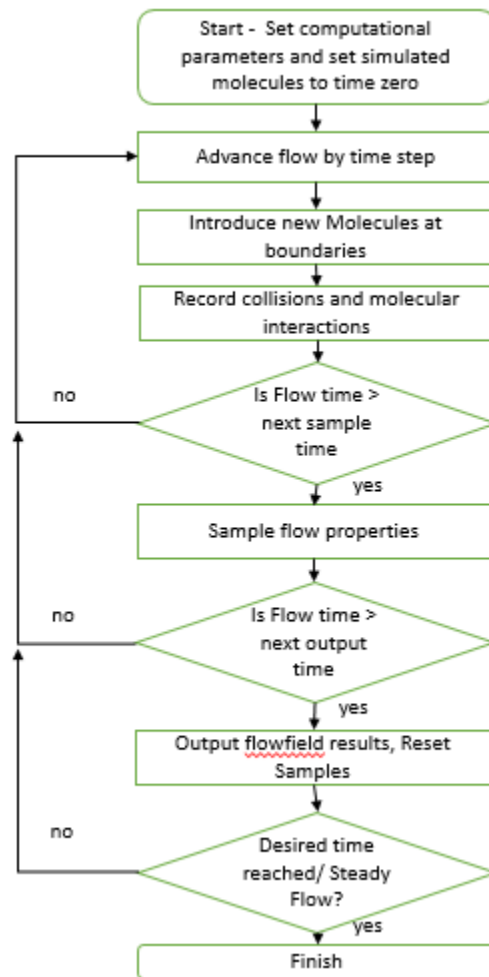


Figure 6: Flow Chart for DSMC Program; most DSMC codes follow this process [7]

The Structure for DSMC computations have kept the same basic algorithm since the first original code. Older codes used to employ a fixed time step where molecular moves and collisions are moved compared to a mean collision time, however this was shown to be inefficient and to yield inaccurate results in

comparison to later versions. Today a variable time step is employed for this. The time step in earlier programs was also set by the user, but now it is set automatically by the code. It is set by the program to a value that is appropriate to the stream and model conditions, then is edited and updated accordingly to the output file and resampled.

The velocity of the incoming particles is determined by the free stream velocity and the thermal velocity of the particles; these particles are moved over the time step generated, from this the particle distance and energy is determined for that sample, and their new positions is determined before commencing the new sample. Particles are generated from the input/ free stream boundaries of the simulation, whether that is from boundary planes, or boundary triangles (in 3D flows). These particles are taken out of the flow when they hit any vacuum interference boundaries or any outlet boundaries/ triangles. After all particles have been indexed by the algorithm when the sample ends, flowfield properties and any molecular interactions are calculated [7] [6]. Molecular reflections are also calculated depending on whether diffuse or specular models are chosen; figure 5 shows the process of the DSMC Program used.

3.1.2 Momentum and Molecule Collisions

The majority of intermolecular collisions will involve only two molecules. This is due to the probability of more than two molecules coming into contact being very low. In elastic collisions, there is no loss or change in momentum or energy in the system. This is stated by Newton's laws of motion, where energy and momentum cannot be created or destroyed. Therefore, to work out the speed of a particle after an interaction, we can use the standard linear equation for momentum:

$$m_1c_1 + m_2c_2 = m_1c_1^* + m_2c_2^* = (m_1 + m_2)c_m \quad (3.1.1)$$

and

$$m_1 c_1^2 + m_2 c_2^2 = m_1 c_1^{*2} + m_2 c_2^{*2} \quad (3.1.2)$$

m is represented by the mass of the molecules involved in the collision, c is the speed of the molecule pre-collision, c^* is the speed of the molecule post-collision, and c_m is the velocity of the centre of mass of the set of molecules. From this, the relative velocity of the particles can be defined:

$$c_r = c_1 - c_2 \quad (3.1.3)$$

and

$$c_r^* = c_1^* - c_2^* \quad (3.1.4)$$

Equations 3.1.1 can be combined with 3.1.3, and 3.1.2 combined with 3.1.4 to make it in terms of relative velocity:

$$c_1 = c_m + \frac{m_2}{m_1 + m_2} c_r \quad (3.1.5)$$

and

$$c_2 = c_m - \frac{m_1}{m_1 + m_2} c_r \quad (3.1.6)$$

From these equations, we can see that the particles are moving away from each other. The post-collision equations can also be given and are similar:

$$c_1^* = c_m + \frac{m_2}{m_1 + m_2} c_r^* \quad (3.1.7)$$

and

$$c_2^* = c_m - \frac{m_1}{m_1 + m_2} c_r^* \quad (3.1.8)$$

From the energy conservation equation given earlier (3.1.1 and 3.1.2), and the equations 3.1.7 and 3.1.8, they can be written in the form:

$$m_1 c_1^2 + m_2 c_2^2 = (m_1 + m_2) c_m^2 + m_r c_r^2 \quad (3.1.9)$$

and

$$m_1 c_1^{*2} + m_2 c_2^{*2} = (m_1 + m_2) c_m^2 + m_r c_r^{*2} \quad (3.1.10)$$

where

$$m_r = \frac{m_1 m_2}{m_1 + m_2} \quad (3.1.11)$$

This is known as the reduced mass. The magnitude of the relative velocities from the equations does not change, therefore:

$$c_r = c_r^* \quad (3.1.12)$$

If F is given as the force between two symmetric points of force in molecules, and r_1 and r_2 are their position vectors in the collision, then the equations of motion for the molecules are given as:

$$m_1 \ddot{r}_1 = F \quad (3.1.13)$$

and

$$m_2 \ddot{r}_2 = -F \quad (3.1.14)$$

Hence, the equations can be combined to give:

$$m_1 m_2 (\ddot{r}_1 - \ddot{r}_2) = (m_1 + m_2) F \quad (3.1.15)$$

If the relative velocity is considered to be $c_r = r_1 - r_2$, then:

$$m_r = \ddot{r} = F \quad (3.1.16)$$

All the equations from section 3 are concluded and summarised with the following figures 7 to 9. Transformation from lab to the centre of mass coordinate system transforms three dimensional trajectories into two dimension trajectories that are symmetrical around the line AA'.

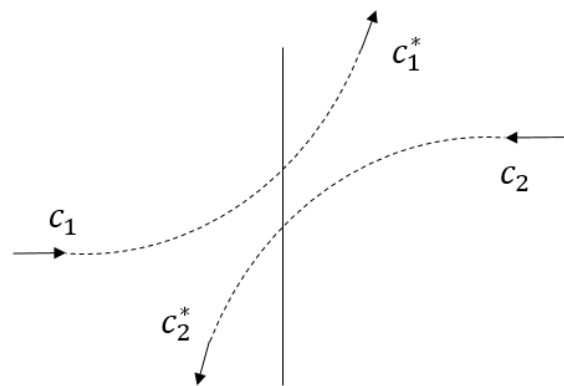


Figure 7: Planer Representation of a collision in the laboratory frame of reference [6]

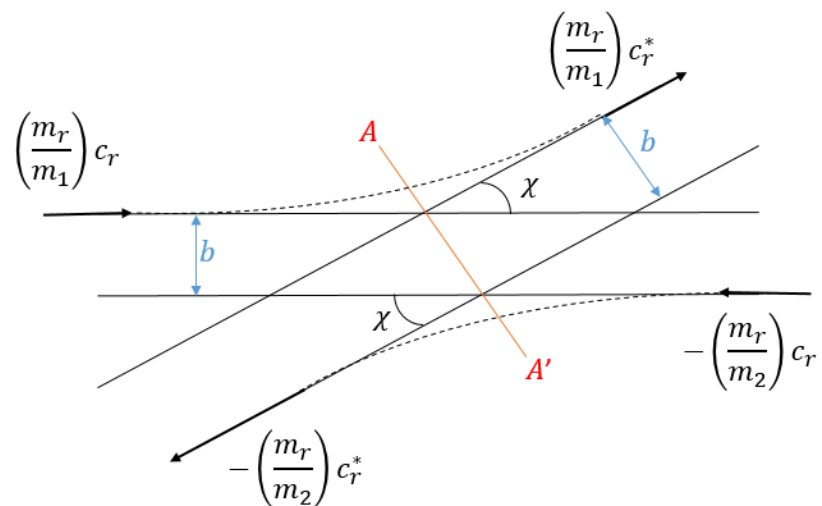


Figure 8: Binary collision in the centre of mass frame reference [6]

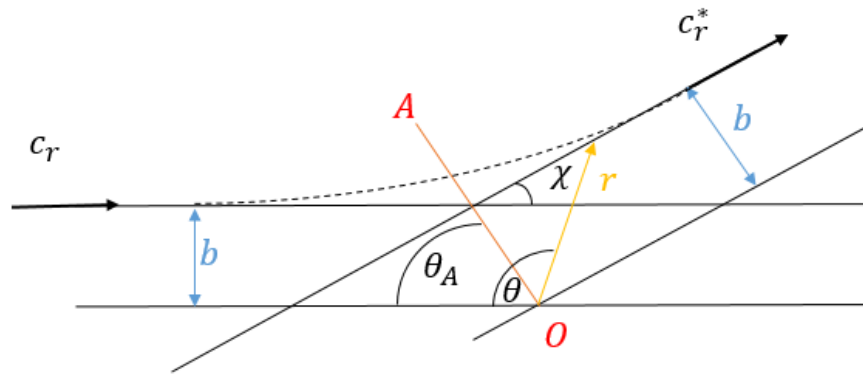


Figure 9: Interaction of the reduced mass particle with a fixed scattering centre [6]

3.1.3 Molecular Model for DSMC

Different molecular models are available to be employed for DSMC simulations. These different models have different properties for the forces between molecules (the intermolecular forces). One of the most common and successful is the Variable Hard Sphere (VHS) Model which was first proposed by G. A. Bird [31]. This model is one of the most popular molecular models used in DSMC simulations. This model is based on the Hard Sphere (HS) model. HS and VHS models are considered to be simple models and are not computationally difficult to run, even though they have shown accurate representations of real viscous gases. The VHS Model treats the particles as 'hard spheres' with a variety of different reflections possible (angles and velocities) from resulting collisions. The collision cross section for the VHS Model can be given as:

$$\sigma \equiv \pi d^2 \propto \left(\frac{1}{2} m_r c_r^2 \right)^{-\omega} \quad (3.1.17)$$

Where ω is given as:

$$\omega = \frac{2}{\eta - 1} \quad (3.1.18)$$

and where the cross section σ is considered to vary with temperature and relative speed between particles, given proportionally as:

$$\sigma \propto c_r^{-4(\eta-1)} \propto T^{-\frac{2}{\eta-1}} \quad (3.1.19)$$

Equations can be derived for the hard sphere model from Figure 8 (the collision diagram), such as the effective radius given as:

$$r = \frac{1}{2}(d_1 + d_2) = d_{12} \quad (3.1.20)$$

where d is the molecular diameter of the given molecules, and d_{12} is the combined diameter of the molecule during the collision. Therefore it can be deduced from Figure 8 that:

$$b = d_{12} \sin \theta_a = d_{12} \cos \left(\frac{1}{2} \right) \chi \quad (3.1.21)$$

One of the disadvantages of the hard sphere model is that the scattering of the particles is not considered to be realistic [6] [32]. The consequence of this lead to Bird developing the Variable Hard Sphere (VHS) Model. In this model the diameter of the molecule d is a function of the molecular speed c_r , which is given by an inverse power law:

$$d = d_{ref} \left(\frac{c_{r,ref}}{c_r} \right)^u \quad (3.1.22)$$

where u is the relative speed exponent of the VHS model, and any values with subscript *ref* are reference values. With the combination of a finite cross sectional area and accurate temperature exponent of coefficient and viscosity for this particle model, it has been shown by Bird that the VHS model provides realistic correlation to real world mean free path and Knudsen number values [33]. From this, the deflection angle of the of the particles can be defined as:

$$\chi = 2 \cos^{-1} \left(\frac{b}{d} \right) \quad (3.1.23)$$

Other molecular models can be used in place of the VHS Model, such as the Variable Soft Sphere (VSS) model. This model was introduced by Koura and Matsumoto [34]. This model is considered to be analytically and computationally similar to the VHS model when used inside Monte Carlo simulations. Although the VHS model has been shown to be effective for many applications, it has not shown good correlation to diffusion coefficients and the Inverse Power Law model. This means that the VHS model is not accurate for simulations where the diffusion in gas mixtures plays an important role. Numerical values for various gasses can be found for the VHS model in Table 10 (Appendix B) of this report; these values can be entered into DSMC software so as to gain an accurate representation of the gas composition; this was taken from Bird [6].

Other important molecular models that have been derived include the Generalised Hard Sphere (GHS) model which was introduced by Hassan and Hash [35]. This model is considered to be an extension of the VHS and the VSS models, but takes into account the attractive and repulsive forces between the particles. This model has been shown to be appropriate for simulations where diffusion plays a big part (similar to VSS), as well as low temperature flows which involve high levels of attractive particles [36] [37].

3.1.4 Direct Simulation 3D Visualisation (DS3V) Program

For the purpose of this project, the original 3D DSMC code by Bird will be used for all simulation work [6] [7] [25]. The program was selected for a number of reasons, including:

- Availability: This program is free to download from Bird's website (<http://www.gab.com.au>). This has meant the program has been used across industry [14] [15] [19]. Most codes are not commercially available to the public (i.e. SMILE, MONACO, DAC), or have to be bought (i.e. PI-DSMC).

- System Requirements
 - This is one of the only DSMC codes that can run on Microsoft Windows. Most codes are written to work on Linux based systems; this makes these codes easier to modify but harder to learn.
 - DS3V has been designed to be able to run on personal computers (usually with RAM \geq 500Mb and processor speeds \geq 2GHz). Most personal laptops have higher specs than this today.
- Ease of use: DS3V uses a set of menus which creates '.dat' files which contain all simulation information and can be read by the program 'DS3V.exe'. The data files can be edited manually through Notepad, or through the program. The program also features an easy to use graphical user interface (GUI) which helps new users to DSMC. For most other DSMC codes the user would need to learn how to program yourself and use external viewers like Paraview (a common CFD and DSMC viewer used on Linux based systems).

However, there are disadvantages associated with the DS3V codes as well. One of these includes 3D geometry creation/ importation. DS3V does not have an integrated geometry package (which is fairly common amongst DSMC packages), neither does it have the ability to accept basic 3D CAD files such as .stp or .stl files. The only file that is accepted by the program is a modified .dat file which is created by the sister application called 'DS3DG.exe'. This sister program can only accept Raw Triangle files (.raw), which is effectively a Notepad file with a series of x, y and z coordinates which form a 'triangle', and when all coordinates are put together they form a mesh (an example of .raw file will be in appendix A). The only commercially available 3D CAD package that can save in .raw format is Rhino3D (package available for student use at University of Hertfordshire). This process,

although simple, takes extra time when compared to other simulation software which can accept generic model files.

One of the other issues when it comes to DS3V, is that it is not designed to run batch simulations or to run simulations on multiple cores. The only way it is possible to run the simulations on multiple cores is to modify the source code of the program (this requires a high level of computer programming skill). The most this program can do is dual – parallel core runs, where computers with two cores can split a simulation into two, allowing each section of the simulation to be run by a different core. This allows simulations to be run quicker, but can also make other processes on your computer function a lot slower, so less powerful computer should only run 1 core.

The DS3V program comes with several features which help in the post processing and characterisation of individual simulations:

- Full 3D simulations, including Internal and External Flow (2D simulations can be run using different program called DS2V)
- Mesh and Cell generation can be carried out by the program
- Fully adjustable gas composition tool. User can input how many molecules are wanted in the simulation, the molecular weight and dimensions of each molecule, and its percentage build up in final gas mixture
- Domain and Boundary conditions. The domain is generated by the program via simple x, y and z dimensions. Different boundary conditions can be set, such as stream boundary, vacuum interface, symmetry plane etc.
- Gas- Surface interaction models can be selected. The two models presented in this program are the Diffuse model (full energy accommodation or ' $\alpha = 1$ ' in accordance to equation 2.3.2) or the CLL model, which is described as a 'clean surface' model [25].

- Molecular model selection. Allowing users to choose between VHS and VSS models
- Chemistry models can be selected along with any chemical reactions/ disassociation/ recombination of gasses.

Although there are many parameters that can be changed in the DS3V program, it is less customisable than most other DSMC programs, but is more suited to beginners in this field. This, combined with its use in industry is the reason DS3V has been selected for use in this Masters level study. If further studies were to be carried out, then potentially other programs would be considered, or even a new DSMC code could be written to specifically meet the needs of the simulations.

3.2 DSMC Validation

3.2.1 Validation against Experimental Data

Experimental data in rarefied gas flows has been an issue for many years, this is due to it being difficult to obtain. In response to this, NATO and the Advisory Group for Aerospace Research and Development (AGARD) set up a group to conduct experiments to help understand hypersonic and rarefied flow better [38]. Data from this report can be used as the experimental data to be compared against data collected from DSMC.

Two of the experiments from this report will be used to validate the DSMC code, this includes flow over a truncated plate and flow past a 70° blunt nose plate. The justification behind this choice of experiments is because they have been studied over again by many authors and researchers, this will help further validate the simulations in this report.

3.2.1.1 Flow past a 70° Blunt Cone

This case has been selected due to its complexities when it comes to wake flow and aerodynamic forces. This phenomenon has been studied intensively over the

past 20 years [39] [40] [41] [42], and has become a benchmark test for validation of DSMC simulations. Initial simulations will be carried out at a range of angles for the incoming flow; results from these simulations will be plotted against the results from the original experimental data, as well as data from other DSMC computations involving this model. Table 2 shows the free stream values used in the validation simulations for the blunt nose cone, and are given below:

Table 2: Freestream parameters for 70° blunt nose simulations

Parameter (Unit)	Values
Velocity (ms ⁻¹)	1502
Mach No.	20.19
Temp (K)	13.32
Density (kgm ⁻³)	1.73E-05
No. Density (m ⁻³)	3.72E+20
Pressure (Nm ⁻²)	6.83E-02
Reynolds No.	7.68E+02
Mean Free Path (m)	1.59E-03
Knudsen No.	0.03176

Free stream conditions were set to the same as the conditions in the experiment carried out by AGARD group 18 [38], this included the use of a non-reactive nitrogen flow. The simulation time step was set automatically by the DS3V program, this is in comparison to other DSMC packages where the time step is set by the user. The VHS molecular model was selected for these simulations due to the ease of computation, and it is a widely used and accepted model.

Figure 11 shows a 2D geometry of the model used by the AGARD group for the experiments, this model was replicated in 3D using Rhino3D CAD software for use in the DSMC program, shown in figure 10. Flowfield cells are generated automatically by DS3V code depending on memory usage selected, and can be

adapted once a steady state has been reached in a preliminary simulation. This cell adaptation is shown in figure 12.

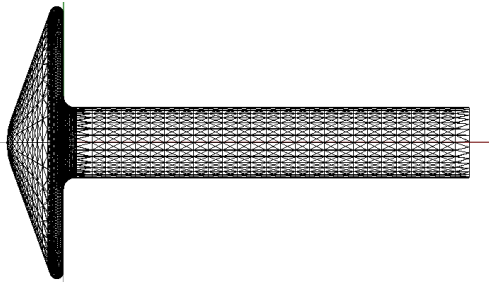


Figure 10: 3D mesh of geometry used in the DS3V program

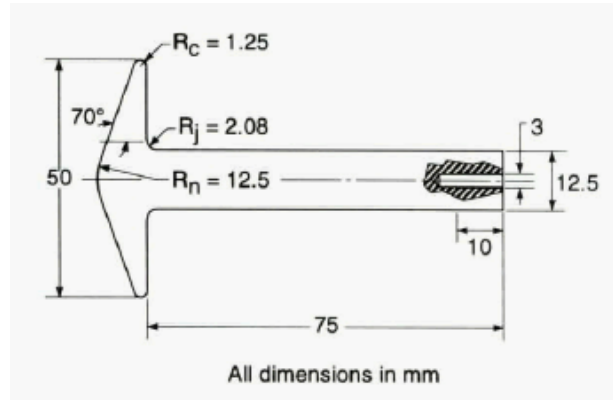


Figure 11: Geometry of model used for experimental wind tunnel experiments

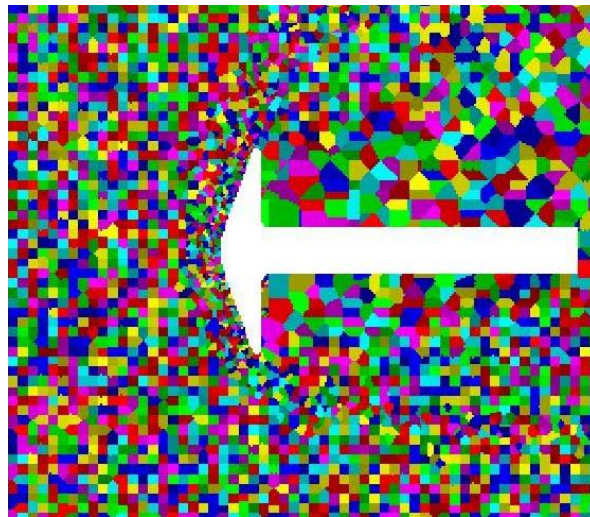


Figure 12: Typical Cell adaptation for the DS3V program

Once the cells have been adapted in the DS3V program, the simulation can be left to run for a desired time or until the program has reached a steady state. Typically, simulation will be left to run for 24 hours.

The coefficients of drag and lift were calculated for each angle of attack and they were plotted against each other in figure 14. Other properties like the flow contours were also compared to help of other validation research papers [43].

Potential errors which may have occurred during the course of these experiments and simulations include systematic errors. These errors may have arisen from unforeseen factors, or even errors in the testing equipment used. All DSMC results from this validation follow a similar trend, with most results being within the error margins of $\pm 3\%$ [42].

3.2.2 DSMC Validation against Analytical Data

Closed form equations have always formed a base to any experimental work that is carried out, and can be described as the ‘theoretical’ method for the calculation of drag on satellites. Results will be taken from reports that have considered analytical ways to calculate the C_D on different shapes in LEO, such as that from Moe *et al* [16] [17] [18]. Various shapes and satellites are used in this report, with the emphasis on looking at the gas-surface interactions and the accommodation coefficient of reflected particles (Equation 2.3.2). In one test they looked at various different shapes and calculated C_D at different altitudes when $\alpha = 1$; this indicates a total diffuse reflection of particles. In these papers, C_D was calculated analytically using Sentman’s model as shown in equation 2.3.6 and 2.3.7 [13]. Drag will be calculated numerically using DSMC and compared next to this data.

Table 3 shows the free stream condition used for each simulation. The gasses used in the simulations are nitrogen, oxygen, and atomic oxygen; Helium will be used in the 300km simulation as it is not negligible at this altitude. Other important data values were taken from the US Standard Atmosphere [1].

Table 3: Important free stream values for DSMC simulations for Analytical vs DSMC Validation

Altitude (km)	Velocity (m/s)	No. Density (/m³)	Temp (K)	N₂ comp	O comp	O₂ comp	He comp
150	7818.23	5.19E+16	634.39	0.603	0.344	0.053	N/A
200	7788.43	7.18E+15	854.56	0.407	0.563	0.03	N/A
250	7758.97	1.91E+15	941.33	0.255	0.732	0.013	N/A
300	7729.83	6.51E+14	976.01	0.147	0.836	0.006	0.011

3.3 Validation Results

The results for the validation against analytical data have shown a strong correlation between the analytical and computational results, this shows that there is a good relationship between the theoretical and DSMC data. Although a limited number of simulations have been completed and they show good results, an accurate conclusion cannot be drawn until a wide range of simulations has been carried out over different altitudes. Figure 13 shows the analytical data compared next to the small number of simulations already carried out.

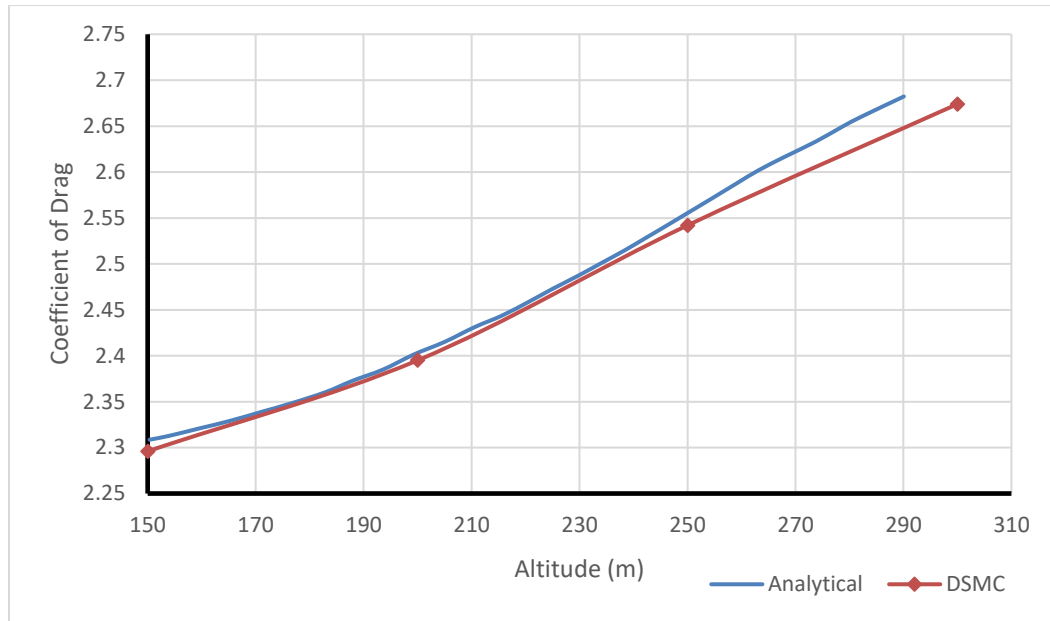


Figure 13: Analytical data from closed-form equations

Below are the results for the blunt nose cone simulations. Table 4 shows the experimental data against the data the values calculated for the coefficient of drag and the coefficient of lift for different angles of attack. The general uncertainty with aerodynamic coefficients is given as $\pm 3\%$ according to Allegre *et al* [42].

Table 4: Coefficient of drag, experimental vs DSMC data

Angle of Attack	Exp	DSMC	% diff
0°	1.657	1.668	0.66
5°	1.629	1.657	1.72
10°	1.615	1.63	0.93
15°	1.569	1.584	0.96
20°	1.538	1.526	0.59
30°	1.432	1.424	0.56

Table 5: Coefficient of Lift, experimental vs DSMC data

Angle	Exp	DSMC	% diff
0°	0	0	0
5°	-0.057	-0.061	6.56
10°	-0.133	-0.123	8.13
15°	-0.2	-0.182	9.89
20°	-0.249	-0.241	3.21
30°	-0.324	-0.346	6.79

Here it can be seen that there is a strong correlation between the experimental results and the results from the DSMC simulations, with most results being within $\pm 3\%$ as described before. Figures 14 and 15 show the results plotted next to each other. Models for the pressure distributions are shown across the surface of the models are shown in figures 20 and 21.

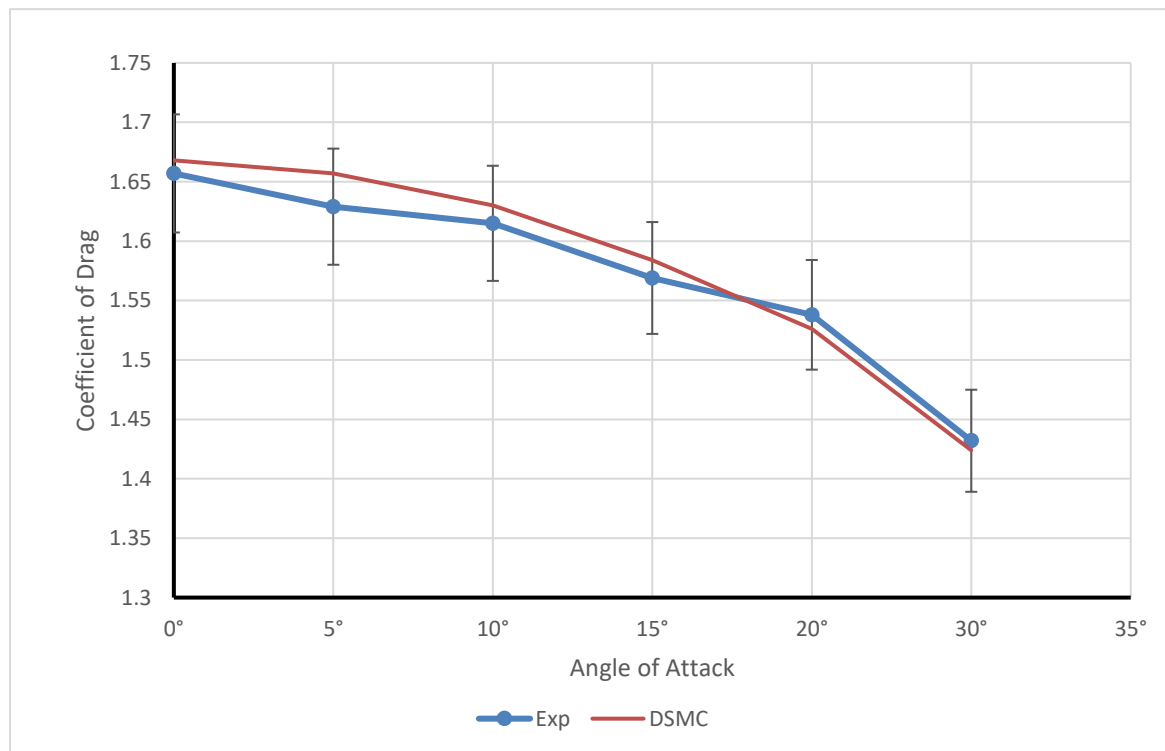


Figure 14: Plot showing Cd plotted against the angle of attack of the Blunt Cone

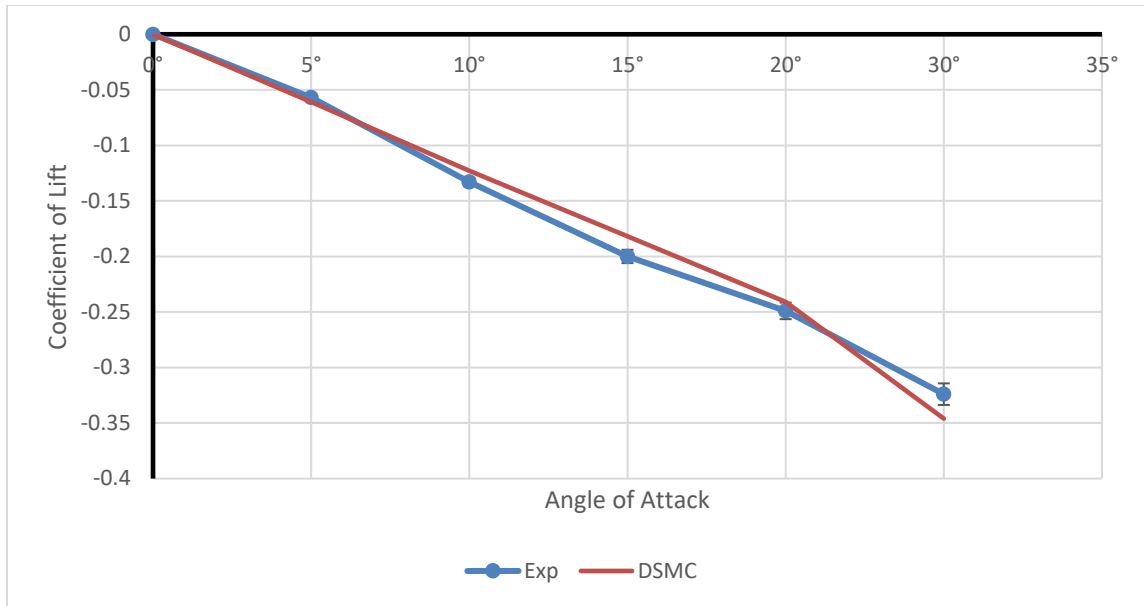


Figure 15: Plot showing Cl plotted against the angle of attack for the Blunt Cone

It can be seen from figure 14 and 15 that there is a strong correlation between the experimental data from the AGARD group and the simulation data collected for this thesis in DSMC. All of the results are within the $\pm 3\%$ aerodynamic variable error stated before. All the figures below show various flow and density patterns of the simulations carried out.

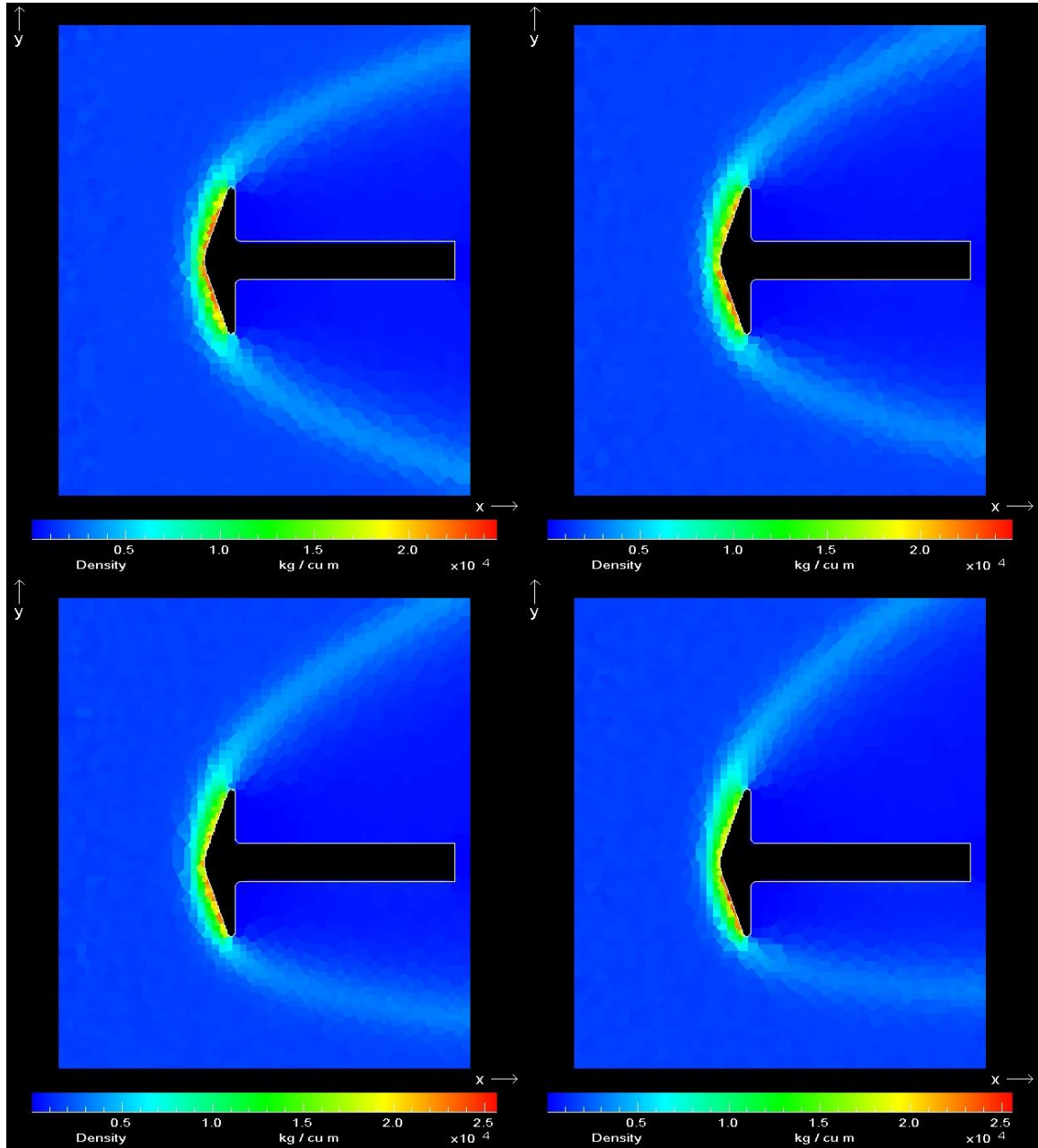


Figure 16: Density contours of blunt cone 0 - 15 degrees

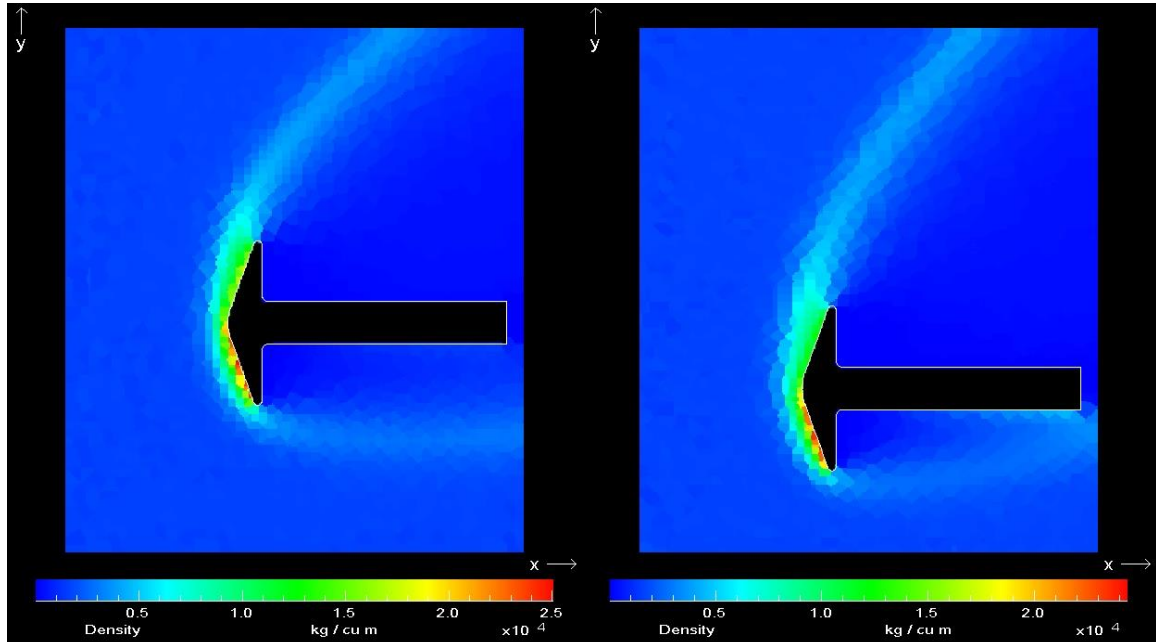


Figure 17: Density contours of blunt cone 20 - 30 degrees

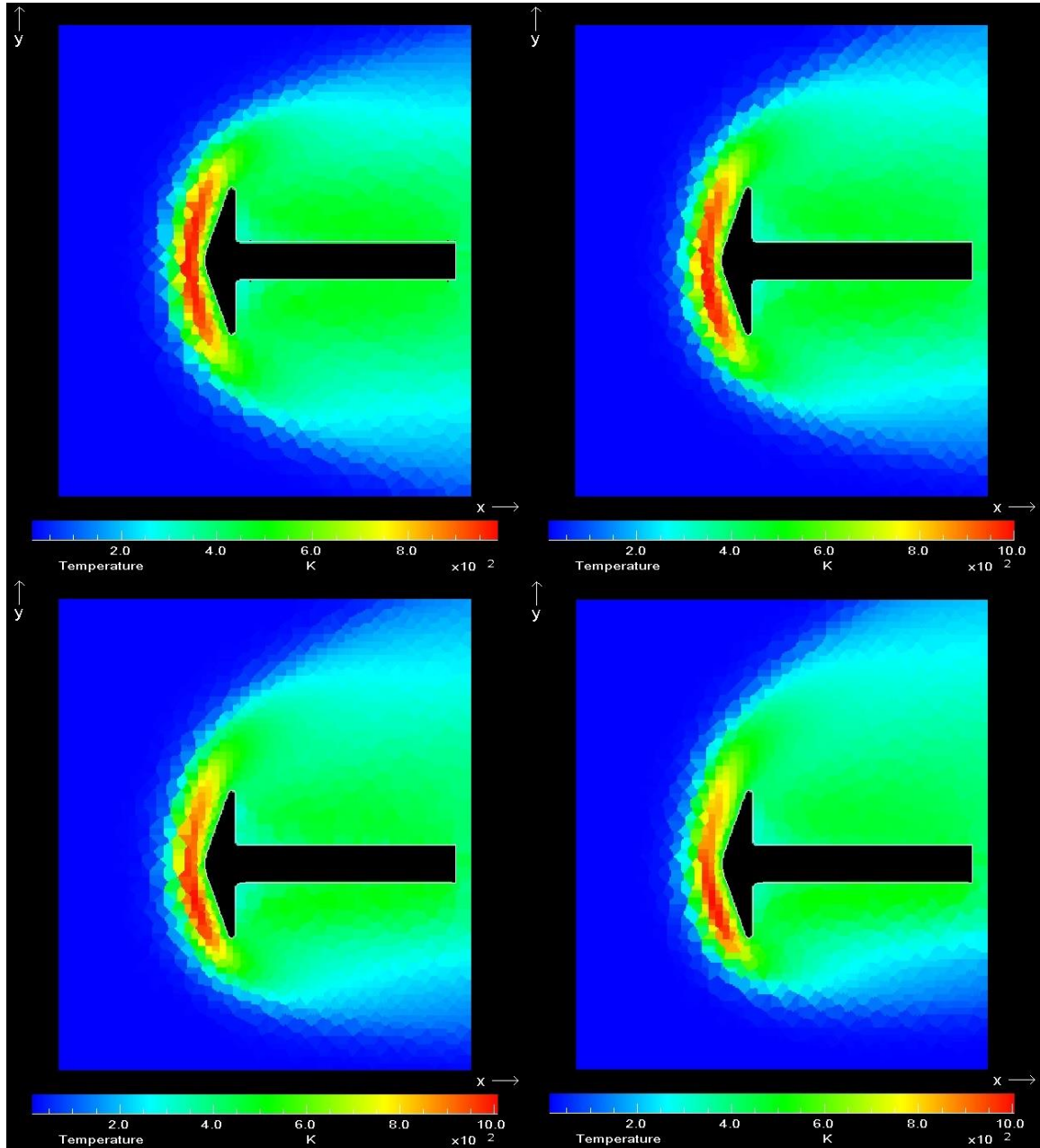


Figure 18: Temperature contours of blunt cone 0 - 15 degrees

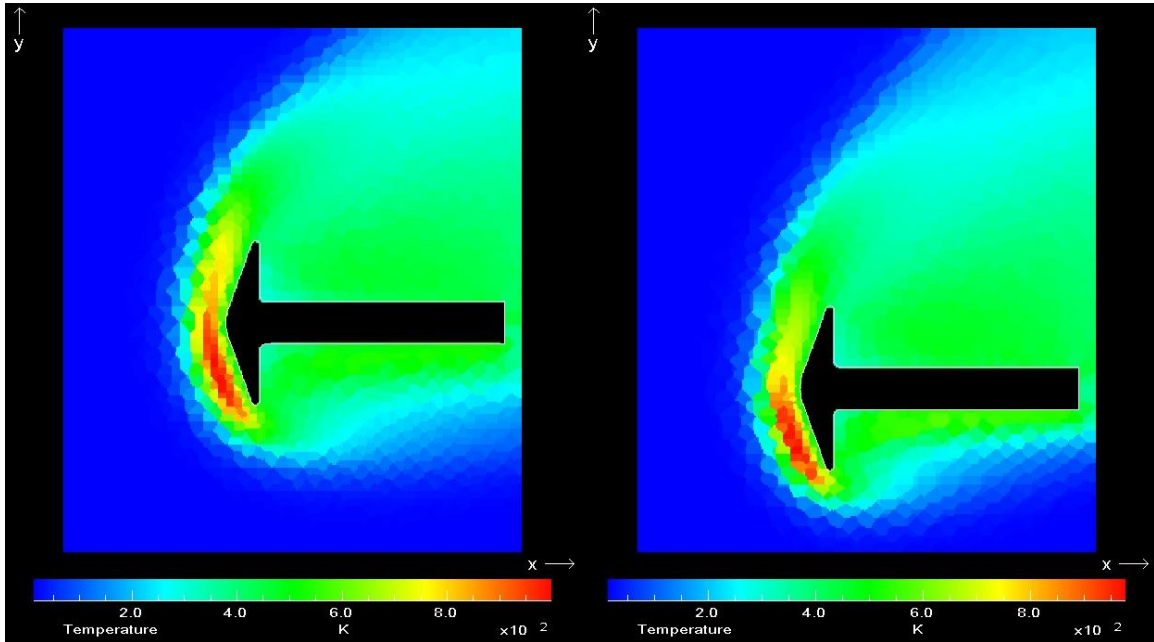


Figure 19: Temperature contours of blunt cone 20 - 30 degrees

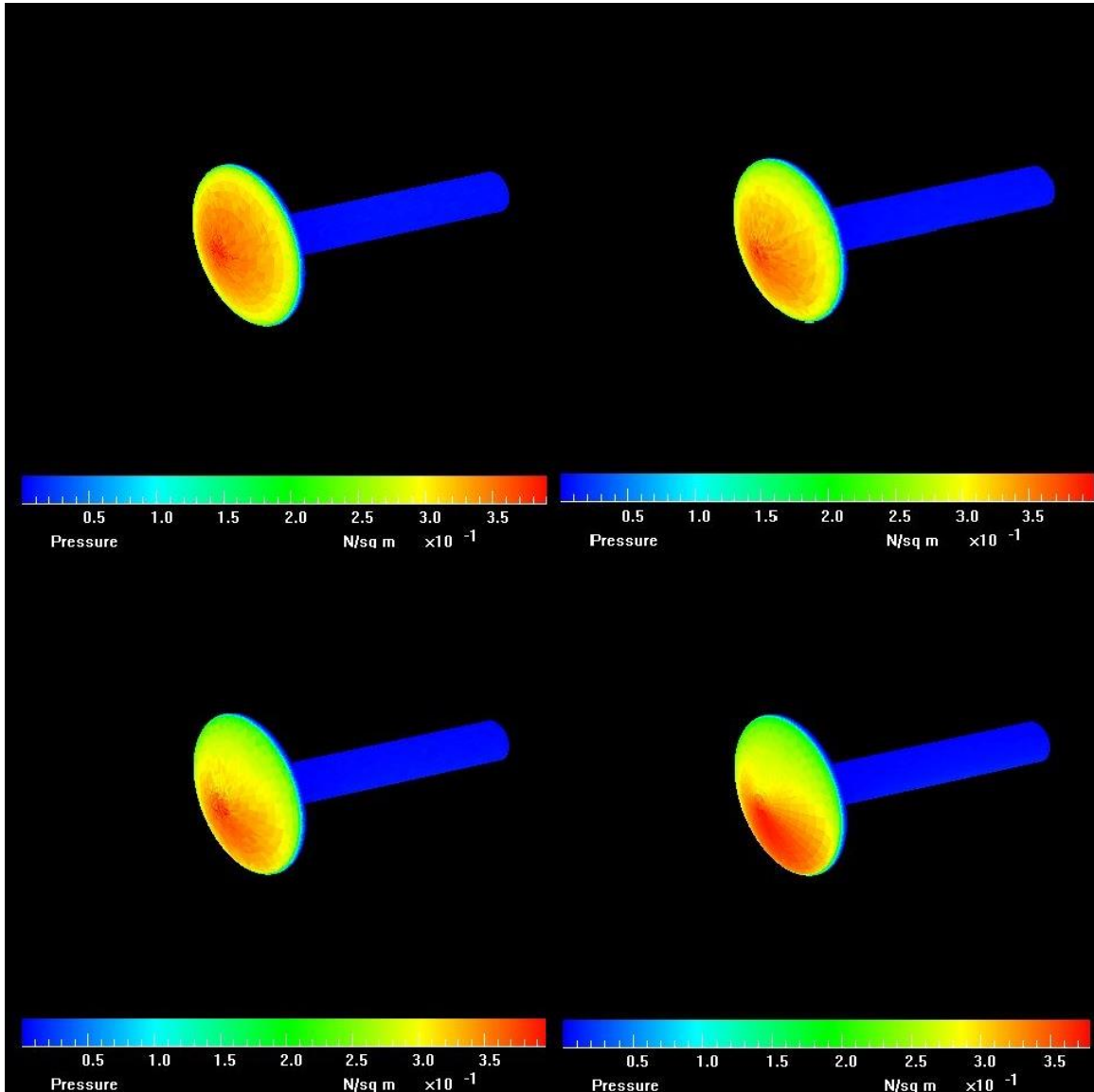


Figure 20: Pressure distributions on blunt cone 0 - 15 degrees

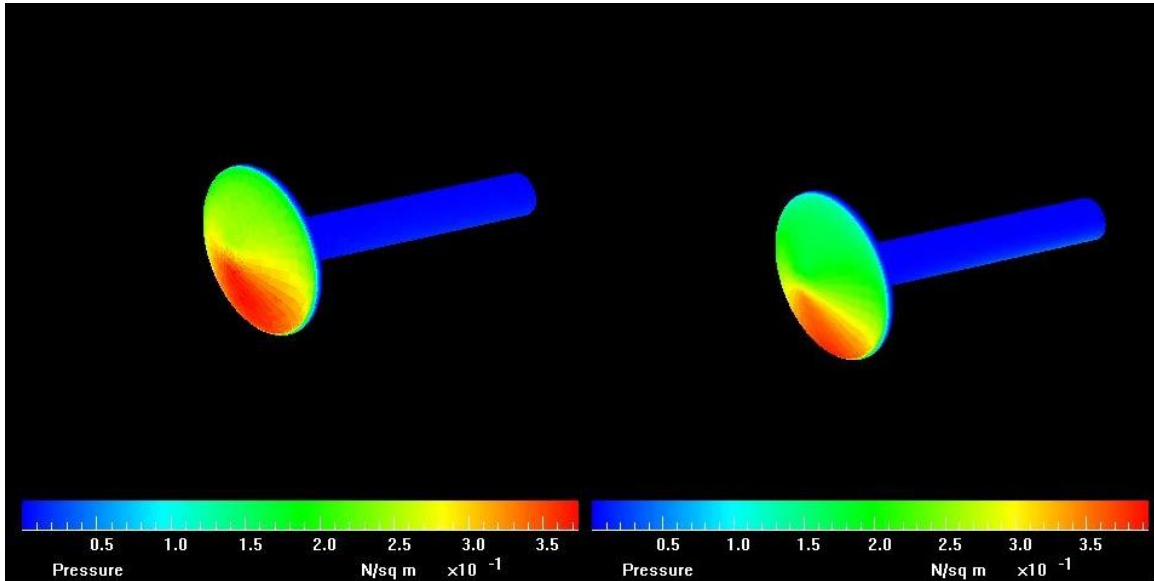


Figure 21: Pressure distributions of blunt cone 20 - 30 degrees

It can be seen from the work by Moss *et al* that the density, temperature and pressure contours from their work closely correlate to the density, temperature and pressure contours to the simulations in this project. This is shown in figures 16 – 21, and these can be closely compared to figure 22 below. It can also be seen that the kinetic temperature from Moss *et al* very close correlates to the simulation in this project.

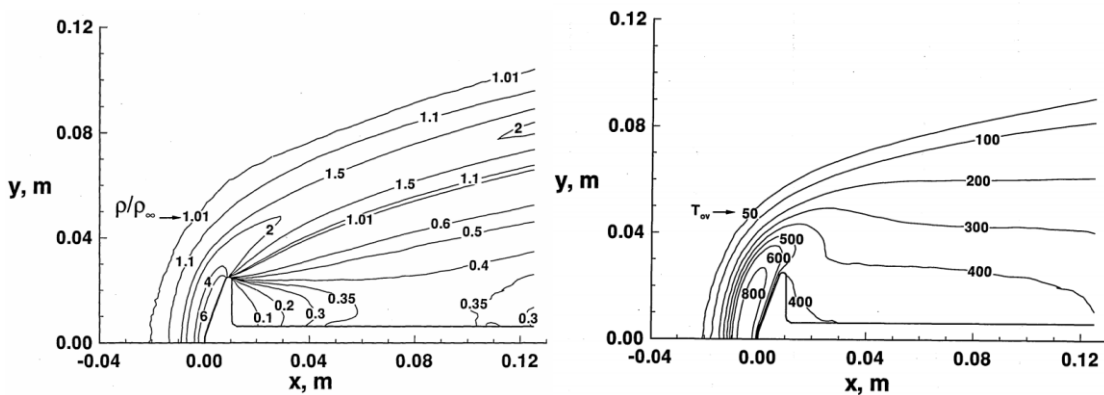


Figure 22: Dimensionless density and Temperature contours from simulations carried out by Moss et al [40]

3.4 Summary

Initial research and validation/ verification DSMC simulations were carried out during the course of this chapter, this was to ensure that DSMC was a viable method for simulating high altitude flows and that future simulations in this project could be trusted. These validation simulations showed good correlation to data collected from analytical calculations and from experimental data from other sources.

A thorough look through of the theory behind DSMC was carried out to ensure that the process was understood fully. This ensured that minimal errors will occur during the entire course of this study. The ground work to the main simulations has been laid out ready for the next chapter.

4. Modelling Satellite Coefficient of Drag Values

There are a number of key factors that can affect the orbital path of a satellite; one of those factors is the coefficient of drag experienced by the satellite. While lowering the coefficient of drag can increase the orbital period of a satellite, increasing the coefficient of drag can decrease its orbital life and allow for the body to be de-orbited at a faster rate than usual. Many satellites are left in orbit once they have reached their end-of-life, which has caused an enormous 'graveyard' of satellites which have the potential to cause problems to other satellites in LEO.

In this chapter, satellite geometries will be analysed while under typical conditions in LEO using DSMC and their drag values, and subsequently their coefficient of drag values will be calculated. The various geometries include distinctive satellite shapes which have been used in the past, such as squares, spheres, cylinders, and satellites with solar arrays attached. Conditions that will be varied will include:

- Freestream Temperature: Molecular activity of incoming particles to the satellite
- Surface Temperature: Heat being emitted by the satellites surface
- Density: number of particles per unit of volume which the satellite is experiencing.

These simulations will indicate which satellites give lower or higher coefficient of drag values. This could help inform to the manufacturer about potential use of geometries.

The second section of this chapter will look at the potential of using high drag devices attached to satellites to increase the coefficient of drag when a satellite reaches its end-of-life. DSMC simulations will be carried out on a number of potential high drag devices and compared . A factor that plays a key role in these

experiments is the size (or effective area) of the high drag device. It is expected that an increase in frontal area will increase the drag values of the satellite, this is confirmed to us in equation 2.3.1 and the deceleration due to drag. What will be tested is the effect this has on the orbital decay of a satellite and whether these devices could bring down satellites at a faster rate than normal.

4.1 Impact of Freestream Temperature on Coefficient of Drag

In order to fully understand how the C_D of a satellite is affected in LEO, we must first look at the conditions this satellite will encounter during a typical orbit around earth. Freestream temperatures tend to fluctuate due to a number of factors, primarily whether the satellite is in sun or shade, and the level of solar activity . Typically the freestream temperature in LEO ranges roughly from 700K to 1500K, but simulations will be carried out between the theoretical minimum and maximum which could be reached at times of extremely high and extremely low solar activities, which is 200K-2000K. These theoretical maximum and minimums are based on the F10.7 Solar index cycles [19].

4.1.1 Simulation conditions

Simulations will be carried out at an altitude of 200km on the variety of geometries including a generic satellite, a cylinder, a sphere and a cube shape. The flow domain will be made up of freestream boundaries to replicate conditions in LEO. The dimensions of the domain will be 9m in the x direction, 10m in the y direction and 10m in the z direction. The geometries will be placed just behind the centre of the flow domain towards the outlet, this is due to the particular style of flow that happens at these altitudes with a high mean free path between particles. This style of flow domain will be used for most of the DSMC simulations in LEO. The surface temperature of the satellite will be set as adiabatic and kept at a constant of 300K.

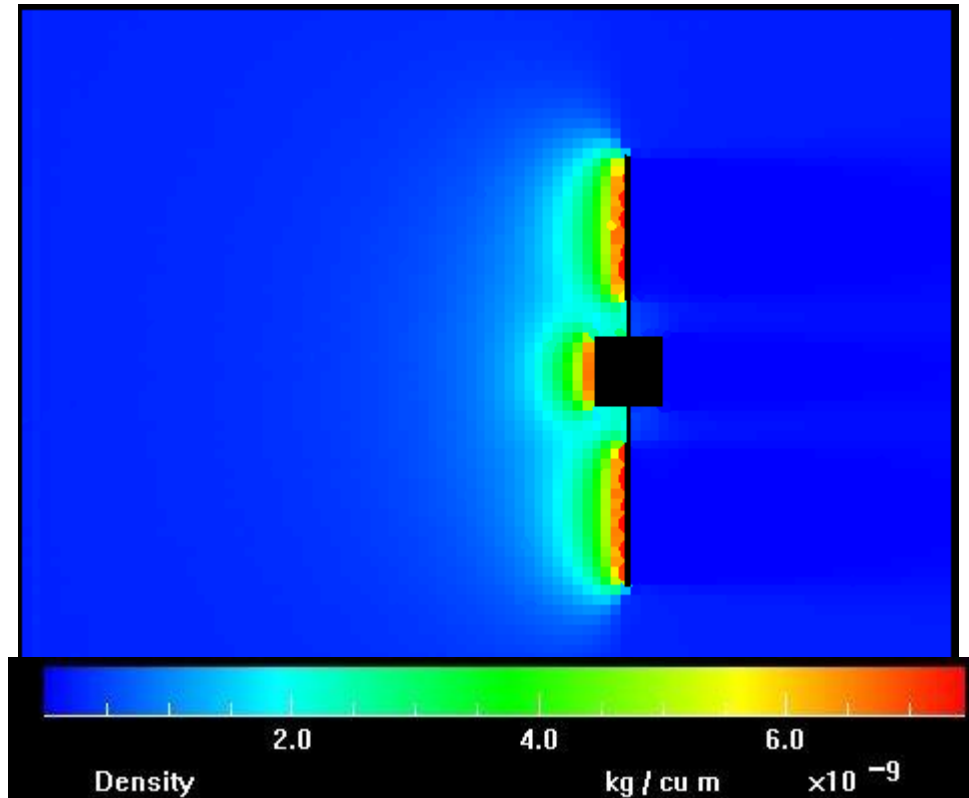


Figure 23: Molecular density formation on the surface of a satellite in LEO

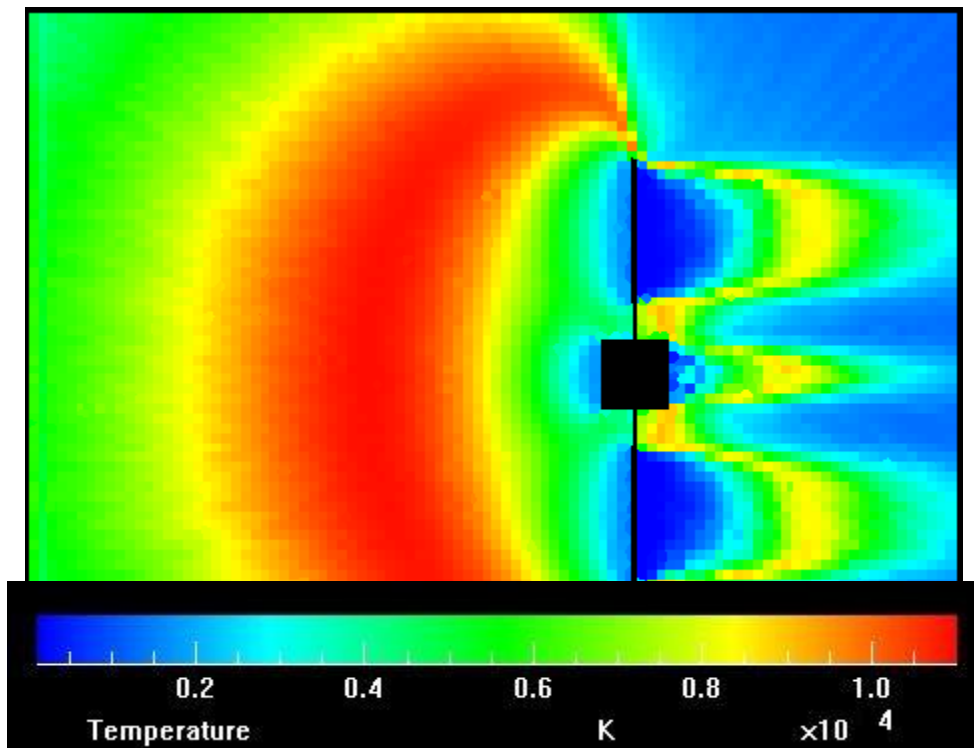


Figure 24: Typical Temperature flow patterns of geometry in LEO

Although the freestream density of the atmosphere at 200km is $2.541\text{E-}10$ kgm^{-3} , the flat surface on the frontal face can experience densities of $0.782\text{E-}8$ kgm^{-3} . While this is still low relative to the earth's atmosphere at sea level, it is a 363 times increase in the freestream density. The main composition of the atmosphere at 200km is Nitrogen (N_2) which accounts for ~41% of the atmosphere at this altitude, atomic Oxygen (O) at ~56% and diatomic Oxygen (O_2) at ~2.5%. This is the composition that will be used in all simulations.

Figure 23 and 24 show the typical Temperature and density flow patterns that can be seen in discrete particle modelling in low densities; these figures were taken from some of the initial benchmark simulations.

4.1.2 Results and Discussions

Each data point for the figure 25 is the result of one simulation which can take at least 2 days to reach a stable state. Simulations were carried out between 200K and 2000K; in 100K gaps.

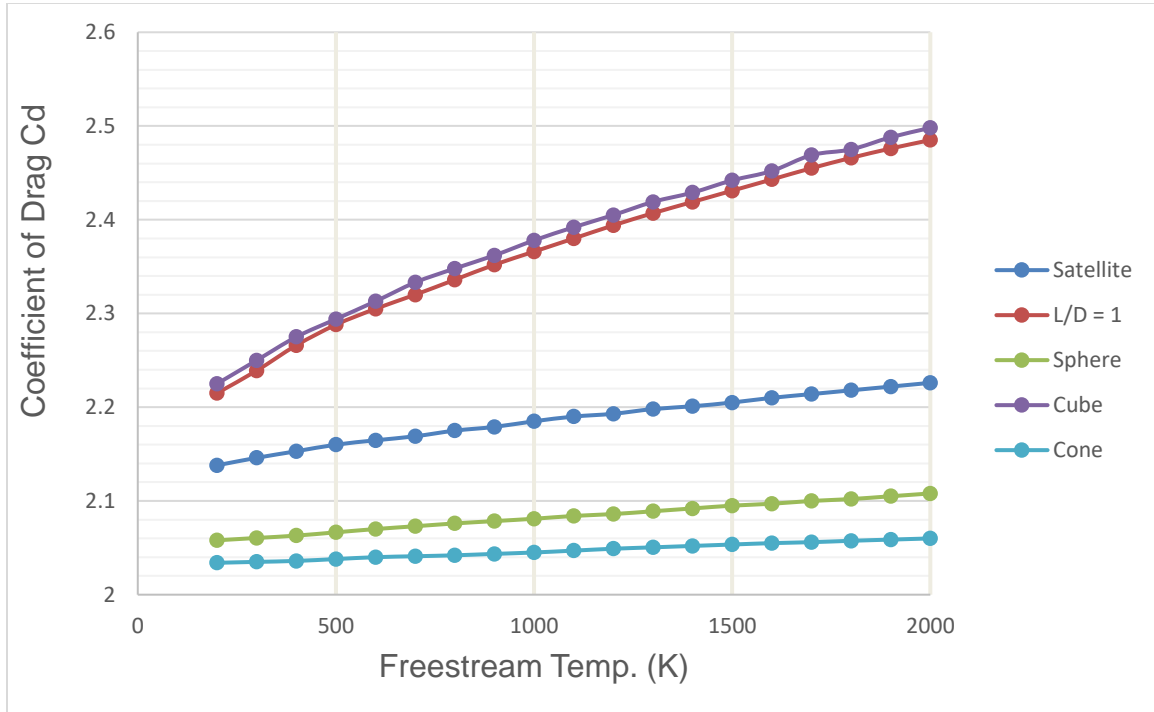


Figure 25: Coefficient of Drag calculated on different geometries at a wide range of freestream temperatures

It can be seen from the results in Figure 25 that the increased freestream temperature has an effect on the coefficient of drag. All of the geometries have shown a positive correlation between freestream temperature and C_D , although some of the geometries have been effected more than others. This shows that satellite manufacturers will have to take into account the average temperature in LEO before launching a mission. This information will help any mission planning and project management.

4.2 Impact of LEO Atmospheric Density on Coefficient of Drag

As shown in equation 2.3.1, the drag coefficient can be calculated using a combination of measurable factors. The drag coefficient is a dimensionless number associated with a particular area or surface, and theoretically should be constant during times of low density where the mean free path is larger than the characteristic area. As the bodies move away from free molecular flow to

transitional flow, the C_D value should start varying due to inconsistencies with the closed form equations and DSMC. Solutions will also be calculated analytically using Sentman's Equations (2.3.6 and 2.3.7) and compared next to the DSMC results. Sentman's Equations are only valid for free molecular flow, therefore a difference between closed form solutions and DSMC solutions will begin to show in the higher densities.

4.2.1 Simulation Conditions

The geometries used will be the same as those from the previous section as these best reflect different satellite geometries. Simulations will be carried out with particle densities between $1E+10$ and $1E+20$ particles per m^3 inside the domain; this roughly corresponds with conditions between 100km and 1000km above the earth's surface [1]. For consistency in the data, and to keep only one independent variable, the gas-surface interaction model used will stay the same throughout the various gas densities. As it can be seen the density decreases, the model changes from a diffuse reflection to a specular reflection, as shown in figure 5 earlier on page 30. Diffuse reflection occurs on satellites below ~500km ($\alpha=1$) due to atomic oxygen build up on the satellite surface. Beyond 500km a more quasi-specular reflection model can be observed [16] [19]. Measuring the exact accommodation coefficient is experimental and therefore would introduce inconsistencies into the simulations.

As shown in figure 25, the freestream temperature can have a profound impact on the satellites coefficient of drag, therefore to keep these simulations consistent a single freestream temperature will be important to reduce the inconsistencies. An average temperature will be calculated from the altitude range and the available data.

4.2.2 Results and Discussions

Below is Figure 26 which is a graph of the completed simulations; each data point represents a separate simulation carried out. DSMC simulations were then compared to analytical results from the Sentman equations (2.3.6 and 2.3.7). As stated in 2.1.3, the Sentman equations are used to characterise the C_D in the free molecular flow range.

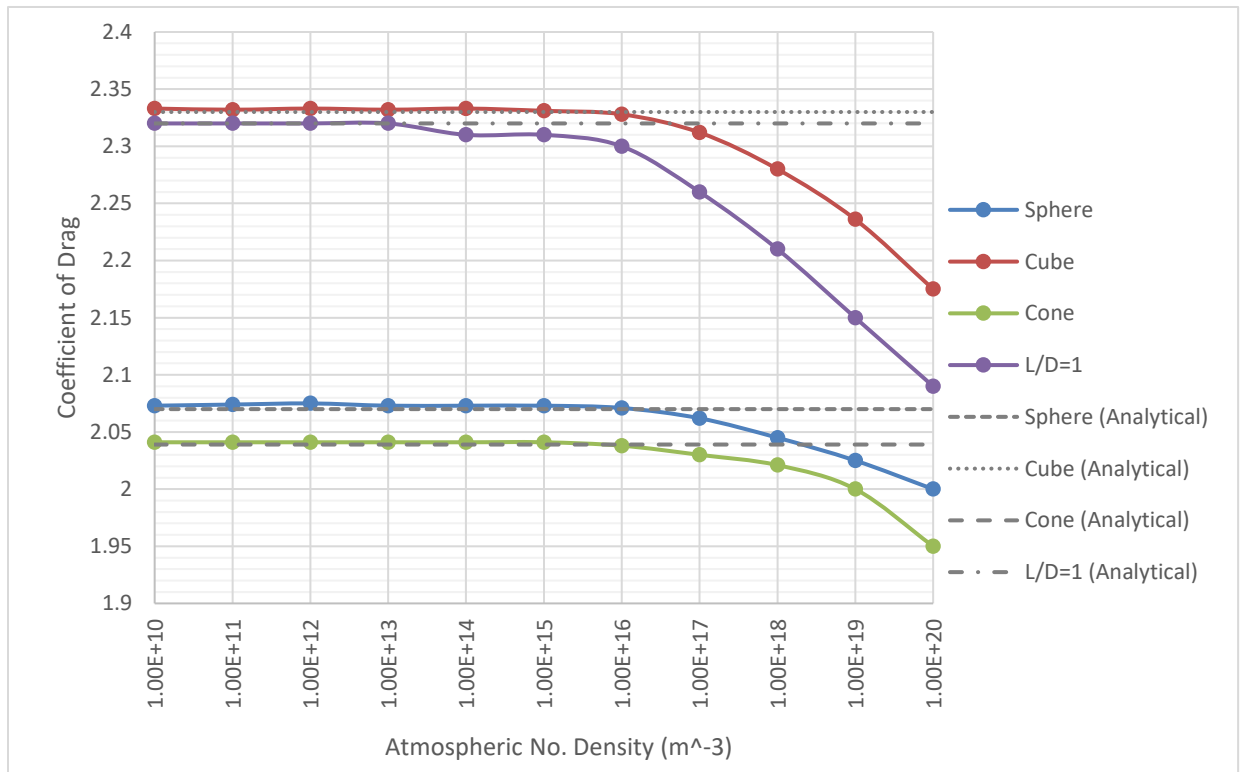


Figure 26: Coefficient of drag on Geometries in LEO against Atmospheric number density; Computational and Analytical

It can be seen from Figure 26 that the coefficient of drag stays practically constant in the free molecular flow regime (roughly from $1E10$ to $1E16 m^{-3}$) which is matched by the analytical closed form calculations. After this the coefficient of drag changes as it goes into the transitional flow regime. In this regime it can be seen that the Sentman equations are not valid.

The limit for the number density was set at $1E20$ particles due to the computational limits of the computer used. The DSMC software effectively simulates a proportion of the real number of particles which makes it very computationally intensive when simulating high densities.

4.3 Effect of Drag Increase Devices on Satellites in LEO

With the ever-growing danger of space junk causing damage to satellites in LEO, it is becoming more important to return to earth any hardware that is no longer needed. This can help reduce the amount of space junk in our orbit. There are two potential ways to combat this problem, the main method of deorbiting satellites and spacecraft is to use thrusters. This method has been researched extensively for example by *Janovsky et al* [44]. In this paper they investigate a variety of methods that can be used on manned and unmanned space vehicles to de-orbit them out of LEO. They only investigate methods which involve propulsion techniques including that of cold and hot plume combustion. This method is expensive as propulsion devices are expensive to fit, and thus limited to high budget satellites, therefore other methods such as drag increasing devices will need to be used for low budget and limited lifespan satellites.

In this chapter a model was designed and developed to add to a satellite which can be put into a DSMC simulation to see whether a significant increase in C_D can be achieved only by changing the geometry. The model started off with only a small drag increasing devices being added, in the form of a single drag plate. The size of the drag plate was then increased and plotted against the C_D calculated. The device may also take the form of a parachute like structure which could be deployed at end-of-life.

After a C_D value has been calculated through use of DSMC, orbital decay calculations were carried out by iterating the two orbital decay equations (2.3.11 and 2.3.12). From this iteration of equations, a theoretical understanding of the orbital life and re-entry time of the satellites was obtained.

4.3.1 Initial Model Development

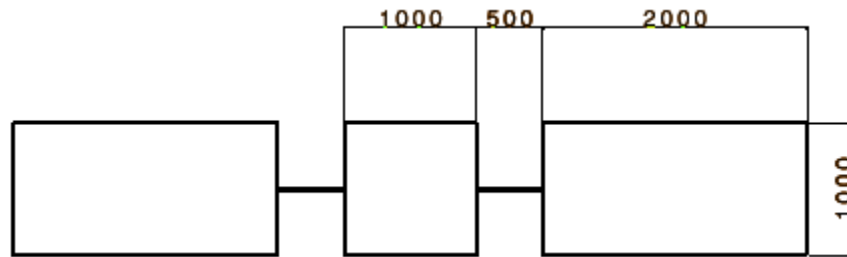


Figure 27: Dimensions (in mm) for the 'generic' satellite for initial testing

An initial model was developed for testing inside DSMC. The model took the form of a generic satellite (as seen in Figure 27 & 28) which served as a 'test bed' for the drag increase devices. After initial testing on the generic satellite was carried out, the model was developed to include a standard drag plate. The frontal area of the satellite was increased on each simulation and the C_D calculated. This C_D was then used for the orbital decay calculations.

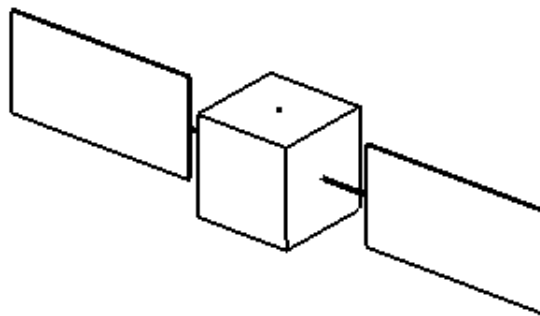


Figure 28: Isometric view of the initial generic satellite

The projections of the satellite in figure 27 & 28 are shown in the maximum frontal area configuration which is the form that will be input into the DSMC program. Further programs with the drag increase devices will also assumed the maximum frontal area.

4.3.2 Drag plate development

A drag plate was developed from a small initial device and was gradually made larger. The drag plate was initially placed at the back of the satellite (the opposite side from freestream inlet) as this would most likely make the satellite more stable. Simulations were also carried out with the drag plate attached to the front.

The frontal area of the main block of the initial satellite is 1m^2 (excluding the solar array that is attached), the first drag plate to be added had an area of 1.5m^2 with subsequent drag plates increasing in size by 0.5m^2 with each iteration of the experiment. Although the main idea for the simulations is to calculate the C_D value from the drag value, pressure distributions on the surface of the satellite and the drag plate will also be documented. This was especially useful for the drag plate that is situated behind the satellite due to the diffuse reflection and interaction with the solar array and satellite. With the drag plate attached to the front of the satellite, there was less interaction with the rest of the satellite but the pressure distribution will also be documented.

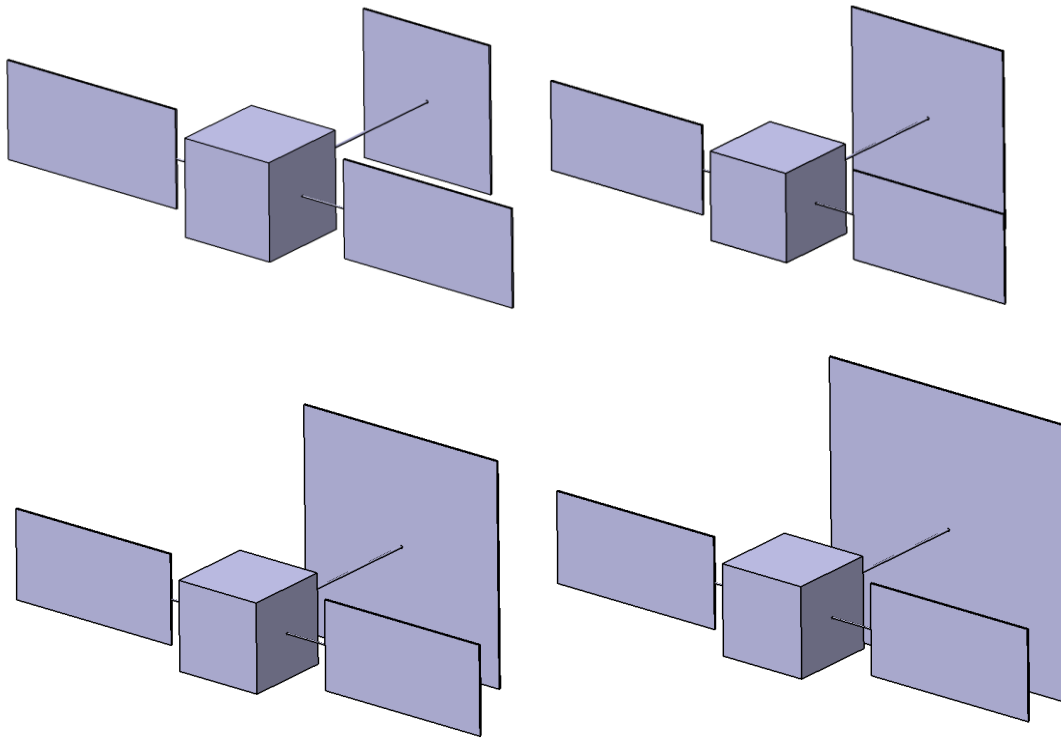


Figure 29: Example of 3D CAD Models for the satellite Drag Plate Experiments

4.3.3 Physics modelling

The physics models and settings used reflected the atmospheric conditions at a given height selected. Although LEO is described as being between 180km and 2000km, simulations were carried out at 300km. This altitude was selected as it allows for a reasonable demonstration for the effects of orbital drag to be shown, and to show when the satellite has eventually decayed into the atmosphere and to be able to graphically display this decay.

At 300km, the atmospheric composition is similar to what it is at 200km (which is the altitude at which most other simulations are carried out). Atomic oxygen, O, is still the primary constituent of the atmosphere at this altitude, indicating that there will be atomic oxygen contamination of the surface of the satellite, and therefore diffuse reflection of the re-emitted particles will occur. As well as

significant atomic oxygen, nitrogen (N_2) and standard diatomic oxygen (O_2) was also form the simulated atmosphere. Although other components such as hydrogen, helium and argon also occur at this altitude, they were not included in the simulation due to the extremely low percentage of these gases being present. The temperature variation of the freestream atmosphere has a huge effect on the C_D calculation on the satellite, as shown earlier in figure 25. As the simulations couldn't be carried out at variable temperatures, a single temperature was selected and kept constant throughout the various simulations. This number was taken from the US Standard Atmosphere [1] and determined by averaging the temperature fluctuations [19]. Below is a table (Table 6) of the conditions that were used in the simulations.

Table 6: Values used for Drag plate simulations

Parameter (Unit)	Values
Velocity (ms^{-1})	7500
Temp (K)	700
Density (kgm^{-3})	1.196E-10
Pressure (Pa)	8.7704E-8
Knudsen No	866
Mean Free Path (m)	2.6E+03

$7500ms^{-1}$ was selected as a baseline velocity for the simulations as it is roughly the orbital velocity at 300km altitude. It can also been seen that the Knudsen number is extremely high and well into the free molecular flow regime, this was calculated using equation 2.1.1.

4.3.4 Computational Results

This section presents the computational results for the drag plate simulations. Graphs will be presented along with density profiles of the various plate sizes.

Coefficients of drag were also displayed on a graph along with the plate area to demonstrate the correlation between these factors. Coefficient of drag was calculated using the theoretical drag equation 2.3.1; using the drag force reading from the x component in the DSMC software.

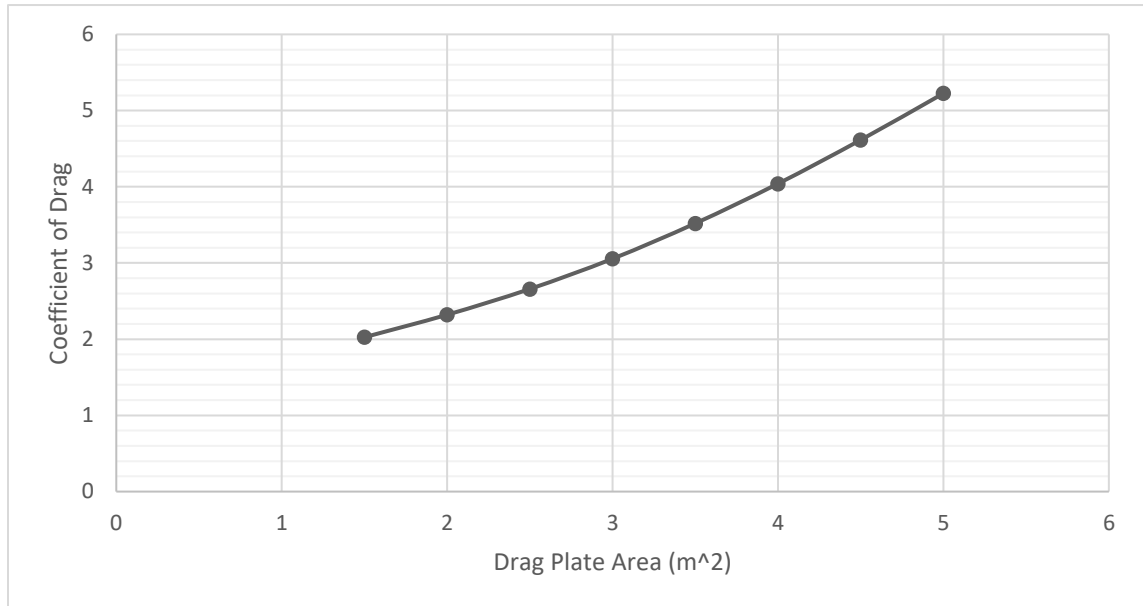


Figure 30: Simulation result for Drag plate size against coefficient of drag

It can be seen in figure 30 that the coefficient of drag of the satellite increased as the drag plate was made larger, indicating that the larger the drag plate is made the greater the effect of orbital decay.

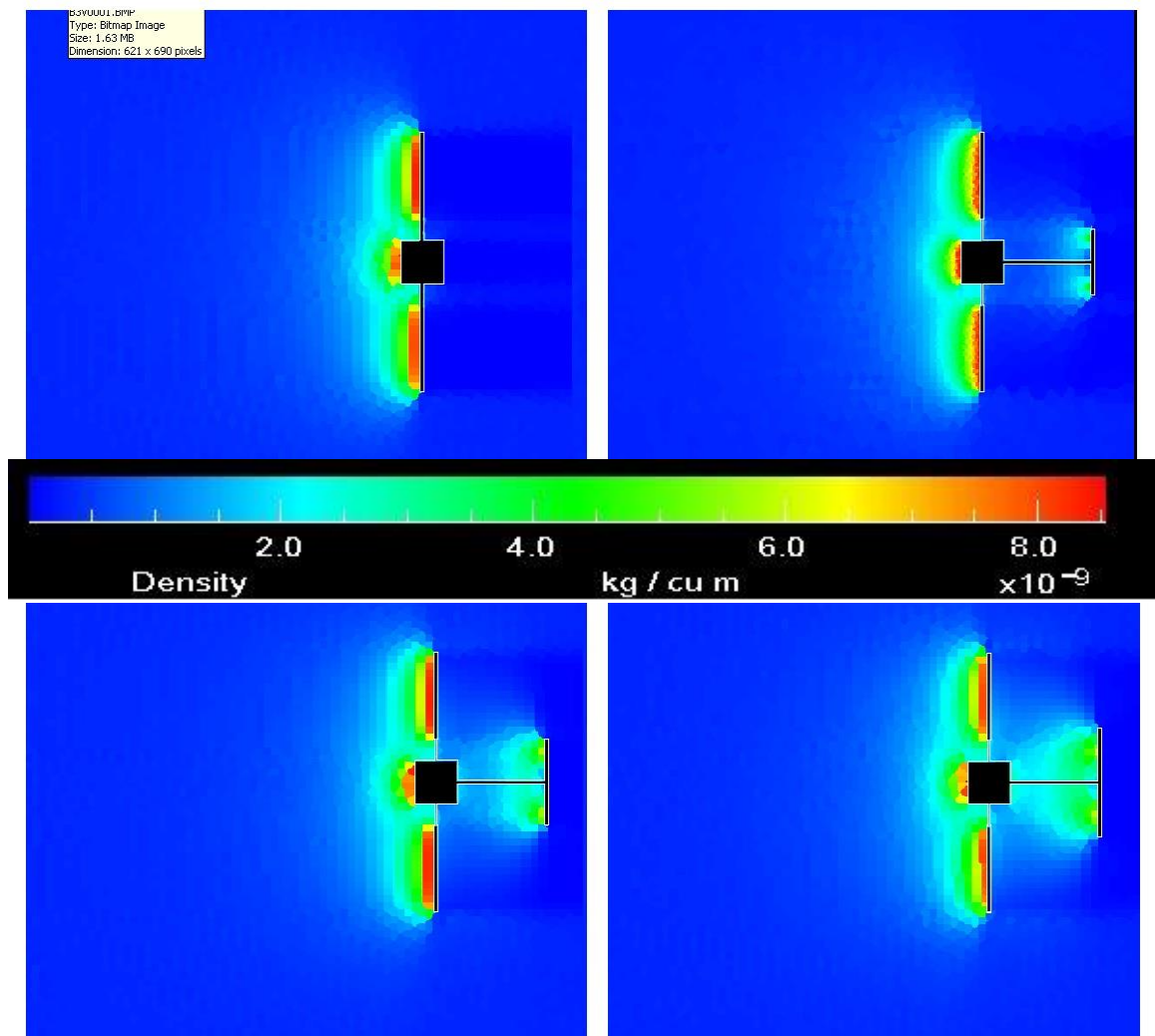


Figure 31: Density flow of the satellites of drag plates from 0 - 2.5m²

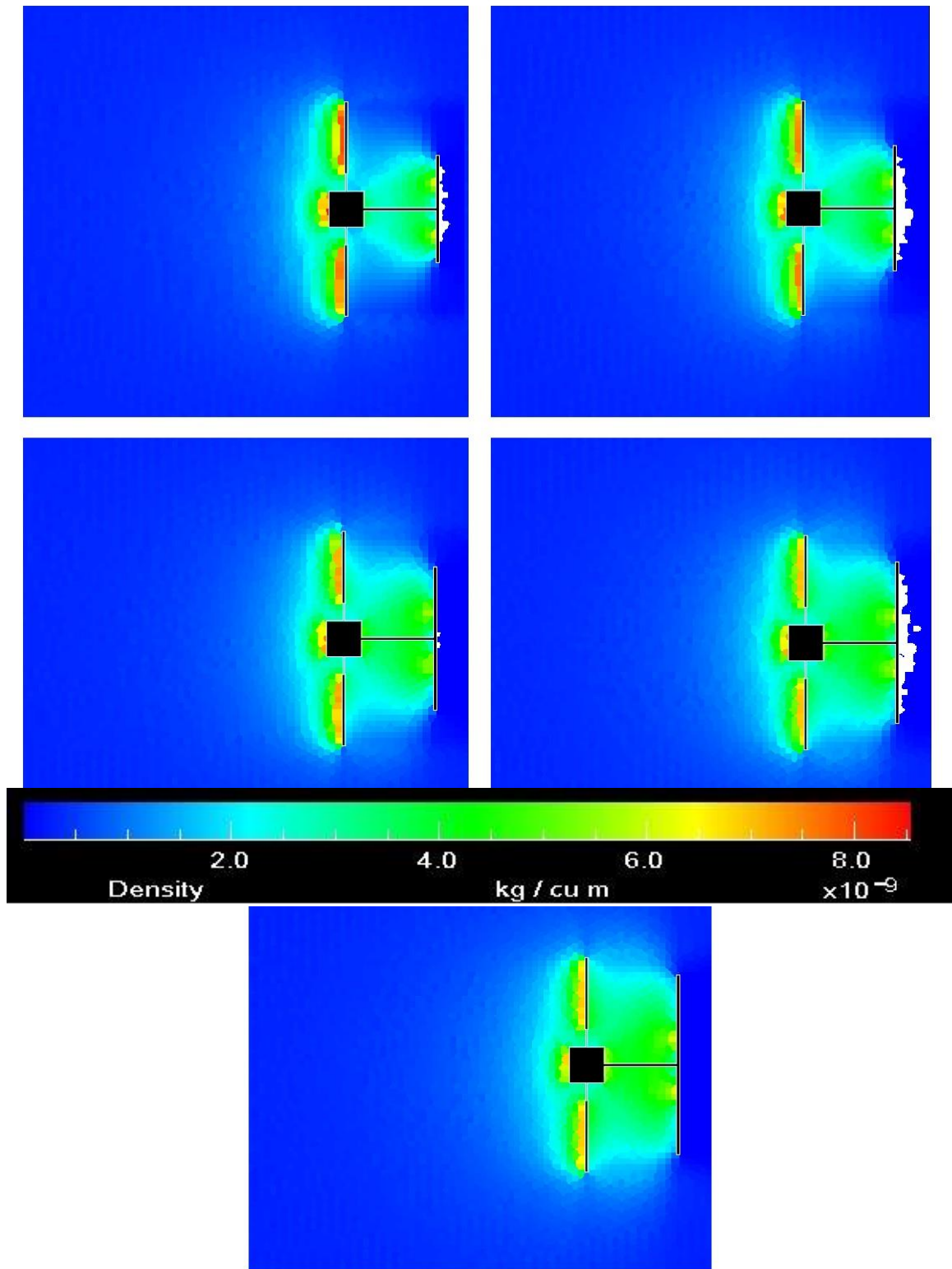


Figure 32: Density flow of the satellites of drag plates from 3 - 5m2

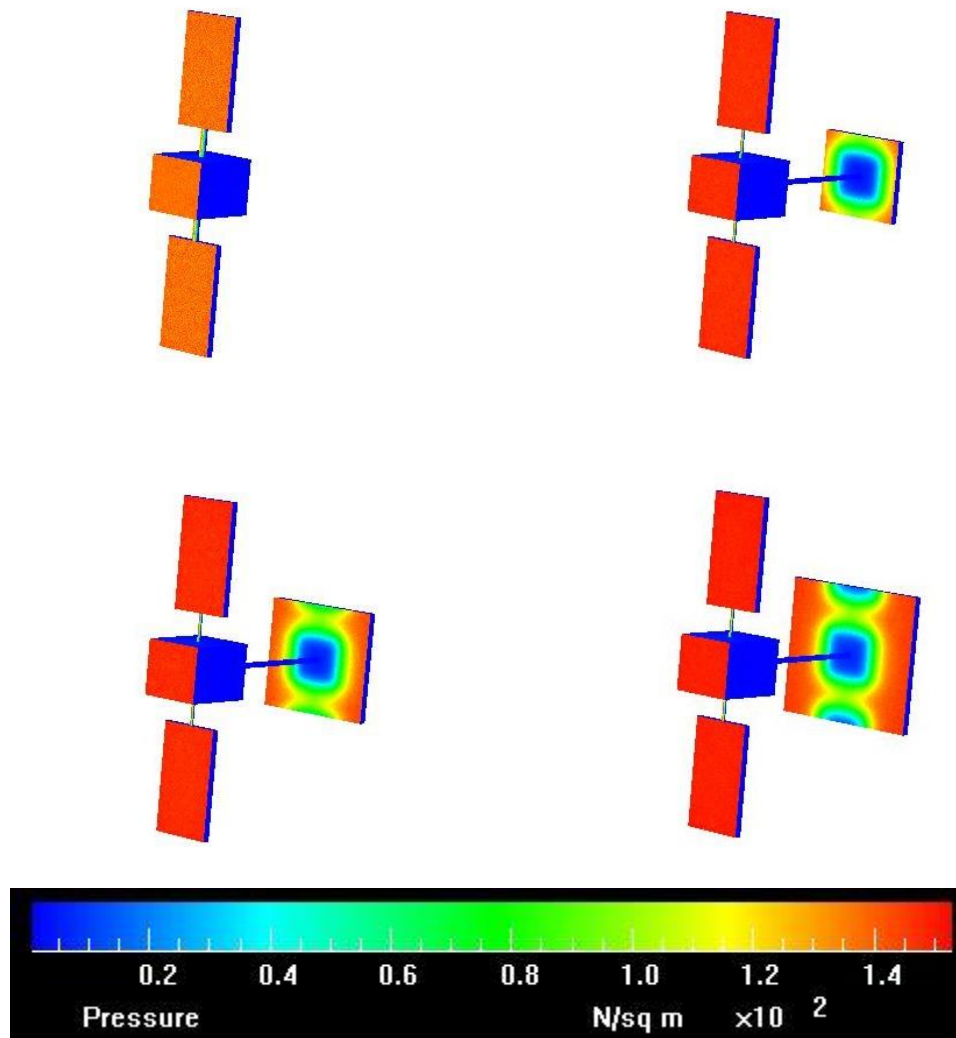


Figure 33: Pressure distribution of satellite drag plates 0 - 2.5m²

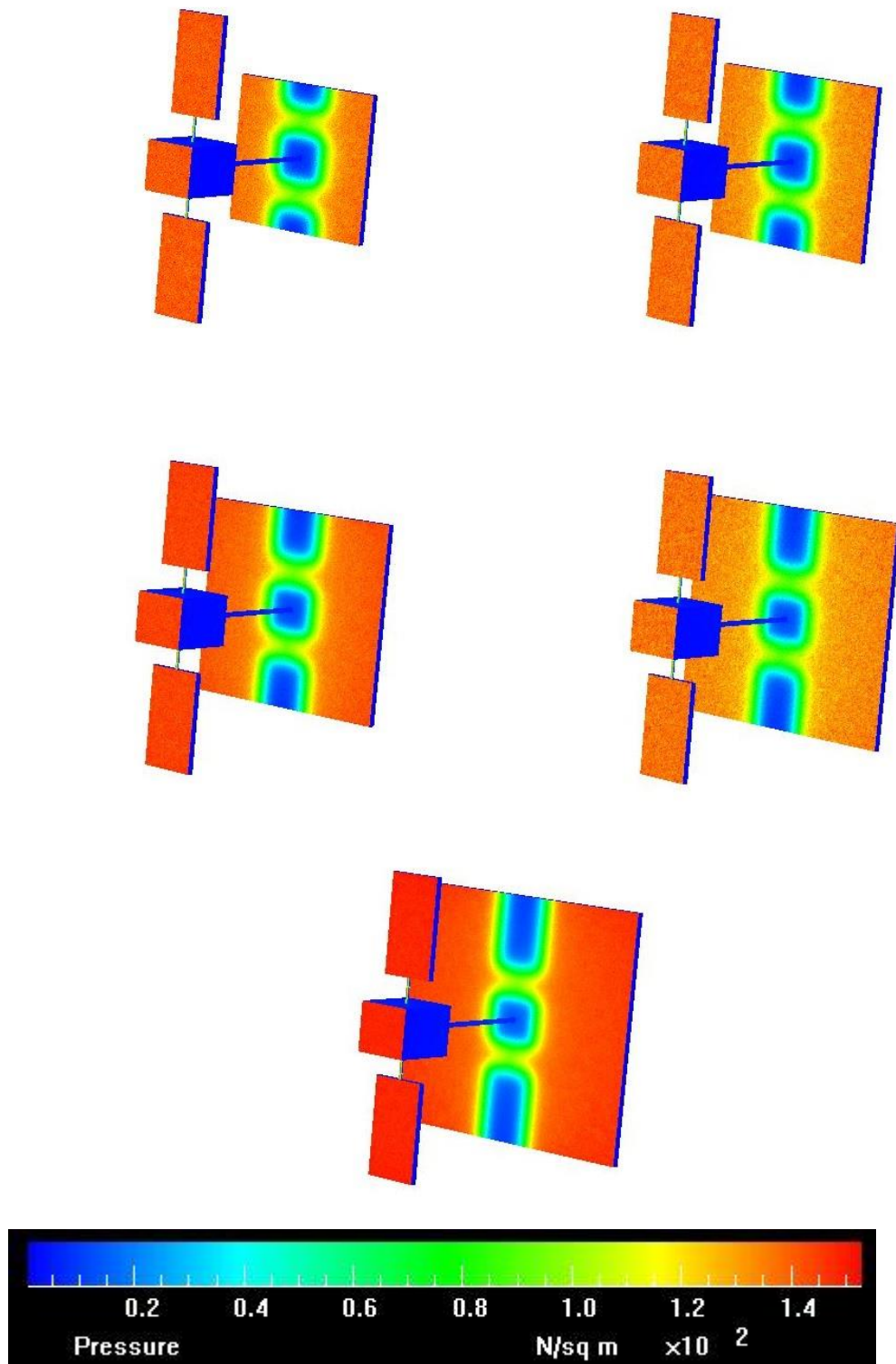


Figure 34: Pressure distribution of satellite drag plates 3 - 5m²

It was seen from figures 31 to 34 above that the larger drag plates can capture more of the particles flow from LEO; figure 31 and 32 shows how a higher density of particles can be trapped between the drag plate and the satellite itself. This phenomenon was investigated further to see whether this helps or decreases effectiveness of the drag plate. It can also be seen that the smaller drag plates in figure 33 have very little increased pressure on the front of the drag plate, this is because the particles are being stopped by the satellite itself before they reach the drag plate, effectively making the drag plate useless in this scenario. It was also seen in figures 33 and 34 that the solar panels from the basic satellite model stop particles from reaching the drag plate, this is shown by the area of lower pressure in blue on the drag plate, meaning a significantly lower number of particles are reaching this area of the drag plate.

All the simulations have indicated that the larger that drag plate the better the drag value achieved; this can also be seen in figure 34 where the area covered by red (higher pressure) is a lot greater than the other drag plates; this is as expected. It was also drawn from these simulations that the design of the satellite could have a significant impact of the performance of the drag plate. The drag plates on satellites with extendable solar panels may not have as great impact as those with built in or attached solar panels. Each satellites individual design was needed to be taken into account for each drag plate to allow for maximum frontal surface area.

4.4 Modelling Orbital Decay

This section (4.4) will focus on how the drag on bodies in LEO can affect the orbital life time of the satellites. As stated in chapter 4.3.4, it is important to know the orbital life time of a satellite to help plan a mission effectively. In chapter 2.3.1 were equations given which were iterated against each other to form a solution for the orbital decay which was calculated using the help of an online calculator; this is shown in appendix A [45]. This chapter looked at the effect of the drag plate (shown in chapter 4.4) attached to a satellite, and how this effects the orbital lifetime of the satellite.

An orbital path was calculated from 300km until its decay in the atmosphere (roughly 160km) and each model will be compared next to each other in figure 35. After the drag plates are compared, orbital decay calculation were made with a varied F10.7 index from the sun. As stated before in chapter 2.1.1, F10.7 index can vary the local density of the LEO region of the atmosphere, which can have an effect on the orbital path and lifetime of the satellite. The large drag plate model

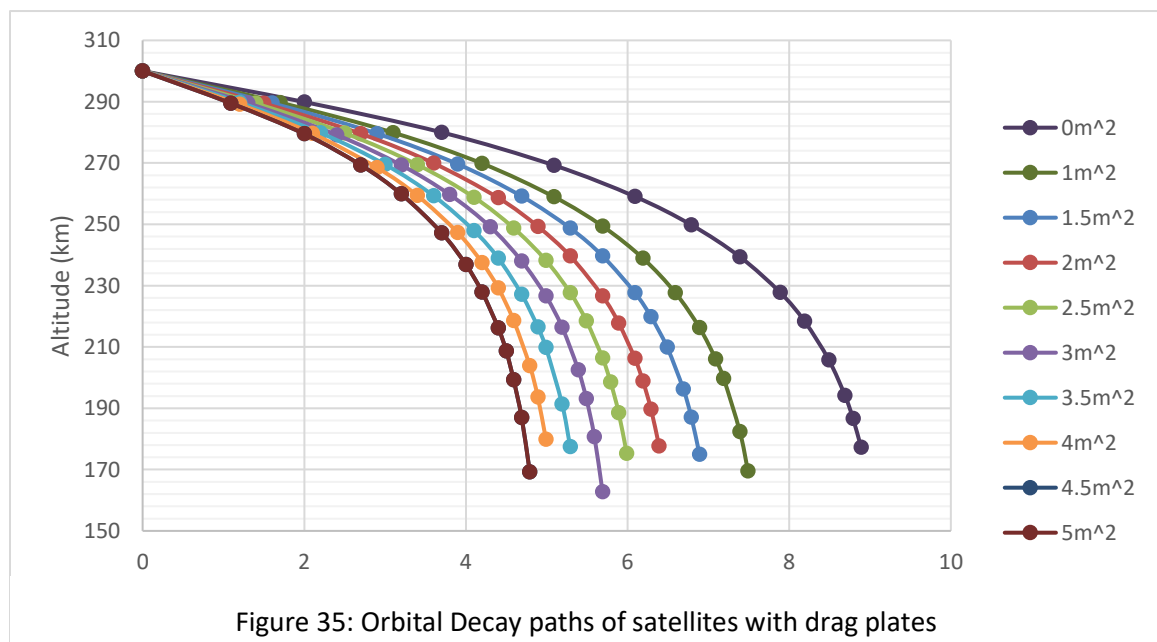


Figure 35: Orbital Decay paths of satellites with drag plates

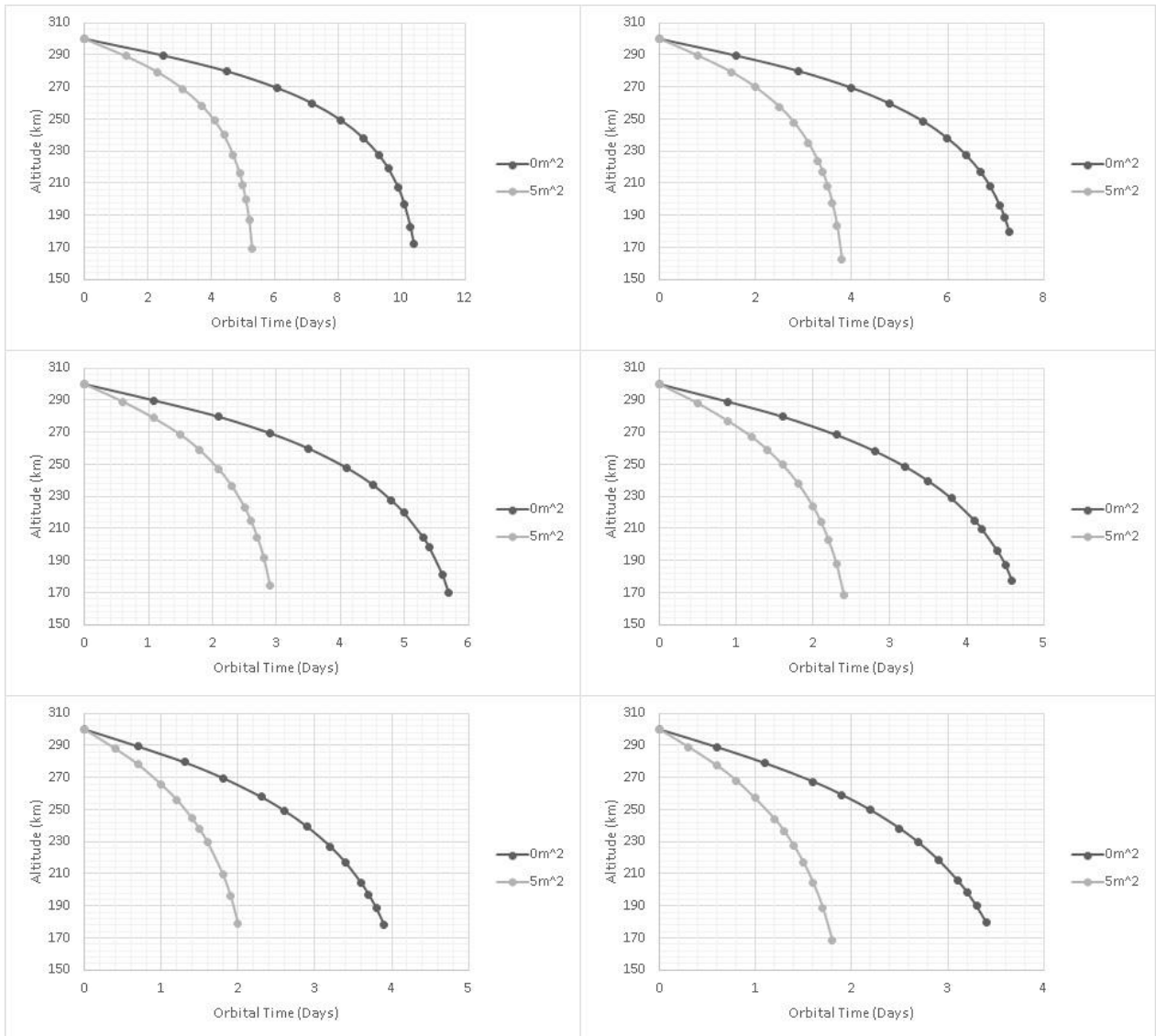


Figure 36: Orbital decay paths of no drag plate and the large drag plate from 50 – 300 sfu

and the standard satellite were compared next to each other in figure 36, and over a range of F10.7 measurements; these measurements vary from 50 sfu to 300 sfu.

Figure 35 indicates the effects the drag plate has on a satellite from 300km to its eventual burn up in earth’s atmosphere are seen. The satellite with no drag plate was not affected very much by earth’s atmosphere in LEO orbit. It dropped 10 km in the first day and then ultimately went on to last for 9 days before; this acted as a benchmark for the following calculations with the drag plates attached.

This satellite decays at a very fast rate compared to the ISS as shown in figure 1 although the starting altitude of the satellites is near enough the same; this is due to the mass of the ISS. The iterative equations 2.3.11 and 2.3.12 require a weight to form a solution to the problem. A weight of 250kg was selected for the drag plates satellites as a bench mark for small-medium size satellites. When the weight of the satellite is increased in the equations, the orbital life is extended which explains how the ISS only needs a re-orbit boost roughly once a month.

After the initial benchmark was carried out with no drag plates, calculations were carried out on the small to large drag plates to find their orbital paths from 300km. As seen in figures 35 and 36, the drag plates have a significant impact on the time it takes to burn up in earth's atmosphere from 300km. Although the small drag plates have a small effect on the orbital decay, the largest drag plate has a noticeable difference which brings the satellite into the atmosphere roughly 4 days sooner than the satellite without the drag plate. This means that the simple drag plate can bring the satellite out of orbit sooner thus decreasing the risk of it being damaged by other satellites or space debris. Looking at the trend of figure 35, it is indicated that the larger you make the drag plate, the greater the effect of the atmosphere on the satellite.

Calculations were also carried out on the effect of satellite drag with different levels of F10.7 Solar flux (refer chapter 2.1.1) and how this affects the orbital path of the satellite. Calculations were carried out from 50 sfu, which is the lowest level of solar activity experienced, all the way up to 300 sfu which is the highest level of solar activity. Figure 36 shows a number of graphs that range from 50 – 300 sfu for the large and no drag plate simulations. It can be seen that very high solar activity can have a massive effect on the orbital performance of the satellite, with an orbital reduction on the larger drag plate of roughly 5.5 days. The satellite with no drag plate with high solar activity re-enters earth's atmosphere just under 2 days from the starting altitude of 300km.

The results from these solar activity calculations reflect the results seen in chapter 4.1 looking at the effect of freestream temperature on satellite geometries.

High solar activity can lead to a greater molecular activity in LEO which leads to larger particle temperatures. The figures in chapter 4.1 show that there is a strong positive increase in the C_D of the geometries as the freestream temperature is increased. Seeing as all other variables in these simulations were kept the same, this showed there is an increase in the physical drag as the temperature increases, therefore de-orbiting the satellite sooner. This matches the data calculated with the varying F10.7 solar flux.

Although the solar activity cannot be changed, satellite manufacturers and space agencies will need to launch satellites as solar cycles lasts for roughly 10-11 years [46]. Therefore, this data is important to satellite manufacturers and space agencies to help them determine the orbital life of their satellites. More considerations to the design of the satellite would have to be taken into account particularly during periods of high and low solar activity. Low solar activity would mean it's more difficult to de-orbit the satellite after its end of life, while a high solar activity would need to be considered before launch to extend its life and allow a full mission to occur.

4.5 Drag Plate Simulations on GRACE Satellite

The previous section (4.4) of the project provides a good basis to determine the effect of a drag plate attached to a 'generic' satellite; this can be classed as a proof of concept for the idea. This section will look at a similar drag plate attached to a real world satellite which has actual data which can be compared to the data from this project.

The GRACE (Gravity Recovery and Climate Experiment) satellite was an orbital experiment put into place in 2002 for a 5 year mission to look at anomalies in the earth's gravity. 15 years later and the satellite is still in orbit collecting data. DSMC simulations have been carried out on this satellite by Mehta *et al* in a number of papers and data from those papers will be compared with data from this project [14] [19]. Currently the GRACE satellite uses a small thruster to adjust its

altitude and potentially to de-orbit when it eventually has no further use to the scientific community. Figure 37 shows how one of the GRACE satellites was laid out.

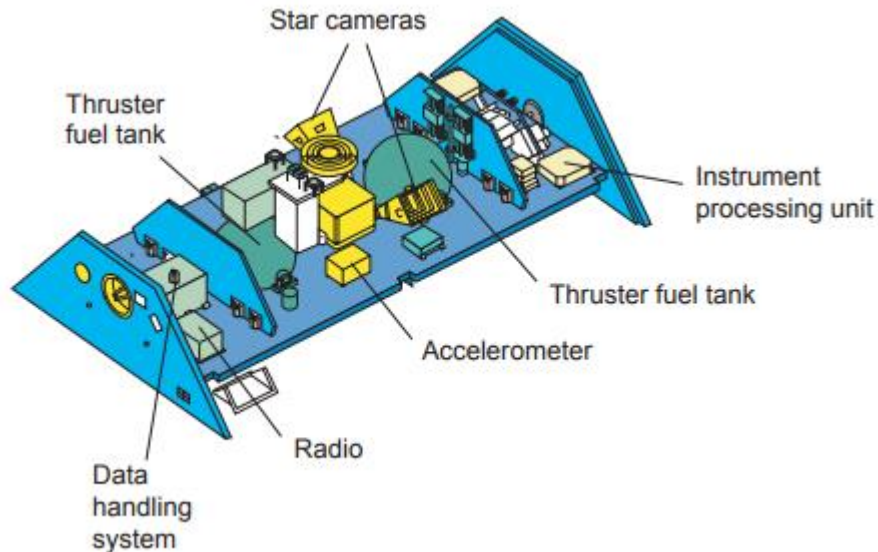


Figure 37: Inside view of the GRACE Satellite [47]

4.5.1 GRACE Model

Models were created with CAD software from technical drawings of the GRACE satellite. These documents gave a good idea of the outside dimensions of the satellite, but did not give anything more detailed than that. However, this was suitable for the project as less detailed models were also used in the papers by Mehta *et al* [14] [19].

A standard model of the GRACE satellite will be simulated as well as a model of GRACE with the larger drag plate from section 4.3, this is because the largest drag plate was shown to have the greatest effect on the orbital decay of the ‘generic’ satellite. Results from the simulations of these models will be compared to each other. The dimensional information was taken from the product specification of the GRACE Satellite [47]. Below Figure 38 & 39 show technical drawings for the satellite as well as the standard and drag plate model.

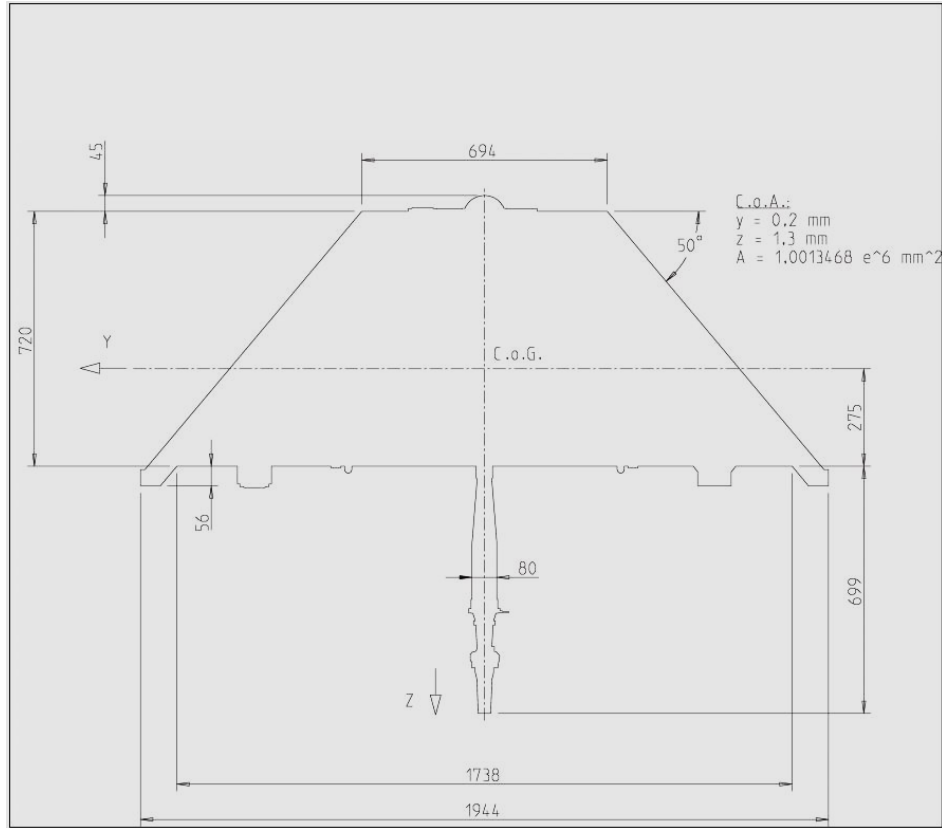


Figure 38: Front on view of Grace Satellite with Dimensions [47]

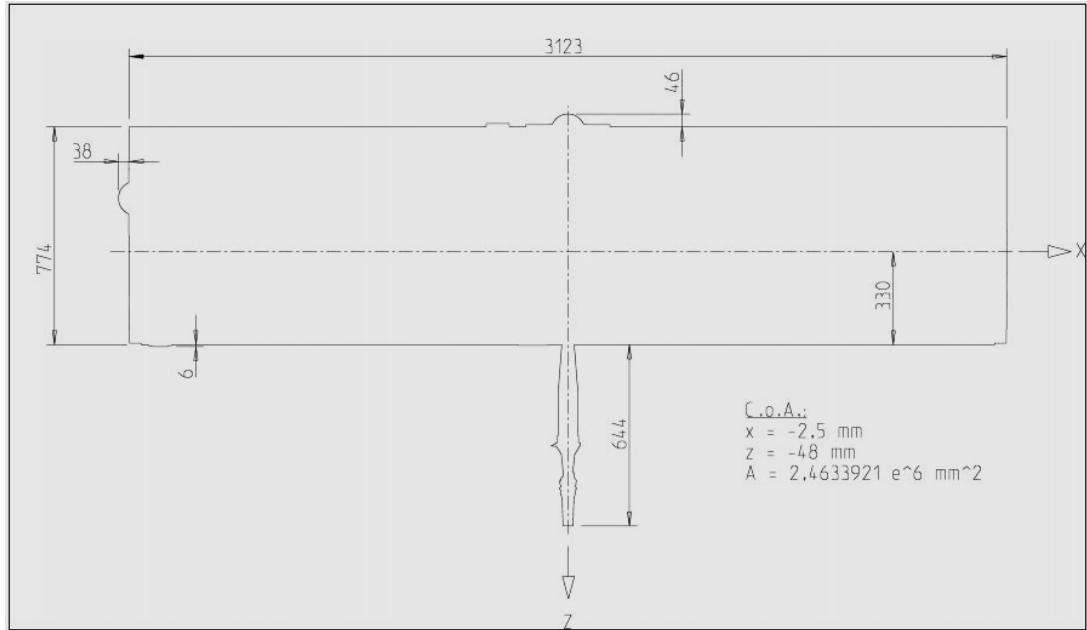


Figure 39: Side on view of GRACE Satellite with Dimensions [47]

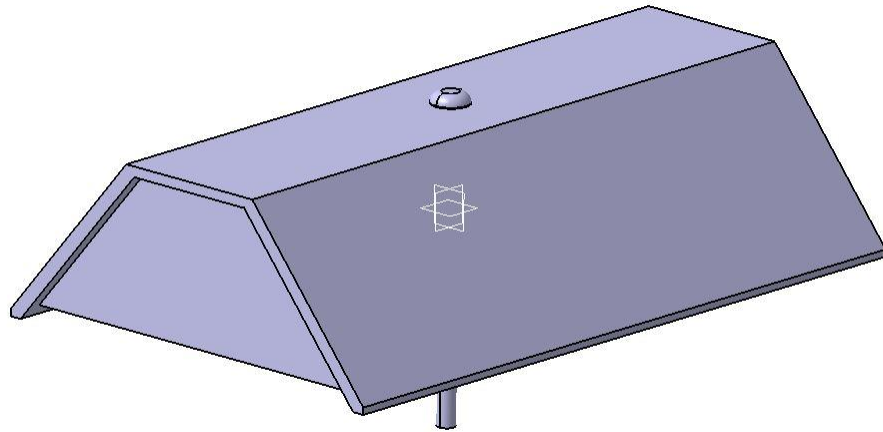


Figure 40: 3D CAD model of GRACE Satellite without drag plate

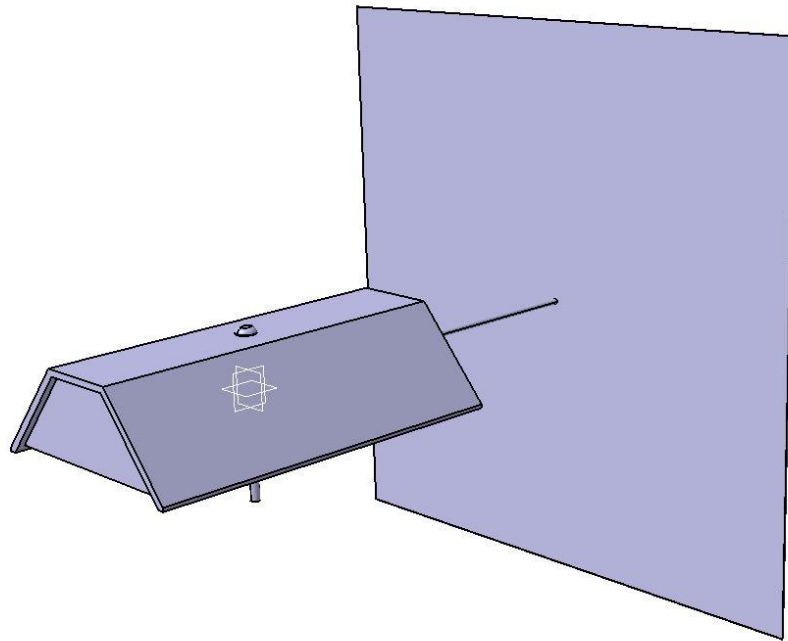


Figure 41: 3D CAD model of GRACE Satellite with large Drag Plate

Figures 40 & 41 show the CAD models made for use in the DSMC software. The models shown should serve as a good base level for the DSMC Simulations. This level of detail was used in the work of Mehta *et al* [14] [19]. The drag plate is the same basic design used in section 4.3.2.

4.5.2 Physics Modelling for GRACE Satellite

The physics models used in these simulations will replicate the conditions used in the previous reports, such as the work from Mehta *et al*, and the conditions the satellite experiences in LEO. The GRACE satellite orbits the earth in a geocentric, near circular orbit (eccentricity – 0.001) with an apogee of 508K and a perigee of 483km. For simplicity the satellite was simulated with conditions at 500km. As with earlier simulations carried out in this project, Atomic Oxygen is the primary gas at 500km which indicates that there will be a more diffused based reflection pattern due to the oxygen sticking to the satellite surface. The Characteristic length of the satellite without the drag plate is 3123mm and 4123mm for the satellite with the

drag plate; this is used to calculate the Knudsen number with the equation 2.2.1. The temperature of the freestream was taken from the NRLMSISE-00 atmospheric model [48] which was used in a number of other reports, including those from Mehta *et al* [14] [19]. The nominal value for the freestream temperature was taken from this. Again, the VHS molecular model was used for these simulations due to its computational simplicity and collision models. Below is a table of all the important variables for these simulations:

Table 7: Values used in the GRACE DSMC Simulations

Parameter (Unit)	Values
Velocity (ms ⁻¹)	7612
Temp (K)	1000
Altitude (km)	500
Density (kgm ⁻³)	5.215E-13
Pressure (Pa)	3.0236E-9
Knudsen No	24655
Mean Free Path (m)	7.7E+04

As stated in the previous paragraph, atomic oxygen is the primary gas at 500km, but there are two other gases that form a part of the atmosphere at this altitude, and that is Nitrogen (N₂) and Helium (He). Other gases are also found at this altitude such as diatomic Oxygen (O₂), Argon (A), and Hydrogen (H); these are at such low quantities in the atmosphere (>0.1%) that these can be neglected from the simulations for computational simplicity.

4.5.3 Results and Discussions

Simulations and orbital decay calculations were carried out on the GRACE satellite with and without the drag plate attached. It was shown that the GRACE satellite would take just over 2.2 years to re-enter the earth's atmosphere from its starting

altitude of 500km. With the drag plate deployed, the satellite would re-enter the earth's atmosphere in just over half a year. This works out to be an 75.7% drop in the orbital period between the standard drag plate and the drag plate model. This means that the simple addition of a drag plate to a satellite in the manufacturing phase could be used to de-orbit satellites without the use of any thrusters. Figure 42 is a graph showing the difference in orbital paths between the 2 satellites.

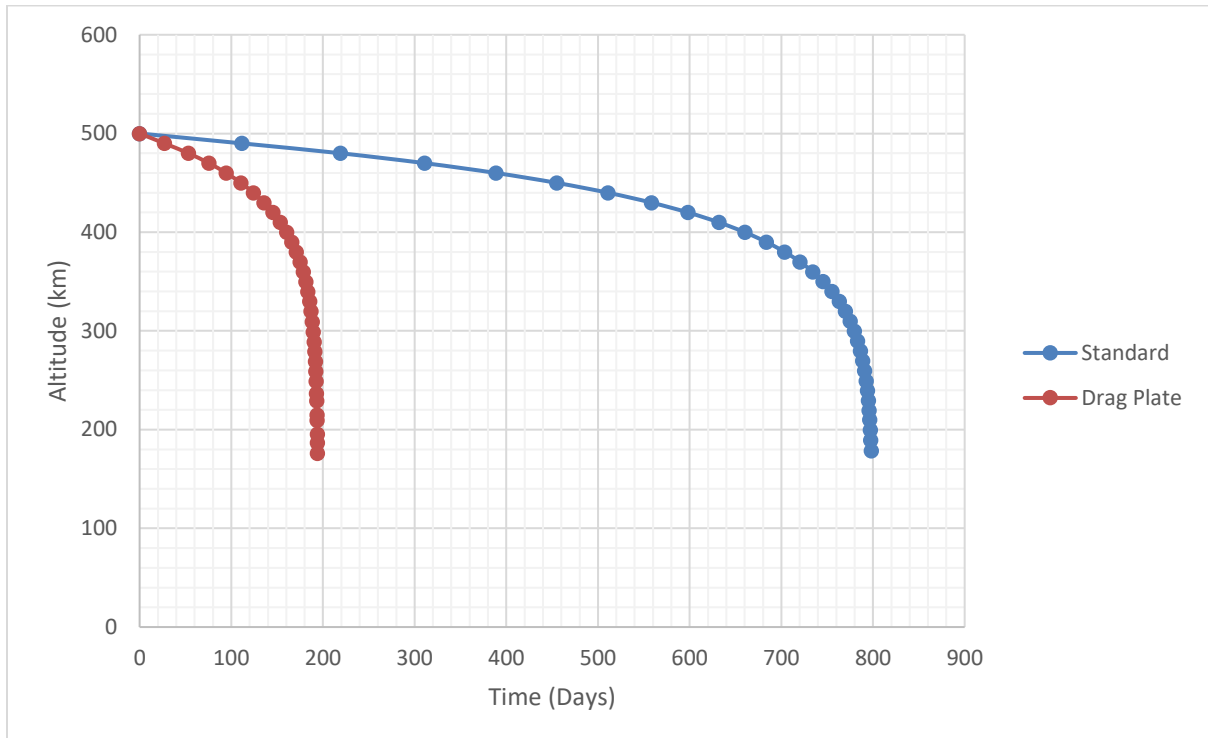


Figure 42: Comparison of the GRACE Satellite with and without an attached drag plate

Although this method has dramatically increased the orbital decay rate of the satellite by 75.7%, this would still not be as fast as the decay achieved by de-orbiting thrusters attached to the satellite. De-orbiting thrusters would most likely be more expensive to design and to implement on satellites, especially if the satellites were relatively small or had small budgets. Research into cost engineering; as well as other areas in engineering and science would be considered later on into future work.

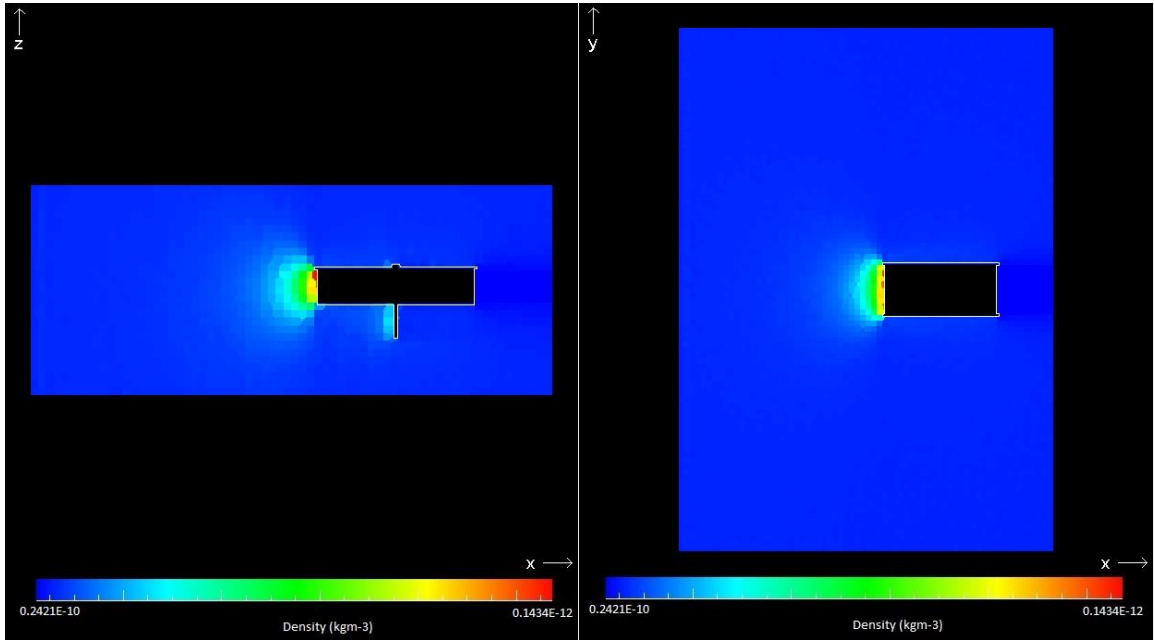


Figure 43: Density of flow around GRACE Satellite looking in Y and Z direction

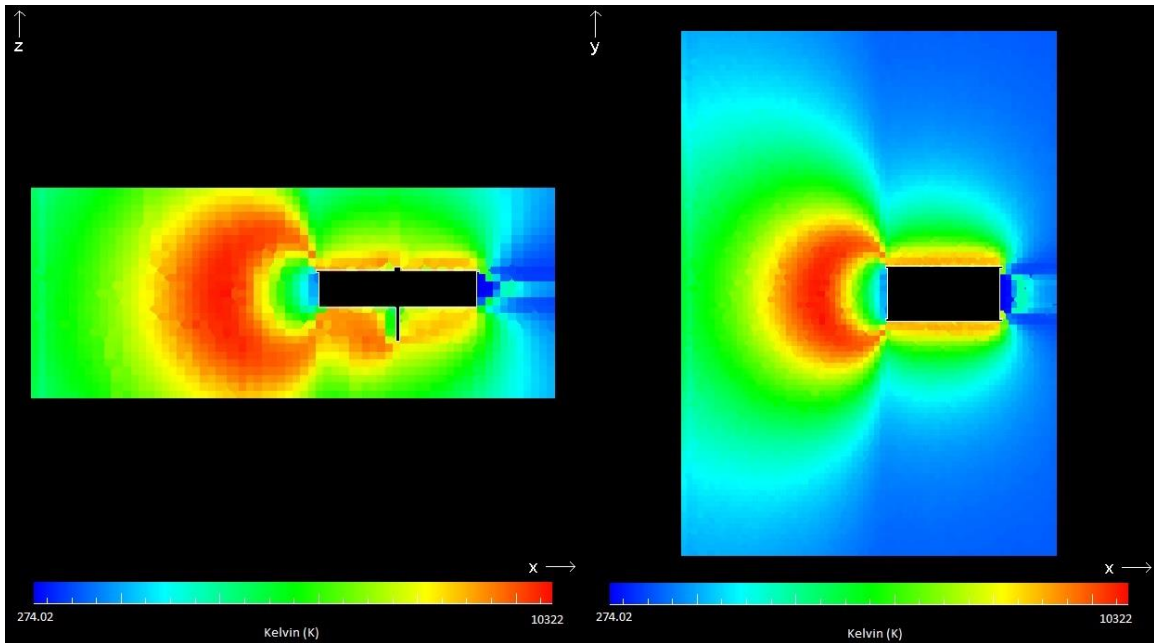


Figure 44: Temperature contours for GRACE satellite without drag plate in Y and Z direction

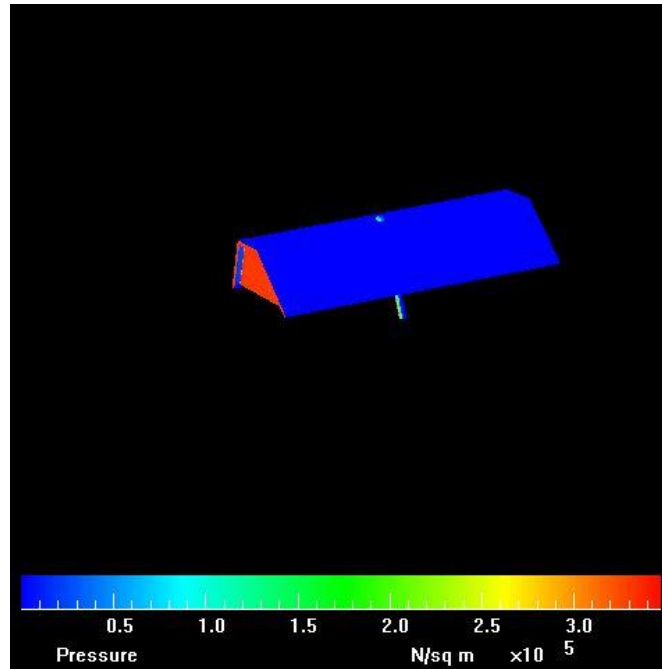


Figure 45: Pressure distribution for GRACE satellite without drag plate

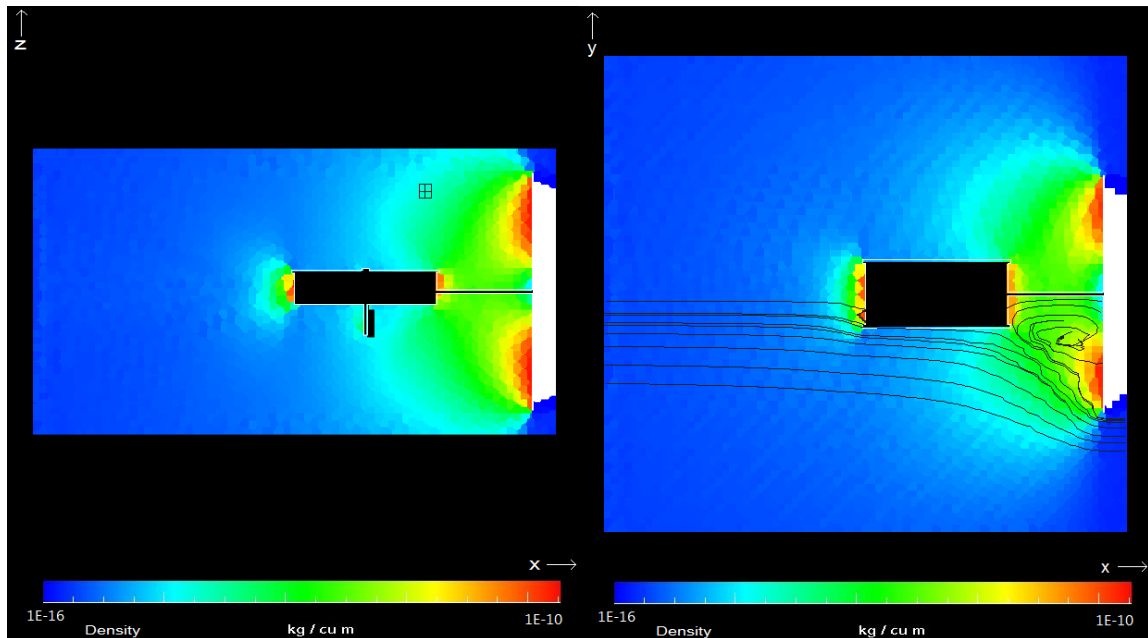


Figure 46: Density contours of GRACE satellite with drag plate

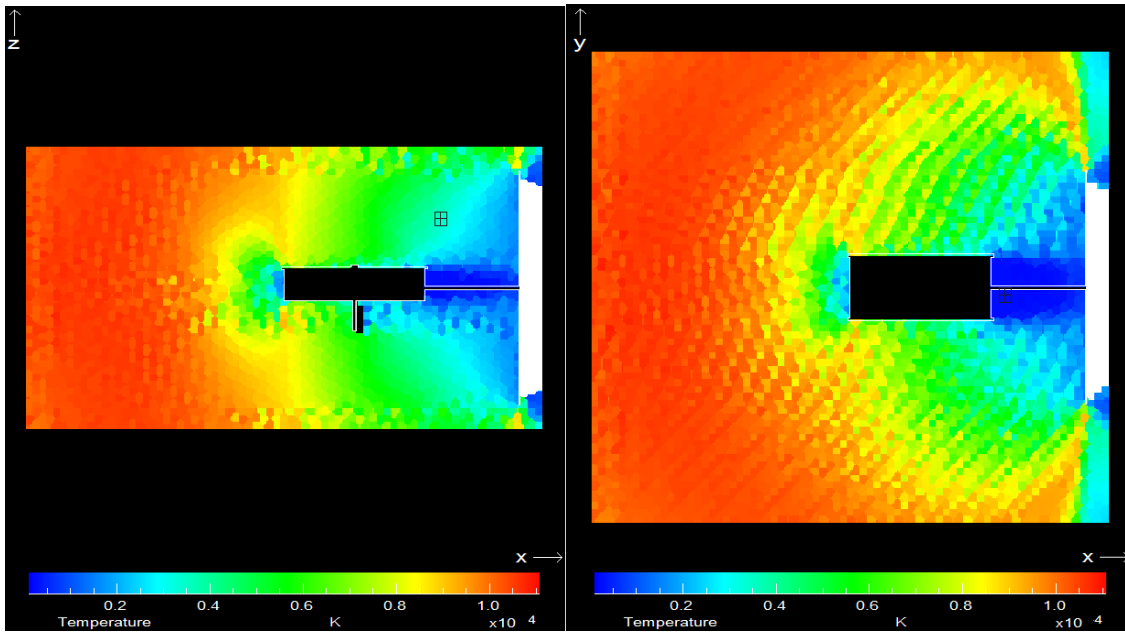


Figure 47: Temperature contours of GRACE satellite with drag plate

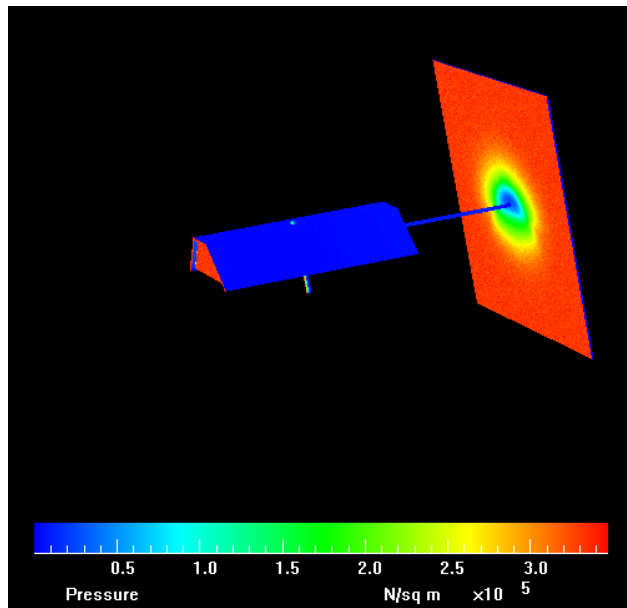


Figure 48: Pressure distribution on GRACE satellite with drag plate attached

Table 8: Drag and C_D of GRACE satellite with and without drag plate

	Standard	Plate
Drag (N)	4.94E-05	8.16E-04
C_D	3.16	2.59

It can be seen in figure 46 that the drag plate attached to the GRACE satellite will cause an area of high density of particles to form behind the satellite and in front of the drag plate; this is compared to the satellite in figure 43. This pocket of high density and pressure which can be seen via the particles tracing lines could cause performance issues to the effectiveness of the drag plate; this would be a factor to consider in a future design phase. This would involve carrying out simulations with the drag plate at different distances away from the satellite body. It can also be seen in Figures 45 & 48 how the surface pressure is distributed along the surface of both the satellites, with and without the drag plate. Table 8 shows how the drag values of the satellite with and without the drag plate compare.

It can also be seen in figure 47 that the temperature contours on the model with the drag plate are significantly bigger than those in figure 44, this indicates that there is a much larger 'bubble' of high energy particles in front of the satellite than before. The contours do not fit inside the domain of the experiment and extend outside the flow domain, this is due to the limited size and computational abilities of the computers used. For future work, higher power machines will be used that will allow for larger flow domains and more detailed mesh.

4.6 Summary

It can be seen from the simulations carried out in chapter 4 that the addition of the drag plate will cause a positive effect on the drag experienced by a satellite in LEO. This indicates that the larger the drag plate attached to the satellite, the faster it will de-orbit and re-enter the Earth's atmosphere.

A number of simulations were carried out on the GRACE satellite as this is a real world example of a satellite that was in orbit up until recently, and was recently de-orbited from space.

Calculations were also carried out to determine the orbital life time of satellites while the drag plate size was changed, as well as the F10.7 Solar Flux (Solar cycle reading) of the LEO regime. This showed that the higher the solar flux of the Leo regime, the faster the satellite would de-orbit from LEO. This information would be useful for satellite mission planning.

5. Conclusions

Validation simulations were initially carried out to compare numerical data collected from DSMC simulation with analytical data collected from equations as well as experimental data. The main focus of molecular reflection modelling was on the diffuse model, due to the amount of atomic oxygen contamination of surface of spacecraft and satellites in LEO which causes chaotic reflection. Simulations involving the Mars Pathfinder probe (70° blunt cone) were carried out with pure nitrogen, non-reacting flow at very low densities. The results from this numerical validation experiment aligned very well with the computational results obtained through DSMC; results were within the $\pm 3\%$ error margins. Simulations were also compared to analytical results collected by Moe *et al* [17] and compared next to the results collected from DSMC simulations from 150km up to 300km; these have shown close correlation with analytical and numerical data which helps validate future simulations.

Various shape geometries were simulated in DSMC while varying the freestream atmospheric temperature at 200km above sea level. The temperatures used in these simulations were based off the theoretical minimum and maximum values achievable contributed by day and night time activity, as well as F10.7 solar flux measurements from periods of high and low solar activity due to solar cycles. It can be seen from the results that there is a positive correlation between the freestream temperature and C_D values. Some of the geometries were affected more than other models, for instance, the sphere's line has a much shallower than the other lines on figure 25. This indicates to satellite manufacturers that specialist considerations need to be taken into account during times of high freestream temperatures.

It can be seen from section 4.2 of this thesis that density variations in the free molecular flow range (high altitudes) do not have an effect on the coefficient of drag value. This is due to the nature of the reflections that take place in free molecular flow; particles that interact with the surface of the satellite do not interact

with any more molecules due to the high mean free path between particles. Particles are not reemitted towards the satellite and more quasi-specular to specular reflection takes place; this is opposed to transitional range altitudes where diffuse reflections take place (see figure 5) [19]. The closed form equations from Sentman for calculating C_D in free molecular flow confirmed this conclusion [13].

A study was carried out to determine what the effects on orbital lifespan are of a drag plate attached to a satellite in LEO. A basic satellite design was taken and simulated at an altitude of 300km above sea level to gain a baseline reading for that specific geometry. Drags plates of various size were modelled and added to the back of the satellite to see if they have an effect on the drag value. The conclusion reached was that the drag plate does have a significant effect on the orbital life of the satellite, with the standard satellite re-entering the atmosphere in 8.9 days, and the satellite with the larger drag plate re-entering in 4.8 days. These designs have shown that satellites can be de-orbited from LEO more easily without the excess weight and cost of thrusters. Satellite with unfoldable drag plates could be designed and manufactured into satellites to allow them to decay more quickly when deployed and reduce the amount of space junk in orbit. Simulations were also carried out on a real-world design of a satellite; the GRACE satellite. The drag plates were shown to have a great effect on the orbital lifetime of the satellite, reducing the orbital life by roughly 81%. Although this addition of the drag plate to the GRACE satellite has made the orbital decay time shrink to 2.5 years from the original 14 years, this is still a reasonably long time to wait for a satellite to re-enter the earth's atmosphere, and extra considerations would need to be taken into account, such as the earth rotation and direction of orbit.

A study was carried out into the effect of solar cycles on the orbital decay of satellite; F10.7 solar flux is the value used in the measurement of solar activity. Solar cycles can last for around 10 years, with times of low activity reading 50 sfu and high activity reading 300 sfu. Orbital decay calculations were carried out between 50 and 300 sfu on a standard satellite. Information on solar flux was used from a report by the Australian Meteorology Department [29] to help carry out the

calculations. It has been shown that that levels of high solar activity decreases the satellite lifespan, with the orbital decay decreasing from 10 days to 3.5 days from 50 to 300 sfu. Satellite design and overall mission organisation needs to consider the level of solar activity as this affects the orbital lifetime of the satellite.

5.1 Future Work

It has been shown that drag plates can be very effective at reducing the orbital life of satellites in LEO, and further work into this field could take the idea and refine it to make it more efficient and achieve higher rates of orbital decay. The design used in the simulations in this project were simple to demonstrate the proof of concept. The next stage would be to make refinements to the design of the drag plates and re-simulate them and further enhance the design for optimal drag increase. This would mean that more models would have to be designed and modelled in CAD packages and transferred over to DSMC software where more evaluations can be made for each design. If sufficient evidence is shown that the designed drag plates can significantly decrease the time to re-entry then physical prototypes could be designed which include deploying mechanisms and packaging.

Further research into the reusability of satellite would also be beneficial. This technology would allow for hardware to be bought back home, whether to analyse physical data or for reusability. DSMC and CFD analysis (along with other potential software) would be used to analyse the forces and heat transfer experienced by the satellite, and from this data potential heat shields and parachutes could be designed and further analysed and refined.

Leading on from the drag plate research would be the main scope for further research relating to this project. Originally a basic cube model with solar panels was simulated which has shown that the concept of a drag plate is feasible; this was followed by the addition of a drag plate to the GRACE satellite which gave a high percentage drop in altitude, even from 500km as the starting altitude. From

this research further development can be carried out into the drag plate. This will include:

- Design: Improvement and re-testing of the drag plate
- Application: Research into whether it can be applied to new satellites
- Costing: Potential pricing of design and manufacture, as well as costing comparison next to de-orbiting thrusters
- Prototyping: creating working models
- Testing: Doing final testing before introduction

Completing a successful test of the drag plates in orbit would be the final stage and would require significant monetary backing before testing could begin.

REFERENCES

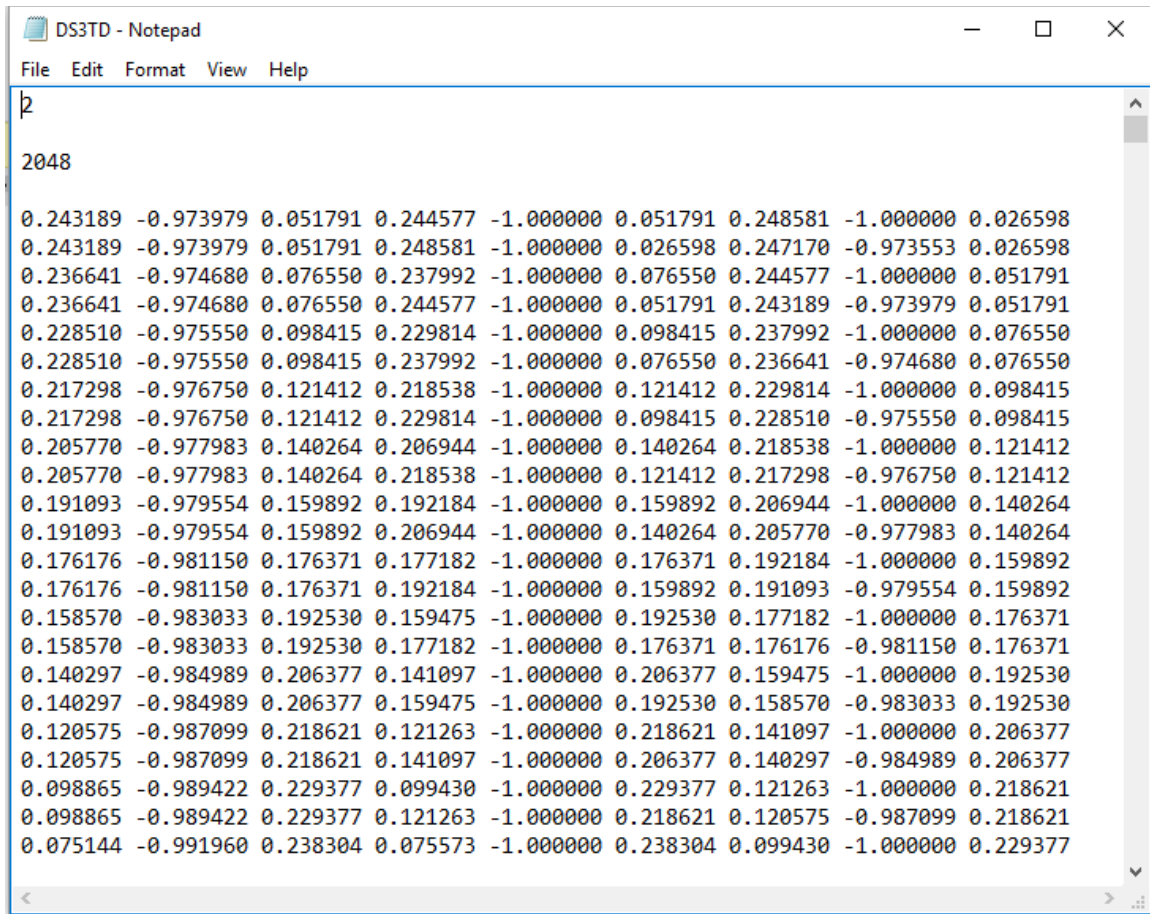
- [1] National Aeronautics and Space Administration, "1976 US Standard Atmosphere," NASA, USAF, 1976.
- [2] Anon., Reference guide to the International Space Station P60-80, 2015.
- [3] The Tauri Group, "State of the Satellite Industry Report," Satellite Industry Association, 2016.
- [4] R. Varvill and A. Bond, "The Skylon Spaceplane: Progress to Realisation," *Journal of the British Interplanetary Society*, vol. 61, pp. 412-418, 2008.
- [5] Inter-Agency Space Debris Coordination Committee, "Space Debris - IDAC Assessment report," IDAC Steering Group, 2011.
- [6] G. A. Bird, *Molecular Gas Dynamics and the Direct Simulation of Gas Flows*, Oxford University Press, 1994.
- [7] G. A. Bird, *The DSMC Method Version 1.2*, Sydney : G.A.B Consulting, 2013.
- [8] A. D. Anderson, "A Simple model for Atmospheric Density Variations between 200km and 800km," in *Journal of the Atmospheric Sciences*, 1962, pp. 207-217.
- [9] K. F. Tapping, "The 10.7 cm solar radio flux (F10.7)," *Space Weather*, vol. XI, no. 7, pp. 394-406, 2013.
- [10] S. H. Knowles, J. M. Picone, S. E. Thonnard and A. C. Nicholas, "The Effect of Atmospheric Drag on Satellite Orbits during the Bastille Day Event," *Solar Physics*, pp. 287-297, 2001.
- [11] M. Knudsen, *The Kinetic Theory of Gases*, London: Methuen Publishing Ltd., 1934.
- [12] G. E. Cook, "Satellite Drag Coefficients," in *Planet. Space Science*, 1965.
- [13] L. H. Sentman, "Free Molecular Flow Theory and its Application to the determination of Aerodynamic Forces," Lockheed Aircraft Corporation, 1961.
- [14] P. M. Metha, C. A. McLaughlin and E. K. Sutton, "Drag Coefficient Modelling for GRACE using Direct Simulation Monte Carlo," Department of Aerospace Engineering - University of Kansas, Air Force Research Lab - Kirtland Air Force Base, 2013.

- [15] C. E. Glass, J. N. Moss and F. A. Greene, "DSMC Simulations of Apollo Capsule Aerodynamics for Hypersonic Rarefied Conditions," NASA Langley Research Centre, Hampton, VA, 2006.
- [16] M. Moe, K. Moe and S. Wallace, "Recommended Drag Coefficient for Aeronomic Satellite," in *The Upper Mesosphere and Lower Thermosphere: Review of Experiment and Theory*, Los Angeles, 1995, pp. 349-356.
- [17] M. Moe and K. Moe, "Gas-Surface Interactions and Satellite Drag Coefficients," in *Planetary and Space Science* 53, 2005, pp. 794-801.
- [18] K. Moe and M. Moe, "The effect of adsorption on densities measured by orbiting pressure gauges," in *Planet. Space Sci*, 1967, pp. 1329-1332.
- [19] P. M. Mehta, A. Walker, C. A. McLaughlin and J. Koller, "Comparing Physical Drag Coefficients Computed Using Different Gas-Surface Interaction Models," in *Journal of Spacecraft and Rockets* Vol 51, 2014, pp. 873-883.
- [20] M. Horsley, "An investigation into using differential drag for controlling a formation of CubeSats," Lawrence Livermore National Lab, 2011.
- [21] C. L. Leonard, W. M. Hollister and E. V. Bergmann, "Orbital Formationkeeping using Differential Drag," in *Journal of Guidance, Control and Dynamics*, American Institute of Aeronautics and Astronautics, 1989, pp. 108-113.
- [22] R. Sutton, K. Eric, S. Merem and J. M. Forbes, "Density and Winds in the Thermosphere Deduced from Accelerometer Data," in *Journal of Spacecraft and Rockets*, 2007, pp. 1210-1219.
- [23] R. Votta, A. Schettino and A. Bonfiglioli, "Hypersonic high altitude aerothermodynamics of a space re-entry vehicle," *Aerospace Science and Technology*, vol. 25, pp. 253-265, 2013.
- [24] S. Mungiguerra, G. Zuppari and R. Savino, "Rarefied aerodynamics of a deployable re-entry capsule," *Aerospace Science and Technology*, vol. 69, pp. 395-403, 2017.
- [25] G. A. Bird, *The DS3V Program Users Guide V2.5*, Sydney, AUS: GAB Consulting, 2006.
- [26] P. Chambre and S. S, *Flow of Rarefied Gasses*, Princeton University Press, 1961.
- [27] W. Watt and R. Moreton, "Technical Note CPM 80," RAE Farnborough, 1964.
- [28] D. King-Hele, *Satellite Orbits in an Atmosphere - Theory and Applications*, Glasgow: Blackie and Son Ltd, 1987.

- [29] Australian Government - Bureau of Meteorology, "Satellite Orbital Decay Calculations," IPS Radio & Space Services, Sydney, 1999.
- [30] W. Wagner, "A Convergence proof for Bird's direct simulation Monte Carlo method for the Boltzmann equation," *J. Stat. Phys.*, 1992.
- [31] G. A. Bird, "Monte Carlo Simulation in an Engineering Context," American Institute of Aeronautics and Astronautics, New York, 1980.
- [32] H. Matsumoto, "Variable Sphere Molecular Model in the Monte Carlo Simulation of Rarefied Gas," in *Rarefied Gas Dynamics: 23rd International Symposium*, American Institute of Physics, 2003, pp. 358-365.
- [33] G. A. Bird, "Definition of Mean Free Path for Real Gases," *Phys. Fluids*, 1983.
- [34] K. Koura and H. Matsumoto, "Variable Soft Sphere Molecular Model for inverse power law or Lennard-Jones potential," in *Phys. Fluids*, 1991, pp. 2459-2465.
- [35] H. A. Hassan and D. B. Hash, "A Generalised Hard Sphere Model for Monte Carlo Simulations," in *Phys. Fluids A* 5, 1993, pp. 738-744.
- [36] H. A. Hassan, D. B. Hash and J. N. Moss, "Direct simulation of a diatomic gas using the generalised hard sphere model," in *Journal of Thermophysics and Heat Transfer*, 1994.
- [37] J. A. Kunc, H. A. Hassan and D. B. Hash, "The GHS interaction model for strong attractive potential," in *Phys. Fluids*, 1995, pp. 1173-1175.
- [38] NATO - Advisory Group for Aerospace Research and Development Group 18, "Hypersonic Experimental and Computational Capability, Improvement and Validation (AGARD AR-319)," 1996.
- [39] J. N. Moss and J. M. Price, "Review of Blunt Body Wake Flows at Hypersonic Low Density Conditions," AIAA, Hampton, VA, 1996.
- [40] J. N. Moss, V. K. Dogra and R. G. Wilmoth, "DSMC Simulations of Mach 20 Nitrogen Flow about a 70° Blunted Cone and its Wake," NASA TM-107762, Hampton, VA, 1993.
- [41] J. Allegre, D. Bisch and J. C. Lengrand, "Experimental Rarefied density flowfield at hypersonic conditions over a 70° blunted cone," *Journal of Spacecraft and Rockets*, vol. 4, no. 36, pp. 714-718, 1997.
- [42] J. Allegre, D. Bisch and J. C. Lengrand, "Experimental rarefied aerodynamic forces at hypersonic conditions over 70-degree blunted cone," *Journal of Spacecraft and Rockets*, vol. 4, no. 36, pp. 718-723, 1997.

- [43] A. G. Klothakis, I. K. Nikolos, T. P. Koehler, M. A. Gallis and S. J. Plimpton, "Validation Simulations of the DSMC code SPARTA," American Institute of Physics, 2016.
- [44] R. Janovsky, M. Kassebom, H. Lubberstedt, O. Romberg, H. Burkhardt, M. Sippel, G. Krulle and B. Fritsche, "End-of-life De-orbiting Strategies for Satellites," Deutscher Luft- und RaumfahrtKongress, 2002.
- [45] I. Kashiwai, "SATELLITE ORBITAL DECAY PREDICTION," Lizard Tail, [Online]. Available: http://www.lizard-tail.com/isana/lab/orbital_decay/.
- [46] E. Friis-Christensen and K. Lassen, "Length of the Solar Cycle: An Indicator of Solar Activity Closely Associated with Climate," *Science, New Series*, vol. 254, no. No 5032, pp. 698-700, 1991.
- [47] S. Bettadpur, "Gravity Recovery and Climate Experiment (CSR-GR-03-02) Product Specification Document," Center for Space Research, University of Texas, Austin, TX, 2012.
- [48] J. M. Picone, A. E. Hedin, D. P. Drob and A. C. Aikin, "NRLMSISE-00 empirical model of the atmosphere: Statistical comparisons and scientific issues," *Journal of Geophysical Research: Space Physics*, vol. 107, no. A12, 2002.
- [49] ITPROSTAR, "n2yo," ITPROSTAR, [Online]. Available: <https://www.n2yo.com/>.

APPENDIX A



```

DS3TD - Notepad
File Edit Format View Help
2048
0.243189 -0.973979 0.051791 0.244577 -1.000000 0.051791 0.248581 -1.000000 0.026598
0.243189 -0.973979 0.051791 0.248581 -1.000000 0.026598 0.247170 -0.973553 0.026598
0.236641 -0.974680 0.076550 0.237992 -1.000000 0.076550 0.244577 -1.000000 0.051791
0.236641 -0.974680 0.076550 0.244577 -1.000000 0.051791 0.243189 -0.973979 0.051791
0.228510 -0.975550 0.098415 0.229814 -1.000000 0.098415 0.237992 -1.000000 0.076550
0.228510 -0.975550 0.098415 0.237992 -1.000000 0.076550 0.236641 -0.974680 0.076550
0.217298 -0.976750 0.121412 0.218538 -1.000000 0.121412 0.229814 -1.000000 0.098415
0.217298 -0.976750 0.121412 0.229814 -1.000000 0.098415 0.228510 -0.975550 0.098415
0.205770 -0.977983 0.140264 0.206944 -1.000000 0.140264 0.218538 -1.000000 0.121412
0.205770 -0.977983 0.140264 0.218538 -1.000000 0.121412 0.217298 -0.976750 0.121412
0.191093 -0.979554 0.159892 0.192184 -1.000000 0.159892 0.206944 -1.000000 0.140264
0.191093 -0.979554 0.159892 0.206944 -1.000000 0.140264 0.205770 -0.977983 0.140264
0.176176 -0.981150 0.176371 0.177182 -1.000000 0.176371 0.192184 -1.000000 0.159892
0.176176 -0.981150 0.176371 0.192184 -1.000000 0.159892 0.191093 -0.979554 0.159892
0.158570 -0.983033 0.192530 0.159475 -1.000000 0.192530 0.177182 -1.000000 0.176371
0.158570 -0.983033 0.192530 0.177182 -1.000000 0.176371 0.176176 -0.981150 0.176371
0.140297 -0.984989 0.206377 0.141097 -1.000000 0.206377 0.159475 -1.000000 0.192530
0.140297 -0.984989 0.206377 0.159475 -1.000000 0.192530 0.158570 -0.983033 0.192530
0.120575 -0.987099 0.218621 0.121263 -1.000000 0.218621 0.141097 -1.000000 0.206377
0.120575 -0.987099 0.218621 0.141097 -1.000000 0.206377 0.140297 -0.984989 0.206377
0.098865 -0.989422 0.229377 0.099430 -1.000000 0.229377 0.121263 -1.000000 0.218621
0.098865 -0.989422 0.229377 0.121263 -1.000000 0.218621 0.120575 -0.987099 0.218621
0.075144 -0.991960 0.238304 0.075573 -1.000000 0.238304 0.099430 -1.000000 0.229377

```

A1: Example of part of a RAW triangle file (.raw) from Rhino3D CAD package, ready for input into first program (DS3DG.exe).

SATELLITE ORBITAL DECAY PREDICTION

Calculating decay rates and orbital lifetimes of satellites in essentially circular orbits below 500 km altitude.

Mass kg
Area m²
Initial Altitude km (range: 180km - 500 km)
Solar Radio Flux (F_{10.7})
Geomagnetic Index (A_p)

Reference

- [Satellite Orbital Decay Calculations](#) * PDF document
(The Australian Space Weather Agency)
- [The Ap-index | Help | SpaceWeatherLive.com](#)
- [Satellites Community Dashboard | NOAA / NWS Space Weather Prediction Center](#)

by isana kashiwai

A2: Online calculator which uses equations 2.3.11, 2.3.12 and information from the Australian Governments Bureau of Meteorology to calculate the orbital decay of satellites up to 500km above mean sea level [29] [45].

See page 80

APPENDIX B

Table 9: 1976 US Standard Atmosphere (Important values)

Altitude (m)	Temp (K)	Pressure (mb)	Density (kgm ⁻³)	No. Density (m ⁻³)	Mean Free Path (m)
200000	854.56	8.47E-07	2.54E-10	7.18E+15	2.40E+02
220000	899.01	5.01E-07	2.37E-10	4.04E+15	4.20E+02
240000	929.73	3.11E-07	7.86E-11	2.42E+15	7.00E+02
260000	950.99	1.99E-07	4.74E-11	1.52E+15	1.10E+03
280000	965.75	1.31E-07	2.97E-11	9.81E+14	1.70E+03
300000	976.01	8.77E-08	1.92E-11	6.51E+14	2.60E+03
320000	983.16	5.98E-08	1.26E-11	4.41E+14	3.80E+03
340000	988.15	4.13E-08	8.50E-12	3.03E+14	5.60E+03
360000	991.65	2.89E-08	5.81E-12	2.11E+14	8.00E+03
380000	994.1	2.04E-08	4.01E-12	1.49E+14	1.10E+04
400000	995.83	1.45E-08	2.80E-12	1.06E+14	1.60E+04
420000	997.04	1.04E-08	1.98E-12	7.58E+13	2.20E+04
440000	997.9	7.55E-09	1.40E-12	5.48E+13	3.10E+04
460000	998.5	5.52E-09	1.00E-12	4.00E+13	4.20E+04
480000	998.93	4.06E-09	7.21E-13	2.95E+13	5.70E+04
500000	999.24	3.02E-09	5.22E-13	2.19E+13	7.70E+04
520000	999.45	2.27E-09	3.80E-13	1.65E+13	1.00E+05
540000	999.61	1.73E-09	2.78E-13	1.25E+13	1.30E+05
560000	999.72	1.33E-09	2.05E-13	9.64E+12	1.80E+05
580000	999.8	1.04E-09	1.52E-13	7.52E+12	2.10E+05
600000	999.85	8.21E-10	1.14E-13	5.95E+12	2.80E+05

Table 10: Important values of gasses for VHS molecular model

Gas	Rotational Degrees of Freedom	Molecular Mass (E-27)	Diameter at 273K (E-10)	Viscosity-Temperature index
Hydrogen H ₂	2	3.34	2.92	0.67
Helium He	0	6.65	2.33	0.66
Carbon Monoxide CO	2	46.6	4.19	0.73
Nitrogen N ₂	2	46.5	4.17	0.74
Nitric Oxide NO	2	49.9	4.20	0.79
Oxygen O ₂	2	53.1	4.07	0.77
Argon Ar	0	66.3	4.17	0.81
Carbon Dioxide CO ₂	3	73.1	5.62	0.93
Nitrous Oxide N ₂ O	2	73.1	5.71	0.94
Xenon Xe	0	218	5.74	0.85

ID	Task Mode	Task Name	Duration	Start	Finish	November							December						
						24/10	31/10	07/11	14/11	21/11	28/11	05/12	12/12	19/12	26/12				
1	★	DSMC Self Teach	67 days	Tue 01/11/17	Wed 01/02/18	[Task bar spanning from 01/11/17 to 01/02/18]													
2	★	Literature Review	15 days	Mon 14/11/17	Fri 02/12/17	[Task bar from 14/11/17 to 02/12/17]													
3	★	Registration Report	36 days	Mon 28/11/17	Sun 15/01/18	[Task bar from 28/11/17 to 15/01/18]													
4	★	Data Collection for Verification and Validation Simulations	19 days	Thu 05/01/17	Tue 31/01/17	[Task bar from 05/01/17 to 31/01/17]													
5	★	Registration Viva	6 days	Wed 01/02/18	Wed 08/02/18	[Task bar from 01/02/18 to 08/02/18]													
6	★	Simulations: Closed form - Computation Comparison	6 days	Mon 13/02/17	Mon 20/02/17	[Task bar from 13/02/17 to 20/02/17]													
7	★	Collect + Analysis of Data from first simulations	11 days	Mon 20/02/17	Mon 06/03/17	[Task bar from 20/02/17 to 06/03/17]													
8	★	Simulations: Experimental - DSMC Comparison (Validation)	16 days	Mon 20/02/17	Mon 13/03/17	[Task bar from 20/02/17 to 13/03/17]													
9	★	Collect + Analysis of Data from second simulations	16 days	Mon 06/03/17	Mon 27/03/17	[Task bar from 06/03/17 to 27/03/17]													
10	★	Thesis Writing (Cont. from this date)	137 days	Sat 01/04/17	Sat 07/10/17	[Task bar from 01/04/17 to 07/10/17]													
11	★	Design Control Model for Drag Plate Simulations	3 days	Wed 05/04/17	Fri 07/04/17	[Task bar from 05/04/17 to 07/04/17]													
12	★	Reserachg into F10.7cm Flux	5 days	Fri 07/04/17	Thu 13/04/17	[Task bar from 07/04/17 to 13/04/17]													
13	★	Simulation: Drag plate simulations	13 days	Mon 10/04/17	Wed 26/04/17	[Task bar from 10/04/17 to 26/04/17]													

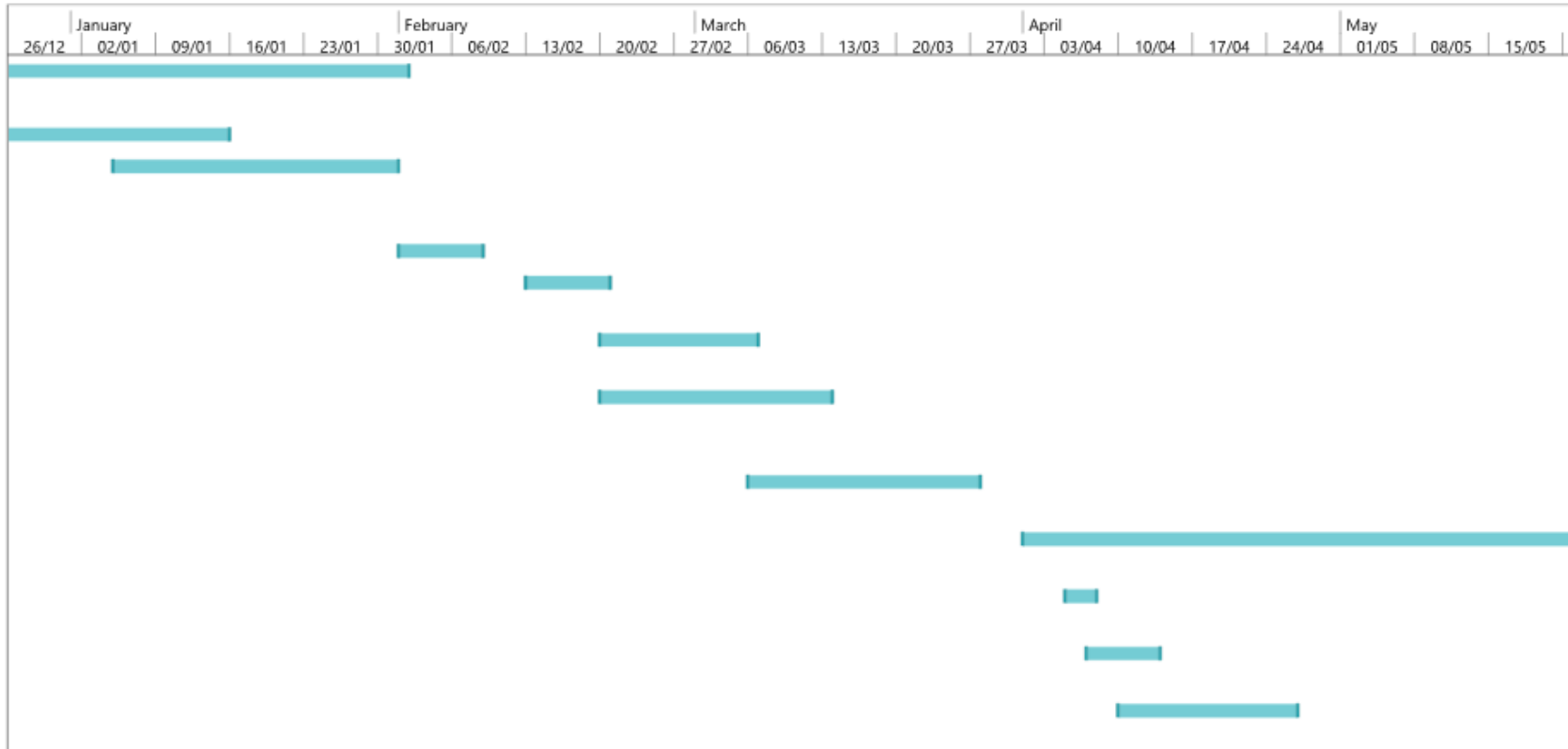
Project: MRes Gantt Chart
Date: Mon 13/11/17

Task		Inactive Summary		External Tasks	
Split		Manual Task		External Milestone	
Milestone		Duration-only		Deadline	
Summary		Manual Summary Rollup		Progress	
Project Summary		Manual Summary		Manual Progress	
Inactive Task		Start-only			
Inactive Milestone		Finish-only			

ID	Task Mode	Task Name	Duration	Start	Finish	November					December						
						24/10	31/10	07/11	14/11	21/11	28/11	05/12	12/12	19/12	26/12		
14		Orbital decay calculations	14 days	Wed 26/04/17	Mon 15/05/17												
15		Analysis: Drag Plate Models	11 days	Mon 17/04/17	Mon 01/05/17												
16		Design: Temperature variation simulation models	4 days	Mon 01/05/17	Thu 04/05/17												
17		Simulation: Temp Var Models	60 days	Mon 08/05/17	Fri 28/07/17												
18		Analysis: Temp Var Models	11 days	Mon 24/07/17	Mon 07/08/17												
19		Design: Density Var Models	5 days	Mon 05/06/17	Fri 09/06/17												
20		Simulation: Density Var Models	10 days	Mon 12/06/17	Fri 23/06/17												
21		Analysis: Density Var Models	11 days	Fri 23/06/17	Fri 07/07/17												
22		Final Analysis of data collected - Any Further Simulations needed	41 days	Mon 10/07/17	Mon 04/09/17												
23		Thesis Writing: Conclusions drawn up	23 days	Mon 04/09/17	Wed 04/10/17												

Project: MRes Gantt Chart Date: Mon 13/11/17	Task		Inactive Summary		External Tasks	
	Split		Manual Task		External Milestone	
	Milestone		Duration-only		Deadline	
	Summary		Manual Summary Rollup		Progress	
	Project Summary		Manual Summary		Manual Progress	
	Inactive Task		Start-only			
	Inactive Milestone		Finish-only			

Page 2



Project: MRes Gantt Chart Date: Mon 13/11/17	Task		Inactive Summary		External Tasks	
	Split		Manual Task		External Milestone	
	Milestone		Duration-only		Deadline	
	Summary		Manual Summary Rollup		Progress	
	Project Summary		Manual Summary		Manual Progress	
	Inactive Task		Start-only			
	Inactive Milestone		Finish-only			

